

AD 740597

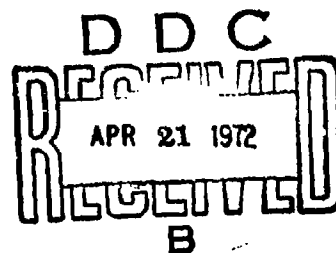
RADC-TR-72-6  
Final Technical Report  
February 1972



NUMERICAL SAMPLING TECHNIQUES INVESTIGATION  
Texas Instruments, Inc.

Approved for public release;  
distribution unlimited.

Reproduced by  
NATIONAL TECHNICAL  
INFORMATION SERVICE  
Springfield, Va 22151



Rome Air Development Center  
Air Force Systems Command  
Griffiss Air Force Base, New York

F  
116

UNCLASSIFIED

Security Classification

DOCUMENT CONTROL DATA - R & D

(Security classification of title, body of abstract and indexing annotation must be entered when the overall report is classified)

1. ORIGINATING ACTIVITY (Corporate author) Texas Instruments, Inc. Digital Systems Division P.O. Box 2909, Austin TX 78767		2a. REPORT SECURITY CLASSIFICATION UNCLASSIFIED	
		2b. GROUP N/A	
3. REPORT TITLE NUMERICAL SAMPLING TECHNIQUES INVESTIGATION			
4. DESCRIPTIVE NOTES (Type of report and inclusive dates) Final July 1970 - August 1971			
5. AUTHOR(S) (First name, middle initial, last name) Dr. Alan L. McBride Dan K. Raley			
6. REPORT DATE February 1972		7a. TOTAL NO. OF PAGES 112	7b. NO. OF REFS 26
8a. CONTRACT OR GRANT NO. F30602-70-C-0180  Job Order No. 45190000		9a. ORIGINATOR'S REPORT NUMBER(S) UI-978101-F	
		9b. OTHER REPORT NO(S) (Any other numbers that may be assigned this report) RADC-TR-72-6	
10. DISTRIBUTION STATEMENT Approved for public release; distribution unlimited.			
11. SUPPLEMENTARY NOTES None		12. SPONSORING MILITARY ACTIVITY Rome Air Development Center (CORS) Griffiss Air Force Base, New York 13440	
13. ABSTRACT <p>This report is devoted to the investigation of techniques for implementing an all digital oscillator and the applications of this oscillator in communication equipment. Two techniques of implementing the digital oscillator are discussed: the recursive technique which uses recursive difference equations as the oscillator algorithm and the nonrecursive technique which uses permanently stored values of sine waves and corresponding control logic to generate output sine waves. The nonrecursive implementation approach was selected for breadboard design. Breadboard design, construction and performance evaluation are considered. The oscillator operates in two modes: as a frequency synthesizer and a digitalized voltage controlled oscillator (VCO). Applications of these two modes in communication function implementations are presented as well as a new technique for implementing digitalized FM demodulation.</p>			

DD FORM 1 NOV 68 1473

UNCLASSIFIED

Security Classification

14 KEY WORDS	LINK A		LINK B		LINK C	
	ROLE	WT	ROLE	WT	ROLE	WT
Digital Oscillator Communication Systems Demodulator Phase-Locked Loop Discriminator In-Phase and Quadrature Sampling Nonlinear Estimation Digital Filtering						

NUMERICAL SAMPLING TECHNIQUES INVESTIGATION

Dr. Alan L. McBride  
Dan K. Raley

Texas Instruments, Inc.

Approved for public release;  
distribution unlimited.

FOREWORD

This final report was prepared by Dr. Alan L. McBride (Project manager) and Mr. Dan K. Raley of the Advanced Development Staff, Digital Systems Division, Texas Instruments, Inc., Austin, Texas. The work was performed under contract F30602-70-C-0180, Job Order Number 45190000, for Rome Air Development Center, Griffiss Air Force Base, New York. The report covers the period from July 1970 to August 1971. RADC Project Engineer is Mr. Charles N. Meyer (CORS). Secondary report number is UI-978101-F.

This report has been reviewed by the Information Office (OI) and is releasable to the National Technical Information Service (NTIS).

This technical report has been reviewed and is approved.

Approved: *Charles N. Meyer*  
CHARLES N. MEYER  
Effort Engineer

Approved: *Alvin Twitchell*  
ALVIN TWITCHELL, Colonel, USAF  
Chief, Communications & Navigation Division

FOR THE COMMANDER:

*Fred I. Diamond*

FRED I. DIAMOND  
Acting Chief, Plans Office

## ABSTRACT

This report is devoted to the investigation of techniques for implementing an all digital oscillator and the applications of this oscillator in communication equipment. Two techniques of implementing the digital oscillator are discussed: The recursive technique which uses recursive difference equations as the oscillator algorithm and the nonrecursive technique which uses permanently stored values of sine waves and corresponding control logic to generate output sine waves. The nonrecursive implementation approach was selected for breadboard design. Breadboard design, construction and performance evaluation are considered. The oscillator operates in two modes; as a frequency synthesizer and a digitalized voltage controlled oscillator (VCO). Applications of these two modes in communication function implementations are presented as well as a new technique for implementing digitalized FM demodulation.

## EVALUATION

This study was concerned with the investigation of techniques for implementing an all-digital oscillator and the applications of this oscillator in communication equipment. Two basic techniques for synthesizing digital oscillators have been discussed. The first, the recursive technique, resulted from the difference equations relating input and output. The error build-up from this approach could not be satisfactorily coped with and consequently, this means was discarded. The second method was the non-recursive technique, using a read only memory. All things considered the non-recursive technique for digital synthesis of oscillators has been shown to operate as well, if not better, than conventional analog circuits in the basic configurations, frequency synthesizer and VCO replacement.

In the course of the study it developed that a particular digital oscillator application, a non-linear demodulator, appears to be capable of providing a near-optimum threshold extension technique for digitalized FM receivers. This idea appears to merit further investigation.

*Charles N. Meyer*

CHARLES N. MEYER  
Effort Engineer

## TABLE OF CONTENTS

Section	Page
I INTRODUCTION	1
A. General	1
B. Outline of the Report	2
1. Implementation Approaches - Section II	2
2. Applications of Digital Oscillator - Section III	2
3. Breadboard Design Discussion - Section IV	2
4. Breadboard Demonstration Evaluation - Section V	3
5. Conclusions - Section VI	3
6. In-Phase and Quadrature Sampling - Appendix A	3
7. A Non Linear Digital Processor For FM Demodulation - Appendix B	3
II IMPLEMENTATION APPROACHES	5
A. Recursive Digital Oscillator	5
1. General	5
2. Error Analysis	8
3. Error Correction Techniques	10
B. Nonrecursive Digital Oscillator	13
1. General	13
2. Fourier Analysis	15
3. Error Analysis	16
III APPLICATION OF DIGITAL OSCILLATORS	21
A. Introduction	21
B. Digitalized Phase - Locked Loops	23
1. Introduction	23
2. Digitalized Loop	24
C. Recursive Nonlinear Demodulator (RNLD)	25
1. Introduction	25
2. RNLD Synthesis	27
3. Single-Pole Filter Example	33
D. Discrete Fourier Transformations	37
E. Synchronization	37

TABLE OF CONTENTS (Continued)

<u>Section</u>	<u>Page</u>
IV BREADBOARD DESIGN DISCUSSION	41
A. General	41
B. Breadboard Configurations	43
1. Frequency Synthesizers	43
a. Frequency Synthesizer	43
b. Frequency Translator	43
2. VCO Replacements	44
a. Tracking Filter	44
b. Frequency Modulator	44
C. Breadboard Description	46
1. Mechanical Description	46
2. Operational Description	46
a. Digital Portion	46
1) Recursive Adder Board (Board E)	46
2) DAC Board F	48
3) Buffer Board I	48
4) Modulation Board D	48
5) ADC Converter Board C	48
6) BCD/Binary Converter Board B	48
7) Clock Board A	51
b. Analog Portion	51
1) Mixer Board G	51
2) Discriminator Board H	51
V BREADBOARD DEMONSTRATION AND EVALUATION	53
A. Demonstration	53
1. Frequency Synthesizers	53
a. Frequency Synthesizer	53
b. Frequency Translator	54
2. VCO Replacement	54
a. Frequency Modulation	54
b. Tracking Filter	55

TABLE OF CONTENTS (Continued)

<u>Section</u>	<u>Page</u>
B. Evaluation	56
1. Frequency Synthesizers	57
a. Stability	57
b. Harmonic Distortion	58
c. Harmonic Content	58
2. VCO Replacement	60
a. Frequency Linearity	61
b. Amplitude and Frequency Stability	61
c. Pull-In Range	61
d. Harmonic Distortion and Harmonic Content	61
e. Application Analysis	61
1) Angle Modulation	61
2) Frequency Shift Keying (FSK)	64
VI CONCLUSIONS	65
A. Summary	65
B. Recommendations	66
APPENDIX A In-Phase and Quadrature Sampling	69
APPENDIX B A Nonlinear Digital Processor for FM Demodulation	79

## LIST OF ILLUSTRATIONS

<u>Figure</u>	<u>Title</u>	<u>Page</u>
2-1	Coupled Recursive Digital Oscillator	6
2-2	Uncoupled Recursive Digital Oscillator	7
2-3	Simplified Recursive Digital Oscillator	7
2-4	Error Correction Filter Applied to Cosine Generator	11
2-5	Phase Circle	14
2-6	Spectral Analysis for $f_o/f_B$ Ratio of 1/11.2	17
2-7	Spectral Analysis for $f_o/f_B$ Ratio of 1/17.3	18
2-8	Spectral Analysis for $f_o/f_B$ for Ratio of 1/22.5	19
3-1	Linearized Phase - Locked Loop Block Diagram	23
3-2	Linearized Digital Phase - Locked Loop	25
3-3	Digitalized Phase - Locked Loop Block Diagram	26
3-4	Block Diagram for Modulator and Demodulator for an FM Process	28
3-5	Block Diagram for Equivalent Baseband FM Process	28
3-6	Single Pole Message Model	29
3-7	Model for FM	30
3-8	Continuous State Variable Representation of FM Process	30
3-9	Block Diagram of the Message Process Illustrating Discrete State Variable Characterization of the Angle $\theta(K)$	32
3-10	Block Diagram Realization of the Recursive Nonlinear Demodulation for a Single-Pole Message Filter	34
3-11	Signal-to-Noise Performance Curves Obtained from Simulation	36
3-12	Block Diagram Showing the Different Time Waveforms Going from Digital to Analog Processing When Using the Digital Oscillator	38
3-13	Block Diagram Showing the Application of a Digital Oscillator to Obtain Timing Marks for Bit Synchronization	39
4-1	Nonrecursive Digital Oscillator Block Diagram	41
4-2	Frequency Synthesizer	43
4-3	Frequency Translator	44
4-4	Tracking Filter	45
4-5	Frequency Modulator	45
4-6	Breadboard Mechanical Package	47
4-7	Breadboard Digital Layout	49
4-8	Analog Layout	52
5-1	Frequency Synthesizer	53
5-2	Frequency Translation	54
5-3	FM Synthesizer	55
5-4	Tracking Filter	56
5-5	DO Stability Measurement	57

LIST OF ILLUSTRATIONS (Continued)

<u>Figure</u>	<u>Title</u>	<u>Page</u>
5-6	Stability Comparison	58
5-7	% Distortion vs Frequency for Digital Oscillator	59
5-8	DO Spectrum for Input Frequency of 186.413 Hz	60
5-9	$\Delta f$ vs Voltage FM Mode Digital Oscillator	62
5-10	Density Function of Sinusoid of Peak "a"	63
5-11	Frequency Spectrum for VCO Configuration	63
5-12	FSK Application of DO	64

LIST OF TABLES

<u>Table</u>	<u>Title</u>	<u>Page</u>
I	Number of Output Samples Obtainable for a Desired SNR	10
II	Digital Oscillator Applications	21

# SECTION I

## INTRODUCTION

### A. GENERAL

The advent of Large Scale Integration (LSI) techniques have made many of the communication functions previously performed by analog techniques amenable to digital implementation. This idea when combined with the versatility of digital components precipitated this contract, entitled "Sampling Numerical Techniques" investigation, directed toward evaluation of techniques for implementing digital oscillators.

A digital oscillator is a device which produces discrete quantized ( $n$ -bits) samples of a sinusoidal waveform at some fixed sample rate. There are basically two methods for generating samples in an all digital oscillator - recursively and nonrecursively. Recursive digital oscillators result from an examination of the different equations relating sinusoidal outputs to previously computed outputs. These different equations are obtained by applying Z-transformation techniques to the Laplace transform of an oscillator output (either sine or cosine). Problems are encountered when a digital oscillator is implemented recursively; the round-off errors associated with each iteration tend to build up and become unbounded, therefore requiring some type error compensation.

The nonrecursive digital oscillator approach, on the other hand, does not have this inherent error build-up. This approach requires that  $n$ -bit samples for one cycle of the sinusoid be stored in a memory, generally a read-only memory (ROM). Since it is physically impossible to store every sample value for one cycle of a sinusoid in a finite size ROM,  $M$  equally spaced sample values of the waveform are stored. This  $M$ -word quantization and the  $n$ -bit discretization of the sampled waveform (sample values stored in an  $M \times n$  ROM) are the two sources of amplitude error for the nonrecursive digital oscillator. These errors however do not build up and are constant for each  $M$  and  $n$  combination.

The choice of which approach to employ in implementing a digital oscillator is usually dictated by the particular application of the oscillator. For example, a nonrecursive digital oscillator which uses a ROM in conjunction with shift registers and simple control circuitry can be used to obtain output waveforms in the neighborhood of 10 MHz using standard techniques. These relatively high sample rates cannot be achieved using the recursive digital oscillator approach implemented with similar logic. However, the recursive digital oscillator under some conditions requires less logic and might be preferred if high sample rates are not required.

## B. OUTLINE OF THE REPORT

### 1. IMPLEMENTATION APPROACHES - SECTION II

The digital oscillator using the recursive approach is discussed first. It is shown that the major difficulty encountered when using this approach is the computational build up error. Two recursive digital oscillators are discussed and their build-up errors evaluated. This evaluation indicates that neither recursive digital oscillator configuration is practical unless this build-up error is corrected. Three techniques for correcting this error are discussed.

The nonrecursive approach to digital oscillator design is then discussed. The amplitude errors for this approach are shown to be fixed and completely determinable for each ROM word size versus bit size (Mxn) combination. The frequency errors result from quantization of the ratio of the synthesized frequency to the sample frequency and are shown to be independent of the (Mxn) combinations. Fourier analysis of various synthesized waveforms are then performed with the results presented.

### 2. APPLICATIONS OF DIGITAL OSCILLATORS - SECTION III

An important part of this effort has been determining those communication functions which could employ digital oscillators and evaluating their respective performances. This section presents the configurations for the digital oscillator approaches. There are essentially two basic configurations in which digital oscillator can function: as a frequency synthesizer, or as a digitalized voltage controlled oscillator (VCO). The nonrecursive digital oscillator approach is directly amenable to these two configurations. The recursive approach on the other hand can not be used in the variable frequency (VCO) configuration because of the difficulty involved in changing the coefficients of the recursive equations. This does not, however, prevent this approach from being used in the frequency synthesizer configuration.

For the above mentioned reasons, this section is devoted to nonrecursive digital oscillator configurations. These configurations include digitalized phase-locked-loop demodulation, linear frequency and angle modulation, discrete Fourier transformation, synchronization, and a new technique called the recursive nonlinear demodulator. This demodulator results from the application of nonlinear filtering and estimation techniques to angle demodulation, and by its very nature provides near-optimum threshold extension (FM). The performance evaluations for these configurations are included in a later section.

### 3. BREADBOARD DESIGN DISCUSSION - SECTION IV

This section presents the basic design considerations for the nonrecursive digital oscillator configurations; i. e., frequency synthesizer, and voltage

controlled oscillator. Also included are descriptions of the mechanical package and the operational procedure.

#### 4. BREADBOARD DEMONSTRATION'S EVALUATION - SECTION V

To effectively evaluate a digital oscillator which outputs digital samples of a sinusoid, these samples must first be converted to analog by digital-to-analog conversion techniques so that a direct comparison can be made with analog waveforms. The breadboard evaluation discussed in this section is based upon making these comparisons with conventional equipment.

#### 5. CONCLUSIONS - SECTION VI

This section contains a summary of the important results obtained during the study effort and a recap of the performance evaluation for the breadboard. Also included are Texas Instruments' recommendations for further efforts in this area.

#### 6. IN-PHASE AND QUADRATURE SAMPLING - APPENDIX A

The in-phase and quadrature sampling idea is used throughout the report. This appendix contains the derivation of this concept for both coherent and noncoherent sampling.

#### 7. A NONLINEAR DIGITAL PROCESSOR FOR FM DEMODULATION - APPENDIX B

This appendix gives a discussion of the synthesis and evaluation of a special type of digitalized FM demodulator that makes use of the digital oscillator. A brief discussion of the same topic is also presented in Section III.

SECTION II  
IMPLEMENTATION APPROACHES

A. RECURSIVE DIGITAL OSCILLATOR

1. GENERAL

The technique used in the recursive digital oscillator has been discussed extensively in references 1, 2, 3 and in the simplest form can be expressed trigonometrically as:

$$\begin{aligned}\cos (m+1)\theta &= \cos m\theta \cos \theta - \sin m\theta \sin \theta \\ \sin (m+1)\theta &= \sin m\theta \cos \theta + \cos m\theta \sin \theta\end{aligned}\tag{1}$$

where the  $(m+1)$ th sine and cosine terms are computed recursively from the last terms and some initialization terms. The recursive relations of equation (1) expressed in block diagram form are shown in Figure 2-1.

These expressions for  $\cos (m+1)\theta$  and  $\sin (m+1)\theta$ , although trigonometrically correct, lead to severe errors when computed on finite bit computers. The problem arises because each output,  $\cos (m+1)\theta$  and  $\sin (m+1)\theta$ , is used to compute the next output. This type of recursive relation is very undesirable because of the error build up.

An alternate method for recursively computing sine and cosine values is based on the application of the  $z$ -transform to an oscillator output; i. e.,

$$\begin{aligned}Z(\cos \alpha t) &= \frac{1 - \cos \alpha T z^{-1}}{1 - 2 \cos \alpha T z^{-1} + z^{-2}} \\ Z(\sin \alpha t) &= \frac{\sin \alpha T z^{-1}}{1 - 2 \cos \alpha T z^{-1} + z^{-2}}\end{aligned}\tag{2}$$

where  $T$  is the sample interval.

These  $z$ -transforms could be considered as transfer functions of a system, i. e.,

$$\begin{aligned}H_c(z) &= \frac{1 - \cos \alpha T z^{-1}}{1 - 2 \cos \alpha T z^{-1} + z^{-2}} \\ H_s(z) &= \frac{\sin \alpha T z^{-1}}{1 - 2 \cos \alpha T z^{-1} + z^{-2}}\end{aligned}\tag{3}$$

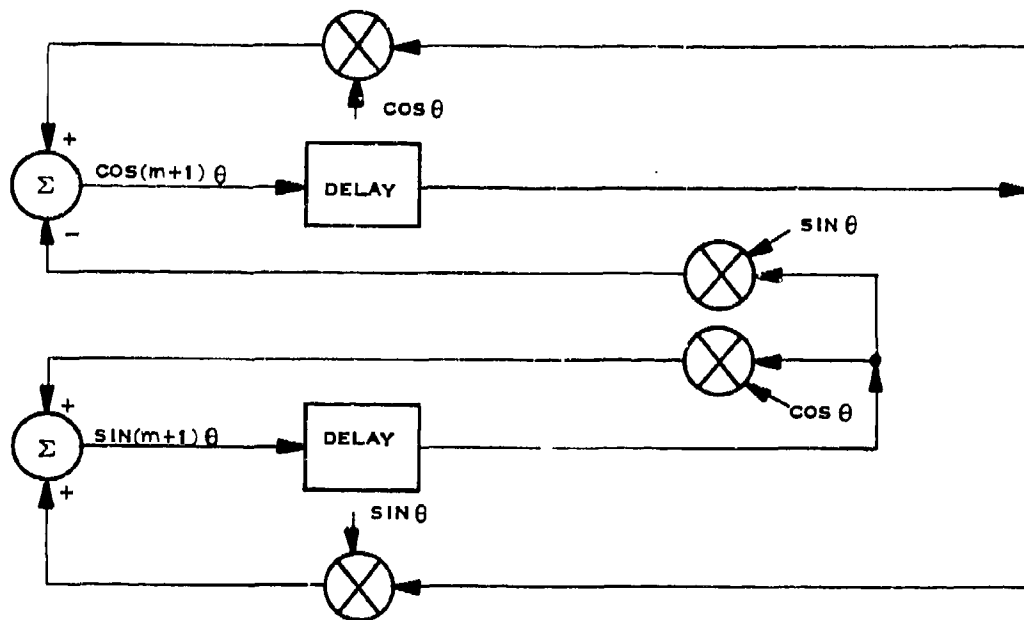


Figure 2-1. Coupled Recursive Digital Oscillator

where  $H_c(z)$  represents a system which outputs a cosine function and  $H_s(z)$  likewise a sine function. The configurations for equation (3) are shown in Figure 2-2.

A method requiring fewer arithmetic operations can be obtained by rearranging the terms of equation (3); e. g. ,

$$H_c(z) = \frac{1}{1 - 2\cos\alpha Tz^{-1} + z^{-2}} (1 - \cos\alpha Tz^{-1}) = H(z) H'_c(z) \quad (4)$$

$$H_s(z) = \frac{1}{1 - 2\cos\alpha Tz^{-1} + z^{-2}} \sin\alpha Tz^{-1} = H(z) H'_s(z)$$

This configuration, shown in Figure 2-3, and the configuration of Figure 2-2 result from the same system function and will have identical outputs. The advantage of the system shown in Figure 2-3 is that it is possible to illuminate the repetitious operations indicated by  $H(z)$ . \*

\*It should be noted, however, that the operations indicated by  $H'_c(z)$  and  $H'_s(z)$  can be eliminated by applying the appropriate initial conditions.

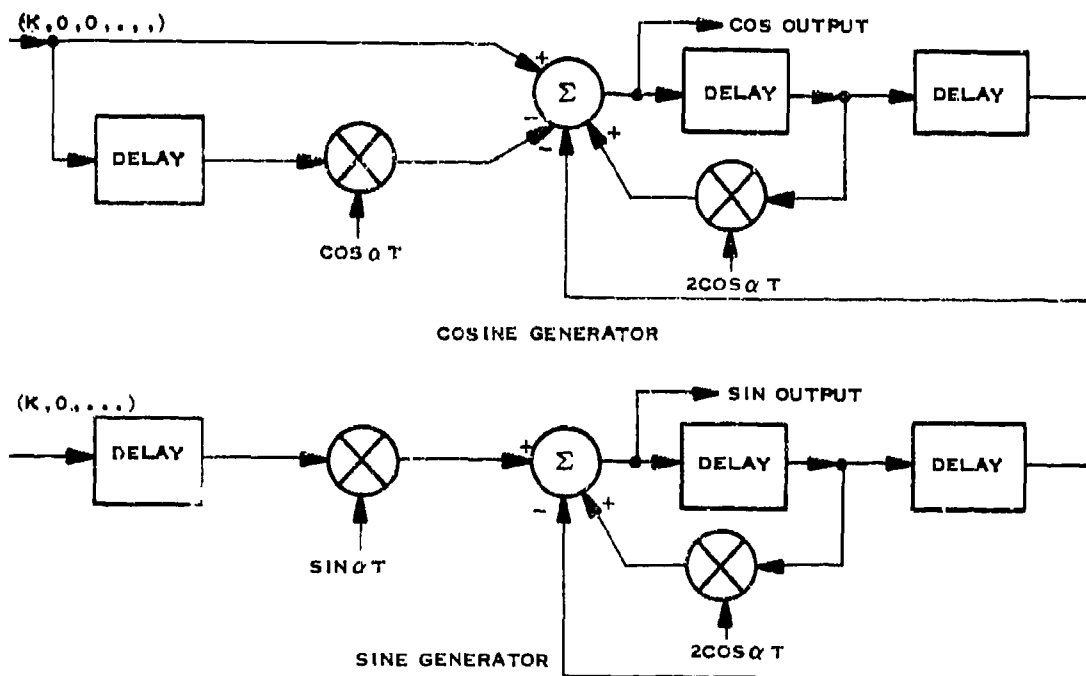


Figure 2-2. Uncoupled Recursive Digital Oscillator

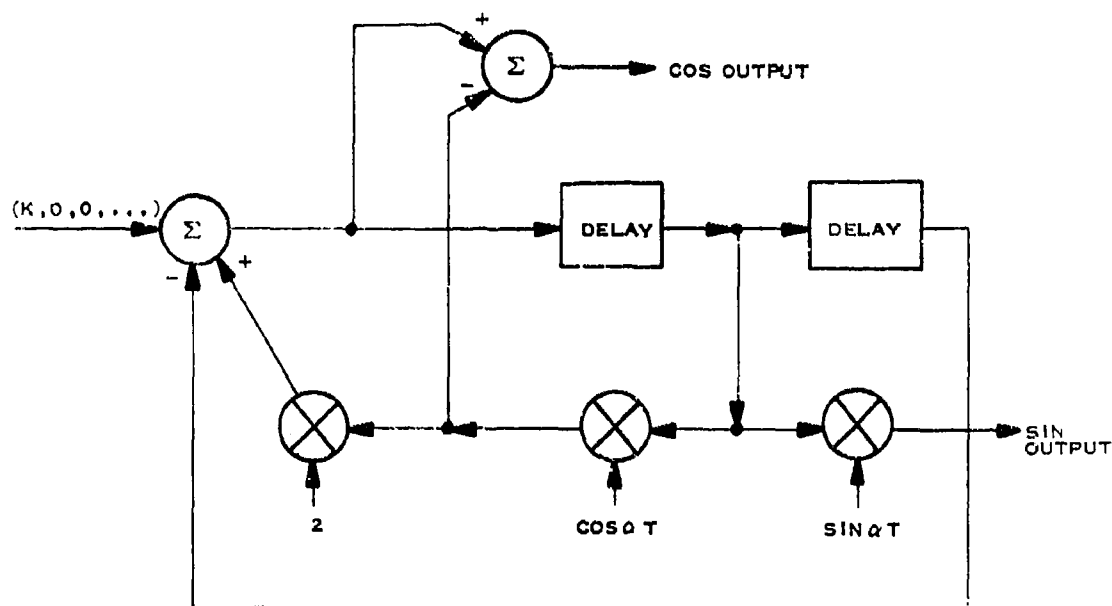


Figure 2-3. Simplified Recursive Digital Oscillator

## 2. ERROR ANALYSIS

When finite word-length computers are used to simulate linear systems (e. g. , digital filters), three types of errors are introduced. They are:

- 1) The error caused by discretization of the system parameters.
- 2) The error caused by analog to digital conversion of the input signal.
- 3) The error caused by roundoff of the results.

Error 1) results in errors in the coefficients of the difference equations and has been shown by Kaiser<sup>4</sup> and Rader and Gold<sup>5</sup> to effectively cause errors in the pole positions of the digital filter (or oscillator). This is an almost intolerable error in a digital oscillator since a digital oscillator is stable only when the poles are exactly on the unit circle. Rader and Gold demonstrated that for poles given by  $z_{1,2} = r \exp(\pm j\theta)$ , the pole position errors are

$$\begin{aligned}\Delta r &\cong \frac{\Delta L}{2r} \\ \Delta \theta &\cong \frac{\Delta L}{2r \tan \theta} - \frac{\Delta K}{2r \sin \theta}\end{aligned}\tag{5}$$

where L and K are the coefficients of the difference equation

$$y(nT) = Ky(nT - T) - Ly(nT - 2T) + x(nT)\tag{6}$$

and  $\Delta L$  and  $\Delta K$  are the respective quantization errors. The errors in pole positions are severe only when  $\theta$  is a small angle. In a digital oscillator this corresponds to the case where the desired output frequency is much smaller than the sampling frequency.

The error 2) has been examined extensively but is of little consequence in a digital oscillator since there is no input.

The error 3) has been shown<sup>2</sup> to be dependent upon the type of representation used to simulate the system. For a coupled system of the type shown in Figure 2-1, the noise variance is shown to be

$$\sigma_n^2 = \frac{E_o^2}{48\epsilon} \left( 1 + \frac{1}{\sin^2 \theta} \right)\tag{7}$$

where  $E_o$  is the digitalization error,  $\theta$  is as previously defined, and  $\epsilon = 1-r$ . Therefore, if  $\theta$  gets small,  $\sigma_n^2$  becomes very large. Likewise as  $r$  approaches 1,  $\sigma_n^2$  becomes infinitely large. For a system of the type in Figure 2-3,

$$\sigma_n^2 = \frac{E_o^2}{48\epsilon} \quad (8)$$

$\sigma_n^2$  is no longer dependent on  $\theta$ , but still becomes unstable for  $r$  equal to 1. This same type analysis was performed for a digital oscillator where  $r$  is equal to 1 with the following result.  $\sigma_n^2$  was found to be

$$\sigma_n^2 = \frac{E_o^2}{12} n \quad (9)$$

where  $n$  is the number of iterations. Therefore, equation (9) indicates that the noise increases linearly with iterations.

To get some indication of the number of samples obtainable before the quantization noise becomes excessive, the signal-to-noise ratio as a function of the number of bits retained and the number of samples obtained is investigated. From equation (9), it can be shown that the output signal-to-noise ratio (SNR) is

$$\text{SNR} = -10 \log_{10} \left\{ \frac{E_o^2}{12} n \right\} \text{ dB} \quad (10)$$

where  $E_o$  is the quantizing level and  $n$  is the number of samples obtained from the oscillator. It should be understood at the outset that the noise here is to be thought of in an ensemble sense; any particular sample may or may not be in error by an amount corresponding to the noise voltage. If it is desired to be sure that the signal output has less than a certain amount of noise disturbance, it will be necessary to be rather conservative in estimating the number of samples obtainable before the noise can exceed the desired level.

Suppose all levels in the oscillator are to be represented by 8-bit binary numbers. Then  $E_o = 1/256$  and

$$\text{SNR} = 59 - 10 \log_{10} n \text{ dB}$$

or (11)

$$n = 10^{\frac{59 - \text{SNR}}{10}}$$

Table I shows the maximum number of samples obtainable before the expected noise degradation will exceed certain levels.

Table I. Number of Output Samples Obtainable For A Desired SNR

Output SNR (dB)	Number of Samples for Oscillator of Figure 2-3	Number of Samples for Oscillator of Figure 2-1 $\alpha T = 45^\circ$
50	8	4
40	79	40
30	790	395
20	7,900	3,950
10	79,000	39,500
0	790,000	395,000

All noise caused by quantizing to 8 bits.

### 3. ERROR CORRECTION TECHNIQUES

The use of an auxiliary storage device to hold the digits which are discarded in computational quantization reduces the error caused by the iterative computations. In essence, this method, diagrammed in Figure 2-4, utilizes a digital filter, the input to which is the sequence of discarded digits obtained from the quantizer Q, and the output from which is an error correction term to be added to the regular output of the digital oscillator.

The expression in the z-domain for the quantizing error may be shown to be

$$E(z) = \frac{Q(z)}{1 + \sum_{j=1}^N b_j z^{-j}} \quad (12)$$

where  $E(z)$  is the z-transform of the error in the oscillator output due to quantizing,  $Q(z)$  is the z-transform of the quantizing error sequence itself, and the  $b_j$  are the coefficients of the denominator polynomial of  $H(z)$ , the system transfer function, given by equation (4) for example. This equation can be expressed in a nonrecursive form yielding

$$e(nT) = \sum_{j=0}^{\infty} C_j q(nT - jT) \quad (13)$$

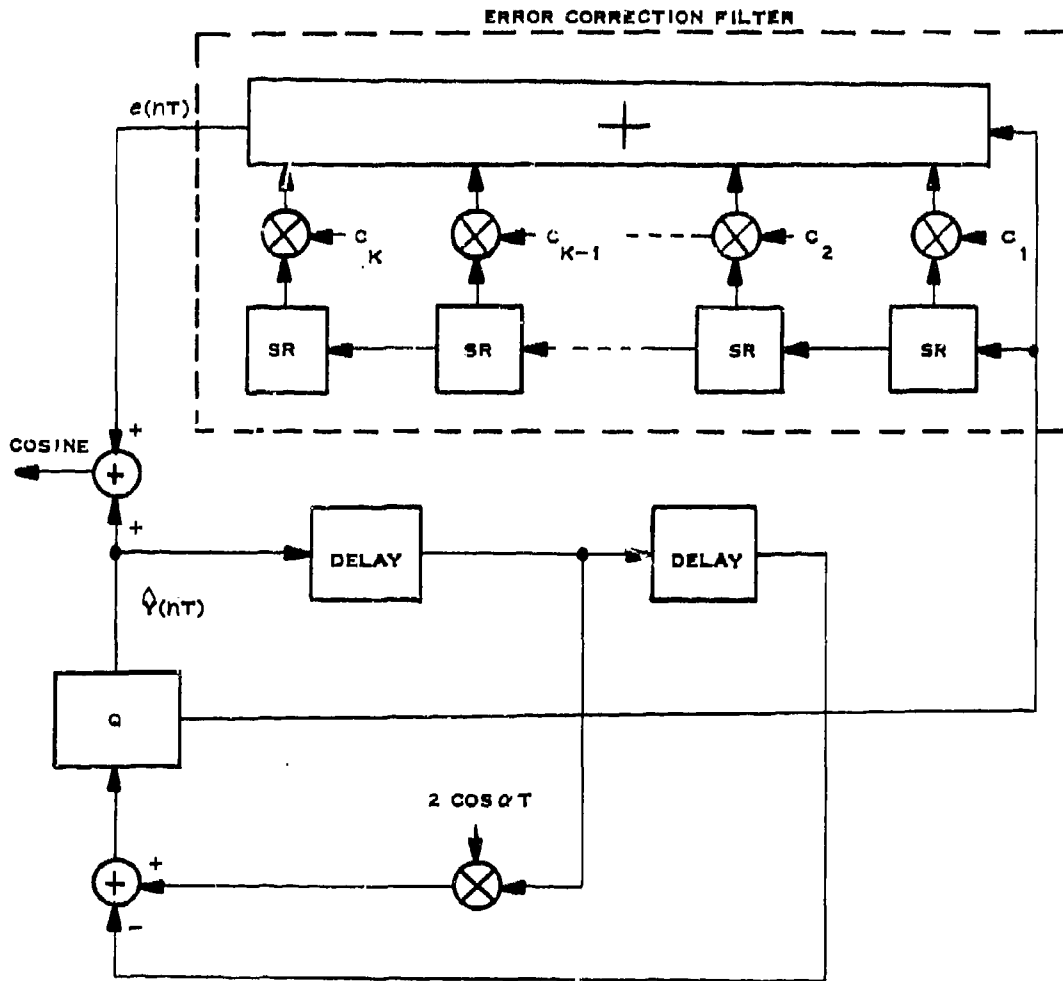


Figure 2-4. Error Correction Filter Applied to Cosine Generator

where the  $C_j$ 's may be found

$$C_0 = 1, \quad C_j = \sum_{l=1}^N b_l C_{j-l} \quad (14)$$

Theoretically, the filter must have a number of storage elements equal to the number of samples to be obtained from the digital oscillator during one run. If the digital oscillator must produce very many samples in one run then the error correction filter may be impractically large.

When this same technique is applied to digital filters to aid in the correction of quantization errors, it is found that the coefficients of the correction filter form a sequence which converges to zero. Thus, it is necessary to store only a certain number of the most recent quantization error values because the correction filter has, for all practical purposes, a finite memory. Unfortunately, this is not the case for unstable filters or oscillators except for special cases. The number of memory stages of the error correction filter necessary to achieve a desired degree of accuracy depends on the relationship of the sampling frequency to the oscillator frequency as well as the quantizing level.

Another technique for reducing the effects of noise from all sources is to periodically restart the oscillator from a point where the conditions are known a priori very accurately. For example, if it is known that the  $k$ th sample output from the oscillator should correspond to the point on the sine wave of  $\sin 2\pi n=0$ , then the oscillator may be restarted at the  $k$ th sample time with the known initial condition.

For example, if  $T$  is the sampling period and  $T_0$  is the oscillator period; both expressed to some finite number of bits, then  $T/T_0$  is a rational number which may be expressed as the ratio of two integers simply by moving the decimal (or binary) point to the right in both  $T$  and  $T_0$  the same number of places. Suppose

$$\frac{T}{T_0} = \frac{a}{b} \quad (15)$$

where  $a$  and  $b$  are both integers. Then  $bT = aT_0$  and it is readily seen that the  $b$ th sample time will correspond exactly to a multiple of the oscillator time period. The oscillator may then be reset to its initial conditions at the  $b$ th sample time to remove any previously built-up error without incurring a phase error because of the correction procedure itself. The smallest number  $b$ , corresponding to the shortest possible time interval between resets, may be found by making  $a$  and  $b$  relatively prime by extracting their greatest common multiple by means of a simple algorithm. An additional technique for error correction takes advantage of the trigonometric relationship between a sine value and cosine value sampled at the same instant, i. e.,

$$\sin^2 \theta + \cos^2 \theta = 1 \quad (16)$$

At any iteration this relationship must hold, and any fluctuation is an indication of amplitude error. The pole locations are fixed (quantized but fixed), therefore the frequency is fixed. The amplitude of the oscillator pair may therefore be adjusted by the scale factor.

$$\text{SCALE} = \frac{1}{\sqrt{\sin^2 \theta + \cos^2 \theta}} \quad (17)$$

The inherent disadvantages of this scheme, however, make it very impractical to use. The scale value itself is a very difficult computation to be performed in real-time, or even near real-time. Also the scale value corrects amplitude variations, but not phase errors which also tend to vary widely as more iterations are performed.

## B. NONRECURSIVE DIGITAL OSCILLATOR

### 1. GENERAL

The nonrecursive digital oscillator algorithm generates sampled approximations to a continuous sinusoid by selectively reading points from a read-only-memory (ROM). The approximations are generated as follows.

Let  $y(t)$  represent a continuous sinusoid of frequency  $f_0$ , e. g.,

$$y(t) = \cos 2\pi f_0 t \quad (18)$$

when expressed discretely,  $y(t)$  becomes

$$\begin{aligned} y(n\Delta T) &= \cos 2\pi n f_0 \Delta T & n = 0, 1, \dots \\ &= \cos 2\pi n f_0 / f_s \end{aligned} \quad (19)$$

where  $f_s$ , the sample frequency, is at least twice  $f_0$ . The ratio  $f_0/f_s$  defines some incremental step or arc around the phase circle, where the phase circle is depicted in Figure 2-5. The quantity  $nf_0/f_s$  represents a complete history of the steps taken around the phase circle. Assume now that the phase circle is discretized into  $M$  equally spaced intervals (where  $M$  is 16 in Figure 2-5), with a sinusoidal value stored in an ROM for each interval. For example the value  $\cos(0)$  would be stored in position (0000) of the ROM; similarly  $\cos(2\pi/M) = \cos(\pi/8)$  in position (0001). There are therefore  $M$  distinct sinusoidal values stored in the ROM.\*

An exact representation for  $y(n\Delta T)$  is obtained only when an infinite number of sample values are stored in a ROM. This is obviously an impossibility. Therefore, once an  $M$  is selected, all arguments for  $y(n\Delta T)$  (i. e.,  $2\pi n f_0 / f_s$ ) lying in an interval are approximated by the argument for that interval, where

---

\*The storage requirement is somewhat simplified since only one quadrant of the sinusoid is unique, therefore requiring only  $M/4$  distinct values in the ROM.

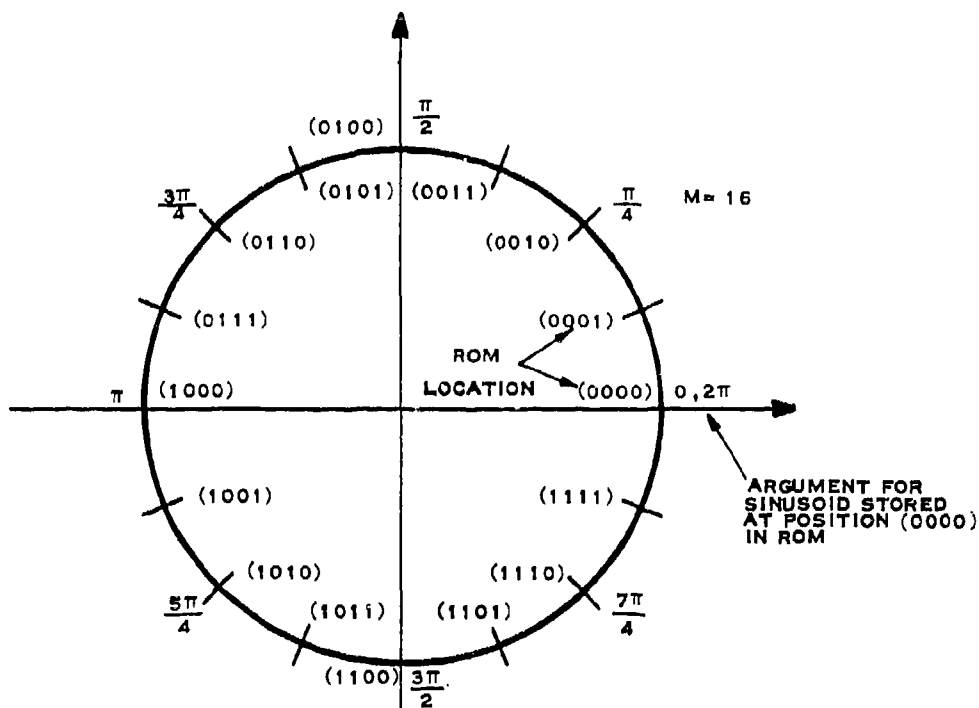


Figure 2-5. Phase Circle

now the arguments  $2\pi n f_0 / f_B$  are constrained to be always in the interval 0 to  $2\pi$ . (This is accomplished simply by performing modulo 1 addition for the quantity  $n f_0 / f_B$ .) The ROM position containing the stored sinusoidal value for a particular interval is obtained by truncating the product  $M n f_0 / f_B$ . Since  $n f_0 / f_B$  is modulo 1, the quantity  $M n f_0 / f_B$  is modulo  $M$ . The truncation ensures only integer values of the product since there are only integer positions in the ROM.

The sinusoidal value extracted from the ROM for a particular  $n$  is therefore given by:

$$\hat{y}(n\Delta T) = \cos \frac{2\pi}{M} [M n f_0 / f_B] \quad (20)$$

where  $\hat{y}$  denotes the estimate of  $y$  and the brackets indicate truncation and modulo  $M$  addition. The quantity  $2\pi/M$  defines the basic phase increments around the phase circle. The product  $2\pi/M [M n f_0 / f_B]$  therefore represents the argument for the sinusoidal value stored at the  $[M n f_0 / f_B]$  position in the ROM.

## 2. FOURIER ANALYSIS

A continuous sinusoid of frequency  $f_0$  has a frequency spectrum composed of two impulses, one at  $-f_0$  and one at  $+f_0$ . The spectrum of a digital oscillator should be the same. Fourier analysis is a tool for comparing the frequency response of the nonrecursive digital oscillator estimate  $\hat{y}(n\Delta T)$  to the ideal spectrum.

The output of the digital oscillator is assumed to be representable as a series of impulse functions of period  $T$ , each impulse having as its magnitude the value of the oscillator at that sample time; i. e. ,

$$y(t) = \sum_{j=0}^{K-1} \cos \frac{2\pi}{M} [Mj f_0 / f_s] \delta(t - j\Delta T) \quad (21)$$

where  $\delta$  is the Kronecker Delta,  $\Delta T$  is the sample interval, and  $K$  is some integer such that  $Kf_0/f_s$  is an integer. The selection of  $K$  ensures that the output  $y(t)$  is periodic in  $T$ .

Using the usual definitions of the Fourier coefficients  $a_n$ ,  $b_n$ , and  $a_0$ ,

$$\begin{aligned} a_n &= \frac{1}{T} \int_0^T y(t) \cos \frac{2\pi n t}{T} dt \\ b_n &= \frac{1}{T} \int_0^T y(t) \sin \frac{2\pi n t}{T} dt \\ a_0 &= \frac{1}{T} \int_0^T y(t) dt \end{aligned} \quad (22)$$

and inserting  $y(t)$  from equation (21),  $a_n$ ,  $b_n$ , and  $a_0$  become:

$$\begin{aligned} a_n &= \frac{1}{T} \int_0^T \sum_{j=0}^{K-1} \cos \frac{2\pi}{M} [Mj f_0 / f_s] \delta(t - j\Delta T) \cos \frac{2\pi n t}{T} dt \\ &= \frac{1}{T} \sum_{j=0}^{K-1} \cos \frac{2\pi}{M} [Mj f_0 / f_s] \cos \frac{2\pi n j \Delta T}{T} \end{aligned} \quad (23)$$

$$\begin{aligned}
b_n &= \frac{1}{T} \int_0^T \sum_{j=0}^{K-1} \cos \frac{2\pi}{M} [Mj f_o / f_s] \delta(t - j\Delta T) \sin \frac{2\pi n t}{T} dt \\
&= \frac{1}{T} \sum_{j=0}^{K-1} \cos \frac{2\pi}{M} [Mj f_o / f_s] \sin \frac{2\pi n j \Delta T}{T} \\
a_o &= \frac{1}{T} \int_0^T \sum_{j=0}^{K-1} \cos \frac{2\pi}{M} [Mj f_o / f_s] \delta(t - j\Delta T) dt \\
&= \frac{1}{T} \sum_{j=0}^{K-1} \cos \frac{2\pi}{M} [Mj f_o / f_s]
\end{aligned} \tag{23}$$

The spectral components are obtained as

$$S_n = (a_n^2 + b_n^2)^{1/2}$$

This analysis has been performed for various  $f_o/f_s$  ratios with a fixed  $M$  of 256. Spectral plots for the ratios 1/11.2, 1/17.3, and 1/22.5 are shown in Figures 2-6, 2-7, and 2-8, respectively. The horizontal scale is normalized frequency; the vertical is normalized to 0 dB. The sidelobes for the three cases are down at least 47 dB from the fundamental.

### 3. ERROR ANALYSIS

The truncation in the model for  $y(n\Delta T)$  obviously causes errors in the approximation to  $y(n\Delta T)$ . An upper bound may be placed on this error as follows: Let  $\epsilon$  represent the error introduced by the truncation; i. e.,

$$2\pi n f_o / f_s - \frac{2\pi}{M} [Mn f_o / f_s] = \epsilon$$

or

$$2\pi n f_o / f_s = \frac{2\pi}{M} [Mn f_o / f_s] + \epsilon$$

Taking the sine of both sides

$$\begin{aligned}
\sin 2\pi n f_o / f_s &= \sin \left\{ \frac{2\pi}{M} [Mn f_o / f_s] + \epsilon \right\} \\
&= \sin \frac{2\pi}{M} [Mn f_o / f_s] \cos \epsilon + \cos \frac{2\pi}{M} [Mn f_o / f_s] \sin \epsilon
\end{aligned} \tag{25}$$

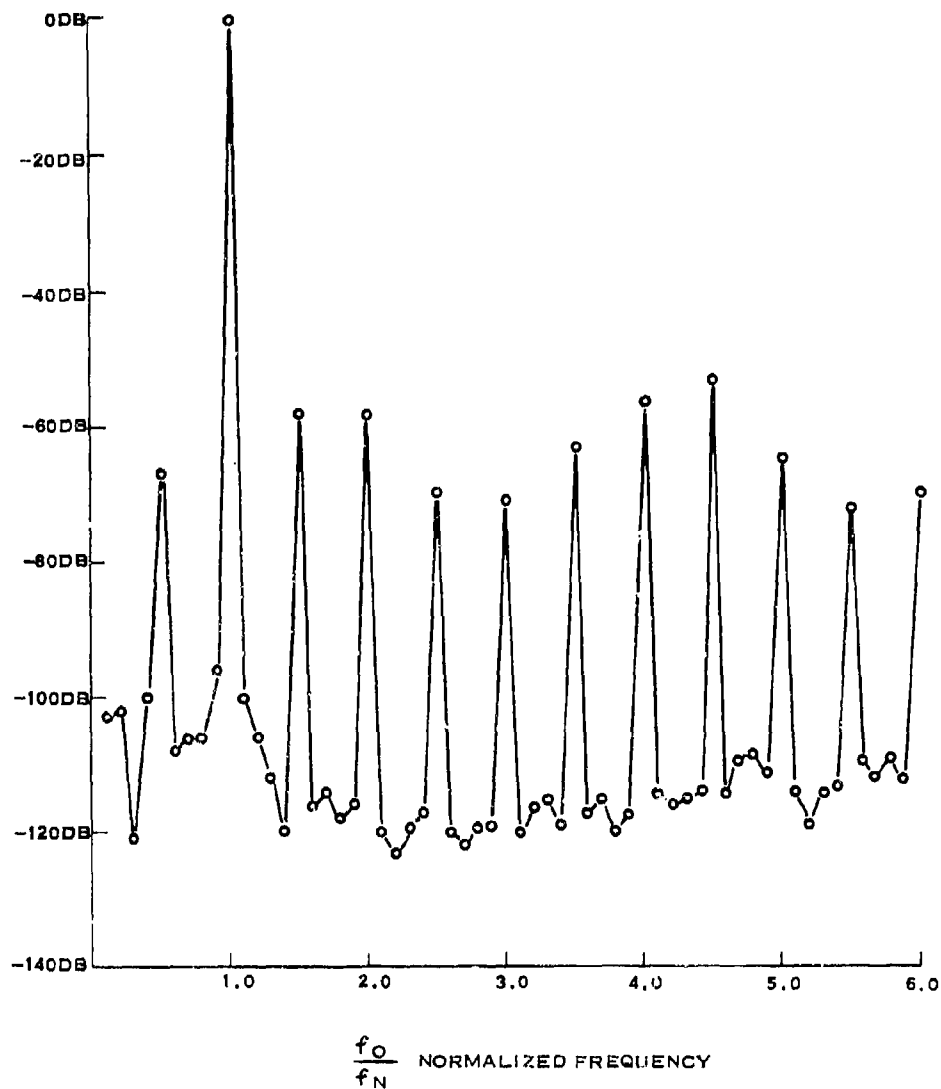


Figure 2-6. Spectral Analysis for  $f_0/f_s$  Ratio of 1/11.2

Using the phase circle of Figure 2-5, the maximum error  $\epsilon_{\max}$  for a particular  $M$  is

$$\epsilon_{\max} = \frac{2\pi}{M} \quad (26)$$

since the truncation can never result in an error of more than one interval. For large values of  $M$ , ( $M \geq 64$ ),  $\cos(2\pi/M)$  becomes very close to one. Using this approximation,

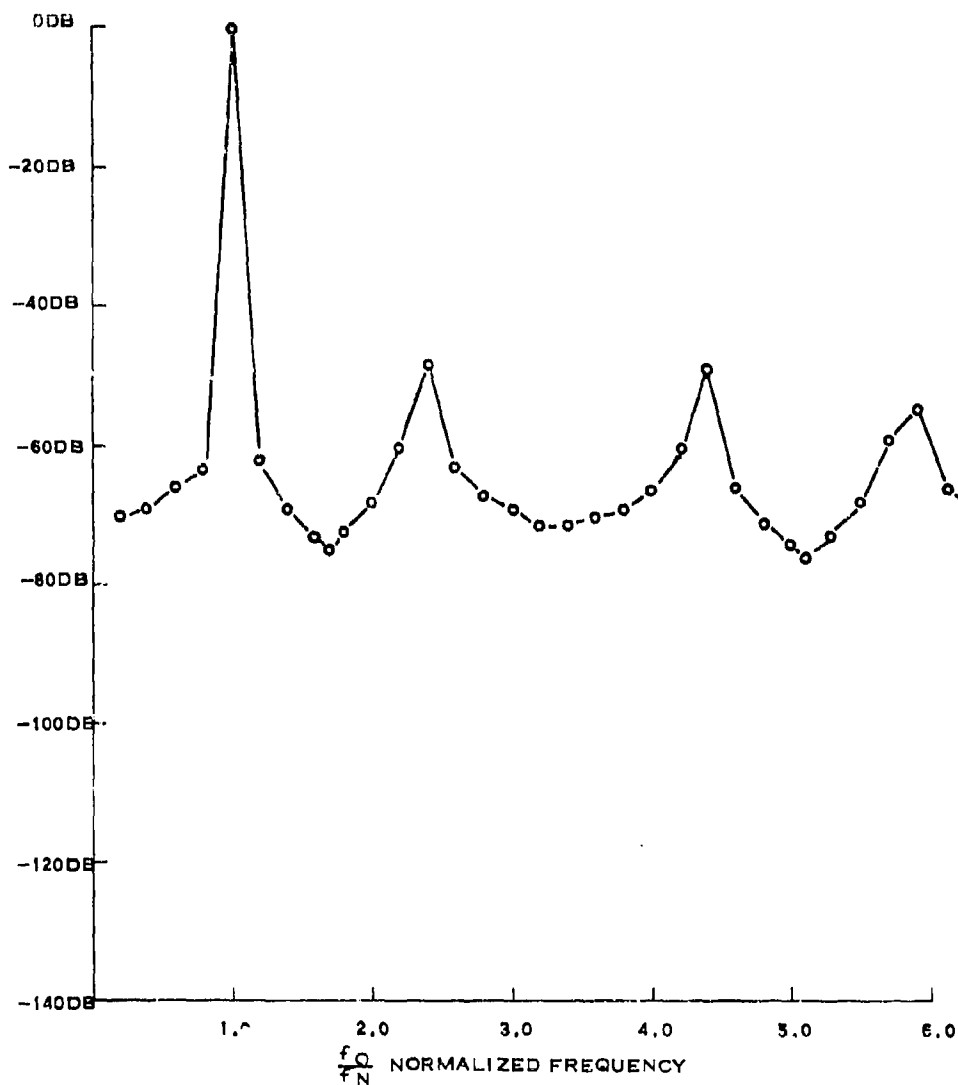


Figure 2-7. Spectral Analysis for  $f_0/f_s$  Ratio of 1/17.3

$$\sin 2\pi n f_0 / f_s - \sin \frac{2\pi}{M} [M n f_0 / f_s] = \cos \frac{2\pi}{M} [M n f_0 / f_s] \sin \epsilon_{\max} \quad (27)$$

The upper bound on the output error is obtained by realizing that  $\cos 2\pi/M[M n f_0 / f_s]$  has a maximum value of one. This results in

$$\left| \sin 2\pi n f_0 / f_s - \sin \frac{2\pi}{M} [M n f_0 / f_s] \right| \leq \sin \epsilon_{\max} \cong \epsilon_{\max} \quad (28)$$

since for small  $\epsilon_{\max}$ ,  $\sin \epsilon_{\max} \cong \epsilon_{\max}$ .

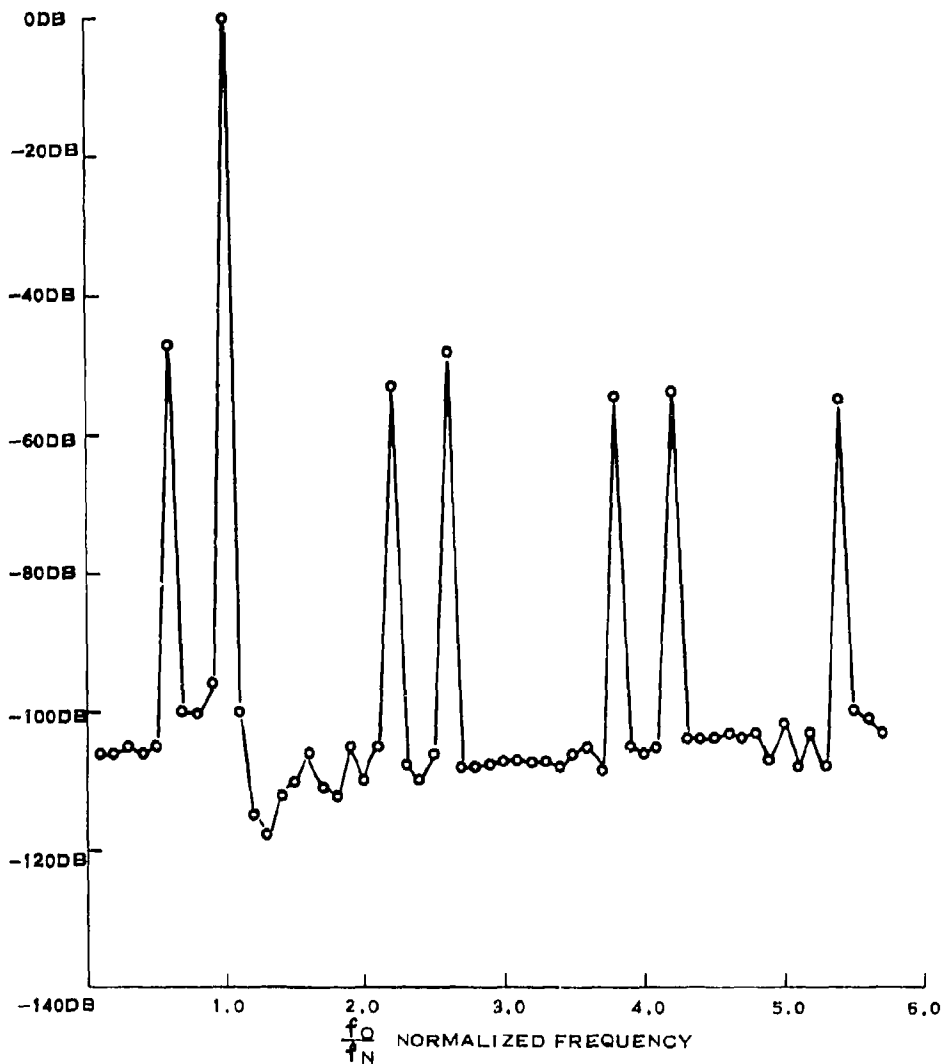


Figure 2-8. Spectral Analysis for  $f_0/s$  Ratio of  $1/22.5$

Therefore, the absolute error in amplitude is bounded by the size of the unit intervals around the phase circle (for large  $M$ ). For the case of  $M = 256$ , the maximum error is  $2\pi/M = 2\pi/256 = 0.0245$ , or 2.45 percent as a maximum.

SECTION III  
APPLICATION OF DIGITAL OSCILLATORS

A. INTRODUCTION

Table II presents the two basic configurations in which a digital oscillator can best function, frequency synthesizers and voltage controlled oscillator (VCO) replacements. A comparison is made between the two implementation techniques, recursive and nonrecursive, with pertinent comments included for each configuration.

Table II. Digital Oscillator Applications

Application Area	Comments
1. Frequency Synthesizers	
a) Nonrecursive	ROM and arithmetic unit limits speed to 10 MHz and below, but relatively inexpensive to build  Shift register technique limited to 100 MHz, and has very high power requirement
b) Recursive	Pipeline techniques allow synthesis to 7 MHz  Necessary arithmetic units expensive and have high power consumption  Error correction a must  Cost approximately twice that of non-recursive synthesizer - not including error correction
2. VCO Replacement	
a) Nonrecursive	Hardware requirements the same as those for frequency synthesizers  Constant phase throughout frequency band  Instantaneous frequency variation with no transient response

Table II. Digital Oscillator Applications (Continued)

Application Area	Comments
2. VCO Replacement (Cont'd)  b) Recursive	Hardware requirements same  Constant phase  Error correction unnecessary in locked loops  Requires calculation of coefficients of difference equation for each frequency change

In frequency synthesizer applications, e. g., conventional frequency synthesizers and frequency translators, synthesis above 1 MHz is possible with either technique, but there are basic cost differentials and differences in complexity.

For the VCO replacement applications, e. g., frequency modulation and tracking loops, there is no change in the logic configuration for the nonrecursive technique. However, the recursive technique requires constant modification of the coefficients of the difference equations describing the output; these modifications effect the necessary frequency change seen at the output when operating as a VCO. Another arithmetic unit must be included to provide the coefficients for each new frequency; this additional unit implies even more complexity for the recursive technique.

The problems encountered when implementing the recursive digital oscillator, problems such as necessary error correction and computation of difference equation coefficients for variable frequency applications, have led to the elimination of the technique from consideration as an efficient useful digital oscillator implementation procedure. Therefore, all applications discussed in this section use nonrecursive digital oscillator configurations. These applications include digitalized phase-locked loops, discrete Fourier transformations, synchronization, and a new technique, the recursive nonlinear demodulator, called RNLD. A complete derivation of the RNLD, including the solution of the filtering and estimation equations, is contained in Appendix B. The recursive nonlinear equations and simulation results are presented in this section.

## B. DIGITALIZED PHASE-LOCKED LOOPS

### 1. INTRODUCTION

Phase-locked loops have been discussed extensively by Viterbi<sup>6</sup> and by Gardner<sup>7</sup>; digitalized phase-locked loops by Larimore.<sup>8</sup> This section examines the possibility of using in-phase and quadrature sampling techniques<sup>9</sup> coupled with a digital oscillator in a digital phase-locked loop. A second order loop was designed as an example. The basic linearized phase-locked loop block diagram is shown in Figure 3-1.

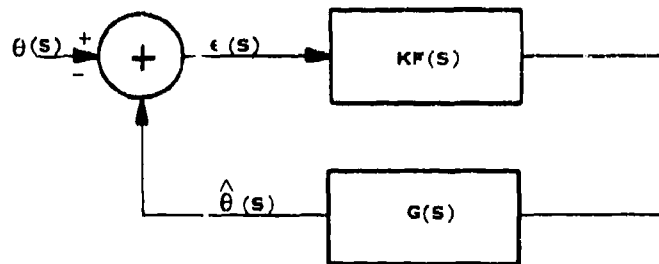


Figure 3-1. Linearized Phase-Locked Loop Block Diagram

This loop has a transfer function given by:

$$H(s) = \frac{\hat{\theta}(s)}{\theta(s)} = \frac{KF(s) G(s)}{1 + KF(s) G(s)} \quad (29)$$

Viterbi<sup>6</sup> shows that for a perfect second order phase-locked loop,  $F(s)$  is given by:

$$F(s) = 1 + \frac{a}{s} \quad (30)$$

which is simply a direct connection and an integrator with gain  $a$ .  $G(s)$  is similarly given as:

$$G(s) = \frac{1}{s} \quad (31)$$

a simple integrator.

Substituting equations (30) and (31) into (29) results in the following transfer function:

$$H(s) = \frac{K(s + a)}{s^2 + Ks + aK} \quad (32)$$

Comparing this transfer function to the general expression for a second order system, given by

$$H(s) = \frac{2\zeta\omega_n s + \omega_n^2}{s^2 + 2\zeta\omega_n s + \omega_n^2} \quad (33)$$

allows one to express K and a as functions of the damping ratio  $\zeta$  and the natural frequency  $\omega_n$ . These expressions are:

$$\begin{aligned} K &= 2\zeta\omega_n \\ a &= \frac{\omega_n}{2\zeta} \end{aligned} \quad (34)$$

## 2. DIGITALIZED LOOP

The digital form of H(s), H(z), given by

$$H(z) = \frac{KF(z)G(z)}{1 + KF(z)G(z)} \quad (35)$$

is obtained by direct digitalization of F(s) and G(s). These transfer functions become:<sup>10</sup>

$$F(z) = 1 + \frac{aTz}{z - 1}$$

$$G(z) = \frac{Tz}{z - 1}$$

where T is the sample time increment.

The block diagram for the direct digitalized loop now becomes as shown in Figure 3-2 with an overall transfer function given by:

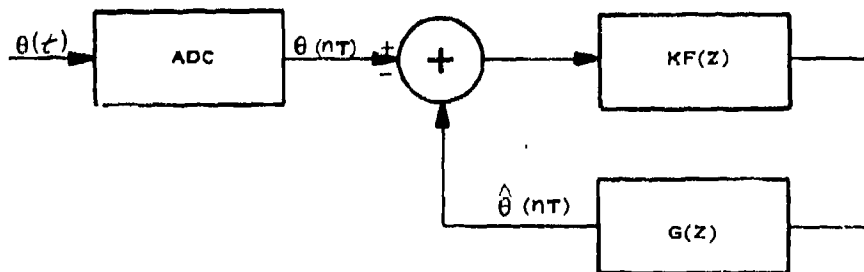


Figure 3-2. Linearized Digital Phase-Locked Loop

$$H(z) = \frac{\hat{\theta}(z)}{\theta(z)} = \frac{KT}{1 + KT(1 + aT)} \cdot \frac{(1 + aT)z^2 - z}{z^2 - z \frac{(2 + KT)}{[1 + KT(1 + aT)]} + \frac{1}{[1 + KT(1 + aT)]}}$$

In the linearized continuous loop, the error  $\epsilon$  is approximated by:

$$\epsilon(t) = \theta(t) - \hat{\theta}(t)$$

when  $\theta(t) - \hat{\theta}(t)$  is small. For small error  $\theta(nT)$ ,

$$\begin{aligned} \epsilon(nT) &= \theta(nT) - \hat{\theta}(nT) \cong \sin[\theta(nT) - \hat{\theta}(nT)] \\ &= \sin \theta(nT) \cos \hat{\theta}(nT) - \cos \theta(nT) \sin \hat{\theta}(nT) \end{aligned}$$

The in-phase and quadrature components of the carrier,  $\cos \theta(nT)$  and  $\sin \theta(nT)$ , respectively, can be obtained by applying quadrature sampling techniques. These techniques are discussed in Appendix A. The  $\sin \hat{\theta}(nT)$  and  $\cos \hat{\theta}(nT)$  estimates are supplied by a digital oscillator.

An overall block diagram for the digitalized phase-locked loop using quadrature sampling and a digital oscillator is shown in Figure 3-3.

### C. RECURSIVE NONLINEAR DEMODULATOR (RNLD)\*

#### 1. INTRODUCTION

Another FM demodulator application of the digital oscillator was investigated during the study effort. It is a near optimum digitalized FM demodulator

\*A Patent disclosure has been submitted by Texas Instruments on the Recursive Nonlinear Demodulator.

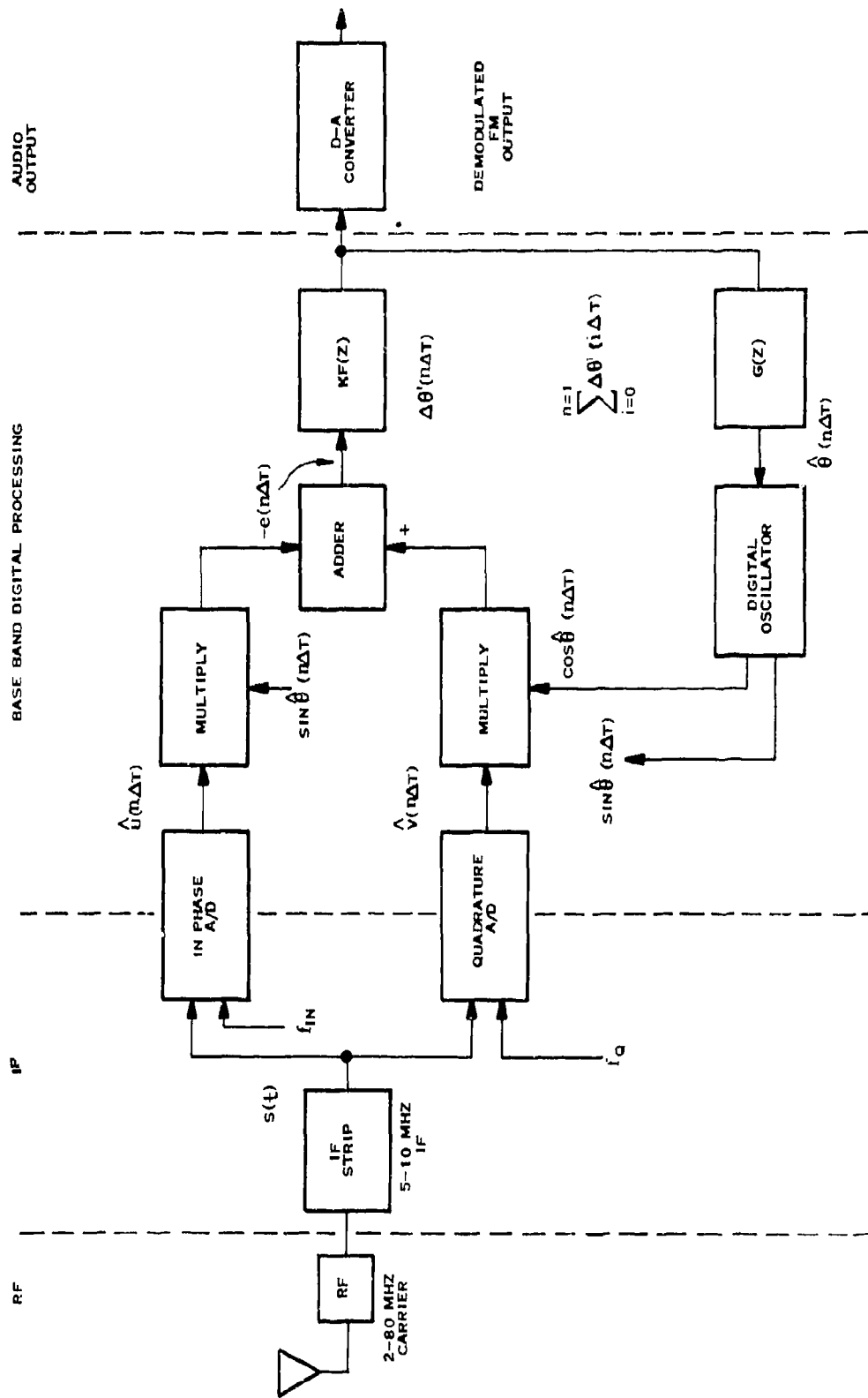


Figure 3-3. Digitalized Phase-Locked Loop Block Diagram

derived from Bayesian estimation and optimal control techniques. It is recursive in that its next output is calculated from its previous value plus weighted samples of the present input signal. In-phase and quadrature sampling techniques (described in Appendix A) are employed to reduce the received narrow-band RF to baseband samples. These samples are then processed to provide the estimate of the original FM modulating signal. Part of the processing algorithm consists of a recursive nonlinear time-varying gain calculation; hence, the name Recursive Nonlinear Demodulator (RNLD). Since it is a digitalized demodulator that also provides threshold extension, it is a natural candidate for future digitalized tactical radios. For example, it will be compatible with present in-the-field tactical VHF/FM radios, i. e., it will operate with standard FM radios, but because of its threshold extension capability, it will provide extended operating range.

In this subsection, the RNLD is discussed in rather general terms. A concise derivation of the demodulator is presented in Appendix B.

## 2. RNLD SYNTHESIS

A block diagram model of the classical FM modulator and demodulator used in the RNLD synthesis is illustrated in Figure 3-4. The input to the FM modulator is  $u(t)$ , a random process. In the synthesis,  $u(t)$  is assumed to be a white gaussian process. This input  $u(t)$  is passed through a linear filter whose output,  $cx(t)$ , represents the weighed modulating signal or the weighted speech process in voice communications. The time varying portion of the output,  $x(t)$ , is the random process and "c" is the so-called frequency derivation in reference to classical FM discussions. The output,  $s(t)$ , of the modulator is given by:

$$s(t) = \sqrt{2} a \cos \left( \omega_0 t + \int_0^t cx(u) du \right) \quad (37)$$

where "a" is the rms value of the carrier of frequency,  $\omega_0$ . Noise is added to  $s(t)$  and this combined signal is supplied to the demodulator. This signal is in-phase and quadrature sampled obtaining two sampled words per sample period,  $z_1$  and  $z_2$ . A discussion of in-phase and quadrature sampling and its applications to narrowband FM processes is given in Appendix A. The output of the estimator or demodulator,  $\hat{x}(t)$ , is the time-varying maximum a posteriori (MAP) estimate of the original signal  $x(t)$ .

An equivalent baseband FM process for this FM carrier process is shown in Figure 3-5. The in-phase and quadrature sampling permits a translation from carrier to baseband representation. Notice that a constant term,  $2\pi\Delta f$ , is added to the modulating signal  $cx(t)$ . This term represents the unavoidable

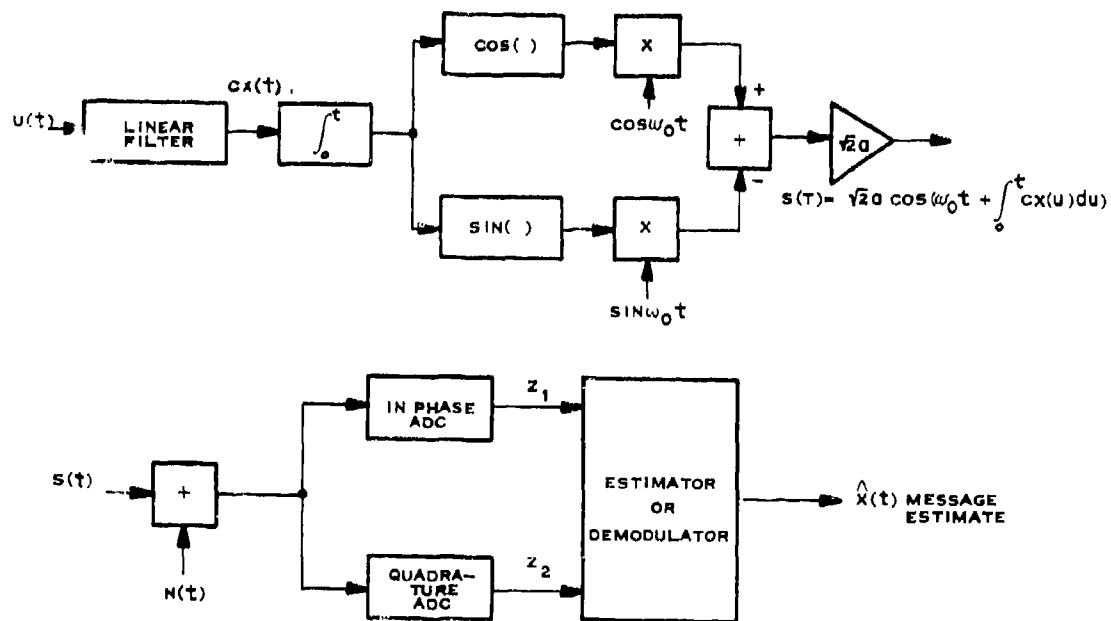


Figure 3-4. Block Diagram for Modulator and Demodulator for an FM Process

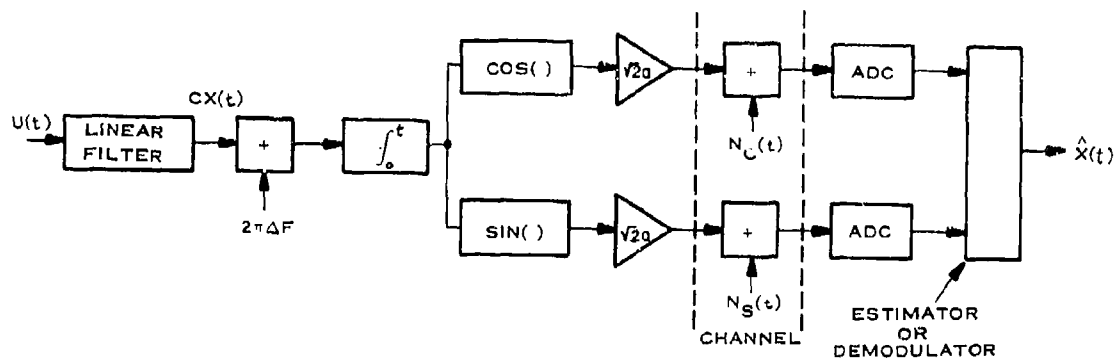


Figure 3-5. Block Diagram for Equivalent Baseband FM Process

frequency uncertainty that exist between the transmitter and receiver frequencies for typical FM links. This frequency uncertainty will be reflected in the observed samples at the receiver and its removal becomes part of the estimator's task.

The linear filter at the modulator is usually referred to as the message filter or filter message model. As part of the synthesis procedure, the modulator is modeled by a state variable representation. This idea is illustrated in Figures 3-6 through 3-8. In Figure 3-6, a single pole RC filter is shown in its state-variable representation. Figure 3-7 shows the model for the FM process using the output,  $x(t)$ , of this filter as the input to the FM process. The complete model for the FM process is shown in Figure 3-8 where the vector differential equations are also given. This same idea can obviously be extended to a multiple pole message filter.

The message model system equation is the linear vector differential equation

$$\dot{Y}(t) = AY(t) + U(t) \quad (38)$$

This equation has a unique solution. <sup>11</sup>

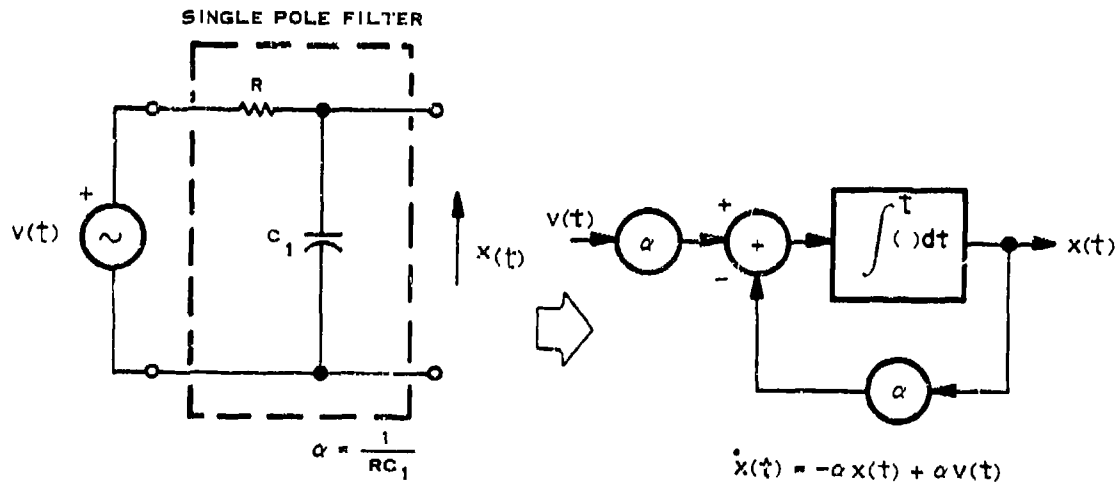


Figure 3-6. Single Pole Message Model.

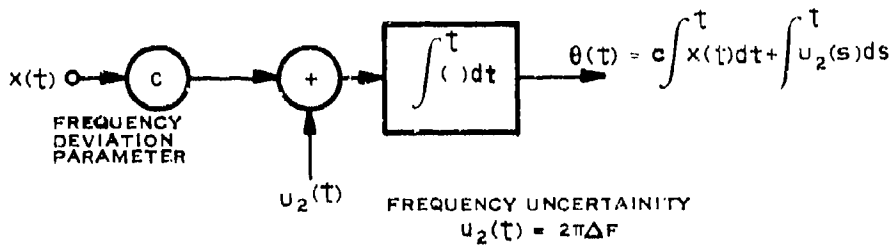
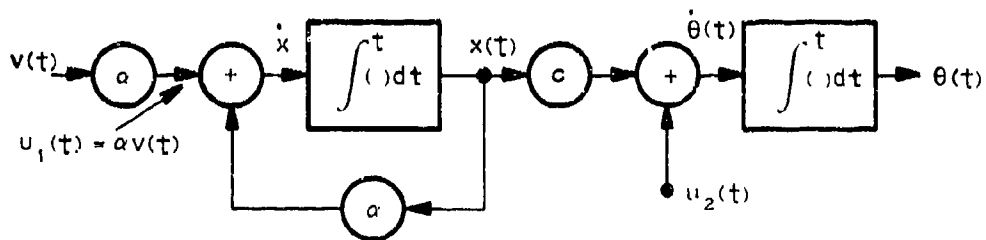


Figure 3-7. Model for FM



$$\begin{pmatrix} \dot{x}(t) \\ \dot{\theta}(t) \end{pmatrix} = \begin{pmatrix} -\alpha & 0 \\ c & 0 \end{pmatrix} \begin{pmatrix} x(t) \\ \theta(t) \end{pmatrix} + \begin{pmatrix} u_1(t) \\ u_2(t) \end{pmatrix}$$

$2 \times 1$  VECTOR  $\dot{Y}(t) = A Y(t) + U(t)$   
 SCALAR  $\theta(t) = \Gamma^T Y(t); \quad \Gamma^T = (0, 1)$   
 $(0, 1) \begin{pmatrix} x(t) \\ \theta(t) \end{pmatrix} = \theta(t)$

Figure 3-8. Continuous State Variable Representation of FM Process

---


$$Y(t) = \Phi(t, t_0) Y(t_0) + \int_{t_0}^t \Phi(t, \tau) U(\tau) d\tau \quad (39)$$

where  $\Phi(t, t_0)$  is the system transition matrix. For linear time-invariant systems,

$$\Phi(t, \tau) = e^{A(t-\tau)} \quad (40)$$

It is shown in Appendix B that the discrete difference equation for FM using the single-pole filter is:

$$Y(k+1) = \Phi Y(k) + w(k) \quad (41)$$

where:

$$\Phi = \begin{bmatrix} e^{-\alpha T} & 0 \\ \frac{c}{\alpha} (1 - e^{-\alpha T}) & 1 \end{bmatrix} \quad (42)$$

$$w(k) = T U(k)$$

$T$  = the sample interval

The equivalent discrete baseband modulator is shown in Figure 3-9 for a general multiple pole filter. The input to the demodulator  $Z(k)$  is a  $2 \times 1$  vector where the equations are also shown in Figure 3-9. This model provides the necessary characterization to synthesize the RNLD.

The algorithm for estimating the original sampled message  $x(k)$  is given by:

$$\hat{x}(k) = S^T \hat{Y}(k) \quad (43)$$

where  $S^T = (1, 0)$ . The recursive algorithm for obtaining  $\hat{Y}(k)$  for inphase and quadrature sampling in white noise is given by a set of coupled recursive equations. These equations are:

$$\begin{aligned} \hat{Y}(k+1) &= \Phi \hat{Y}(k) - \frac{\sqrt{2a}}{\sigma_n^2} P(k+1) \Gamma \{z_1(k+1) \sin \hat{\theta}(k) + z_2(k+1) \cdot \\ &\quad \cos \hat{\theta}(k)\} \\ P(k+1) &= [\Phi P(k) + Q \Phi^{-T}] \left\{ \left[ \Phi^{-T} + \frac{\sqrt{2a}}{\sigma_n^2} \Gamma \Gamma^T (\Phi P(k) + Q \Phi^{-T}) \right. \right. \\ &\quad \left. \left. \{z_1(k+1) \cos \hat{\theta}(k) - z_2(k+1) \sin \hat{\theta}(k)\} \right] \right\}^{-1} \end{aligned} \quad (44)$$

where  $P(k+1)$  is a  $N \times N$  matrix.

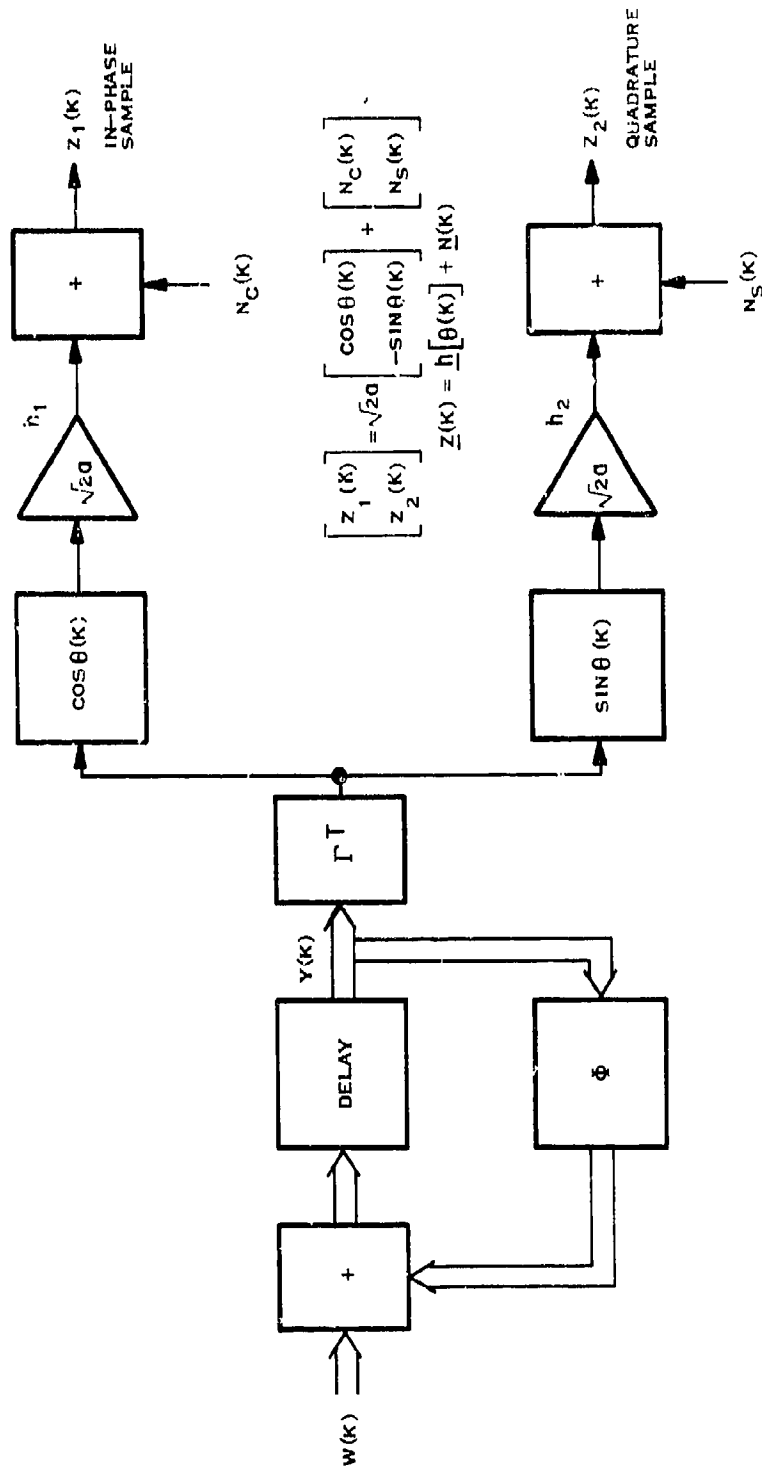


Figure 3-9. Block Diagram of the Message Process Illustrating Discrete State Variable Characterization of the Angle  $\theta(k)$

### 3. SINGLE-POLE FILTER EXAMPLE

For a single-pole message model, the parameters of the recursive algorithm are:

$$\hat{Y}(k)^T = [\hat{x}(k), \hat{\theta}(k)] \quad (45)$$

$$\Phi = \begin{bmatrix} \phi_{11} & \phi_{12} \\ \phi_{21} & \phi_{22} \end{bmatrix} = \begin{bmatrix} e^{-\alpha T} & 0 \\ \frac{c}{\alpha} (1 - e^{-\alpha T}) & 1 \end{bmatrix}$$

$$Q = \begin{bmatrix} \sigma_q^2 & 0 \\ 0 & \sigma_2^2 \end{bmatrix}$$

$c$  = frequency deviation

$\alpha$  = 3 dB frequency of the filter

$T$  = sample interval

$\frac{a}{\sigma_n^2}$  = input carrier-to-noise ratio

The  $\hat{x}(k)$  element of  $\hat{Y}(k)$  is the estimate of the message that is sought. In the  $Q$  matrix,  $\sigma_q^2$  is the variance of the message filter input,  $u_1(t)$ , and  $\sigma_2^2$  is the variance of the frequency uncertainty  $2\pi\Delta f$ , where for convenience  $\Delta f$  is assumed to be a Gauss Markov white sequence. The part of the last assumption pertaining to the white sequence is difficult to justify; however, when crystal controlled frequencies are used  $\sigma_2^2$  is quite small compared to  $\sigma_q^2$  and the degradation is most likely insignificant.

A realization of these estimation equations is illustrated in Figure 3-10. In the absence of noise, the input to the fixed gain  $G_1$  is:  $\sin[\theta(k) - \hat{\theta}(k)] \cong \theta(k) - \hat{\theta}(k)$ . Under the same input situation, the input to the nonlinear time-varying gain processor is  $\cos[\theta(k) - \hat{\theta}(k)]$ . The realization of these two signals resemble the in-phase and quadrature detectors sometimes used in phase-locked loop (PLL) receivers. It is clear that the form of the demodulator resembles a PLL demodulator where the loop filter and the digitized VCO (digital oscillator), constitute the other elements of the loop. The main departure from the phase-locked loop demodulator is the time-varying gain processor; the algorithm for this processor is defined by the equation for  $P(k+1)$ .

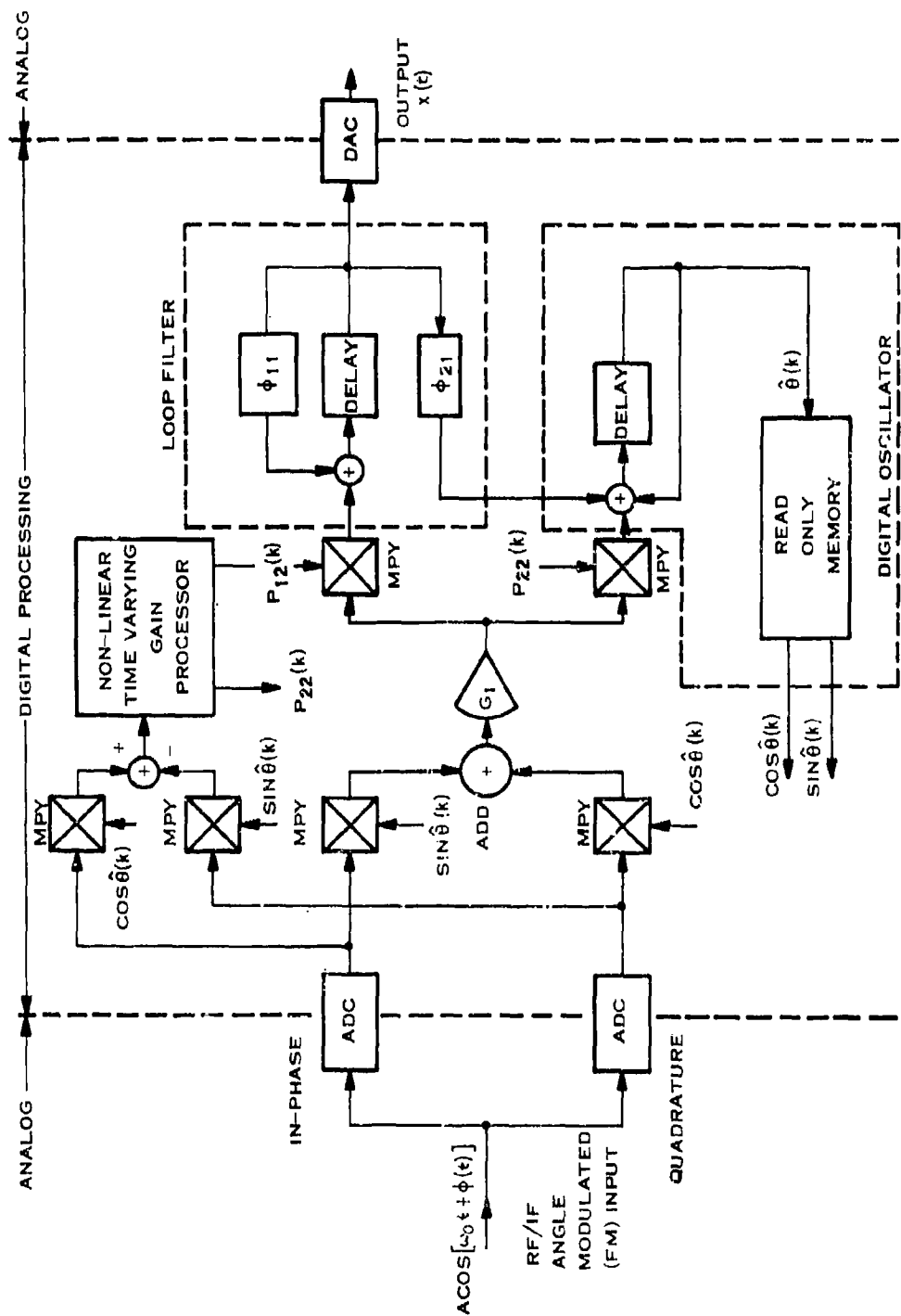


Figure 3-10. Block Diagram Realization of the Recursive Nonlinear Demodulation for a Single-Pole Message Filter.

The gain term  $G_1$  is given by:

$$G_1 = \sqrt{2} a / \sigma_n^2 \quad (46)$$

where  $\sigma_n^2$  is the noise power, defined in the input IF bandwidth, and "a" is the rms carrier voltage. It is interesting to note that the input to the time-varying gain processor is the quadrature phase component which is often used for automatic gain control (AGC) in phase-locked loop receivers. This might be the reason that matching  $G_1$  to the input carrier and noise power was not too critical as far as the demodulator performance was concerned. This fact was discovered during the simulation of the demodulator.

The simulation of the demodulator of Figure 3-10 was accomplished using digital computer simulation techniques. Of particular importance in determining the performance of FM demodulators are curves relating the output signal-to-noise ratio in the message bandwidth (SNR) to the carrier-to-noise ratio in the IF bandwidth\* ( $CNR_{IF}$ ). Consequently, the ultimate purpose of the simulation was to obtain these SNR performance curves; Figure 3-11 illustrates the SNR performance curves obtained by simulation of the single-pole message filter example of Figure 3-10.

In these curves  $\beta$ , the modulation index, is defined as:

$$\beta = \frac{c}{\alpha} \quad (47)$$

where  $c$  is the radian frequency deviation and  $\alpha$  is the 3 dB bandwidth of the single-pole filter. Curve A is the SNR performance curve for the demodulator for  $\beta = 5$  and fixed gain  $G_1$  matched to  $CNR_{IF} = 20$  dB. Both curves were obtained for a sinewave test signal of frequency  $(1/50)T$  where  $T$  is the sample interval. Curve B was obtained from an identical simulation as was curve A, except a single-pole digital filter like that used in the message filter was also put at the output of the demodulator. Since sinewave test signals were used, this filter should and did improve the above-threshold performance. However, the threshold (1 dB below the linear extension of the curve) is almost identical on each curve occurring at  $CNR_{IF} \cong 4$  dB.

This would tend to indicate a threshold improvement of about 6 dB over conventional discriminator demodulators when using sinewave test signals. A very important factor associated with threshold performance of FM demodulators is the type of message spectrum employed. Van Trees<sup>12</sup> illustrates this where he compares FM threshold performance single-pole and two-pole Butterworth message spectrum. The two-pole message characteri-

---

\*Carson rule bandwidth definition was used in the simulation.

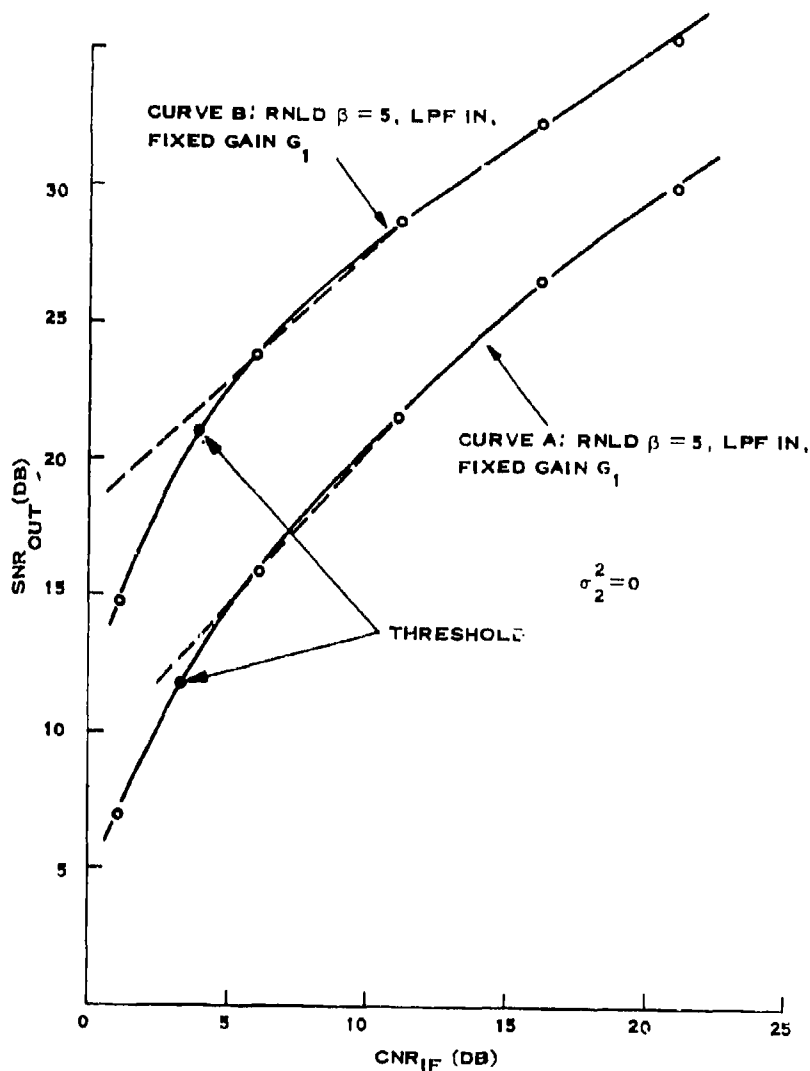


Figure 3-11. Signal-to-Noise Performance Curves  
Obtained From Simulation

zation has about a 2 dB threshold improvement above that for a single-pole message characterization. In the simulated test, single unfiltered sinewave test signals were employed. An ensemble of sinewaves with random phase passed through the message filter would be a more meaningful test. However, the demodulator of Figure 3-10 does appear to provide threshold extension equal to or better than the analog threshold extension demodulators reported in the literature.<sup>13</sup>

#### D. DISCRETE FOURIER TRANSFORMATIONS

Nonrecursive digital oscillator schemes have been used for some time in the well-known and many-times-published Fast Fourier Transform (FFT) algorithm. In the FFT, an array of sine and cosine values are appropriately prestored by taking into account the symmetries involved in the transform and the sinusoid itself. These sampled values are then used repeatedly in the transform.

For many applications the FFT is either too complicated or lacks versatility; the discrete Fourier transform (DFT) is usually preferred for these applications. A nonrecursive digital oscillator is also well suited to this type transformation. All that is required (at least hardware wise) to perform the DFT is a fast multiplier and adder to perform the necessary convolutions and a digital oscillator for providing the various frequencies required. The Fourier coefficients are then available directly in the adders.

#### E. SYNCHRONIZATION

Synchronization is one of the fundamental requirements in coherent communication systems. In transmission of information in the continuous wave or analog mode, synchronization implies precise knowledge of the phase of the incoming carrier before the near-optimum coherent demodulation can be implemented. In digital data transmission, the elements of synchronization include carrier sync, bit sync, and frame sync. Bit synchronization is always required in digital data reception, but carrier requirements and frame synchronization requirements are dictated by the demodulation performance desired and the type of data, respectively. To determine the role of the digital oscillator in implementations of synchronization systems, we will review what the digital oscillator provides as its output and where this particular type of output is useful in synchronization.

The output of the digital oscillator is sample values of the amplitude of sine and cosine waveforms, i. e.,  $\sin \omega_0 t_i$  and  $\cos \omega_0 t_i$  where  $t_i$  is the sample time. These outputs are binary words which occur at the basic clock time of the digital oscillator.

Frequency, as such, is not a direct output, but is implicit in the sequence of output binary words. When we consider the output as zero-width spikes occurring at the sample time and whose height represents the amplitude of the sampled sine or cosine value, the frequency spectrum has one form. When, however, the spikes are connected to form a staircase waveform (a zero-order hold) the spectrum will change. It will again change when this staircase waveform is passed through a filter as is done to generate continuous time waveforms for analog processing. Figure 3-12 illustrates this concept by

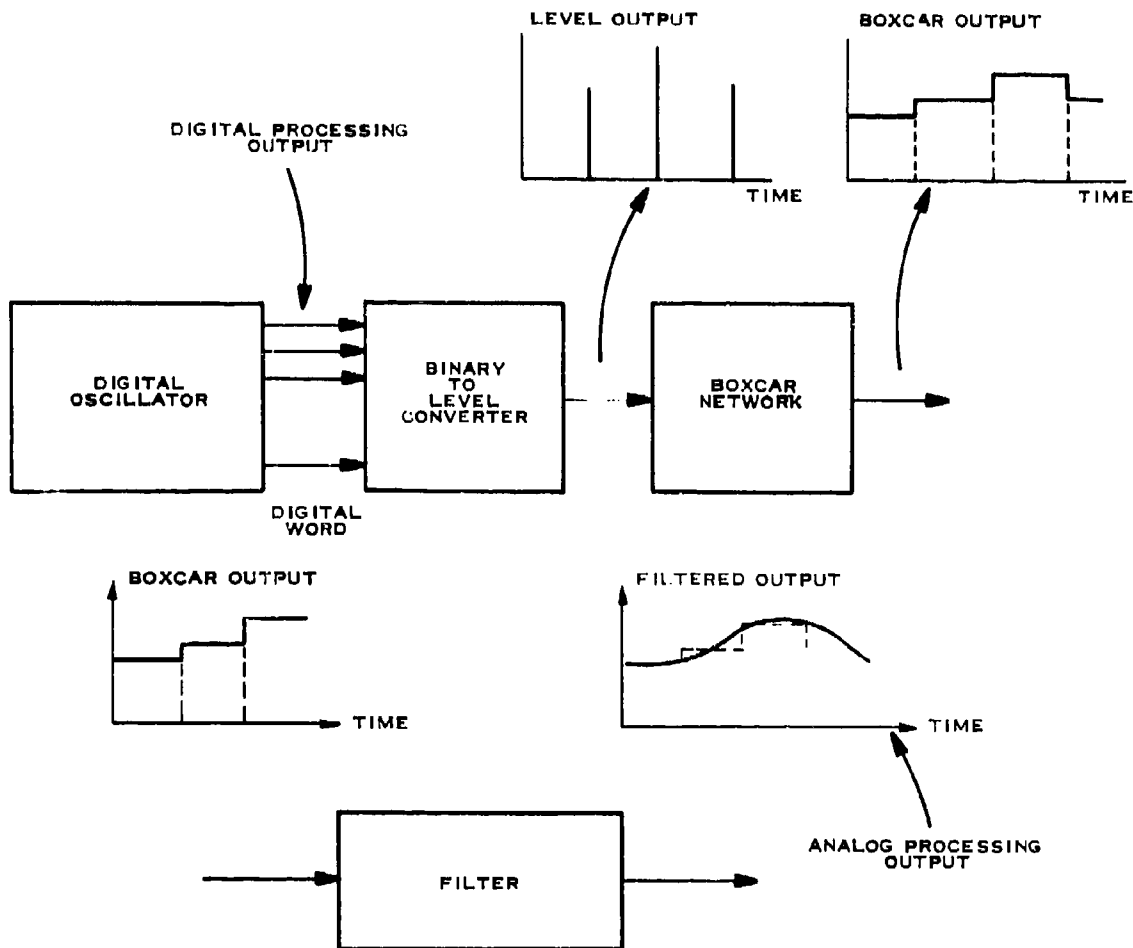


Figure 3-12. Block Diagram Showing the Different Time Waveforms Going from Digital to Analog Processing when using the digital Oscillator

showing the different types of waveforms which evolve when going from a sequence of digital words to a continuous waveform.

Suppose that the digital oscillator is to be used to obtain bit timing marks which can be varied in both phase and frequency. Then the output of the digital oscillator would not only have to be D/A converted to obtain a sinewave waveform but this sinewave would have to be further processed as illustrated in Figure 3-13 to obtain the bit timing marks. Obviously, the important

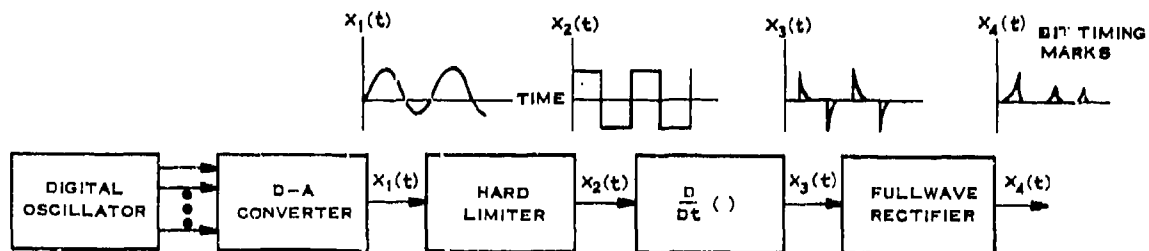


Figure 3-13. Block Diagram Showing the Application of a Digital Oscillator to Obtain Timing Marks for Bit Synchronization

attribute desired of the sine wave at the output of the D/A converter is the zero crossing purity, since in this bit sync scheme, these carry all the bit timing information.

This bit sync example illustrates an important point: the digital oscillator does not generate timing marks. It does, however, generate numbers from which timing marks can be obtained. Evidently, timing mark generation is necessarily an analog type of process which requires additional analog circuitry for its implementation. Thus, bit synchronization, which is mostly timing mark generation, is not too amenable to digital oscillator application. Nevertheless, it can be implemented through use of the digital oscillator which could be advantageous when the digital oscillator is already available.

The major role the digital oscillator has in synchronization is that of the VCO replacement in digitalized feedback control loops, e. g., the digitalized phase-locked loop. The breadboard model discussed in Section IV of this report can easily be modified to operate in a phase-locked-loop configuration for carrier synchronization. Unfortunately, the upper frequency bounds ( $\approx 10$  MHz) on the design of the oscillator limits the frequency of the carrier to be acquired to the lower HF and below frequency spectrum.

Wireline modem synchronization is an area of intense interest at the present time. The digital oscillator used as a VCO replacement in a carrier synchronization scheme should have wide application either in a PLL configuration or a modified version of the recursive nonlinear demodulator (RNLD) discussed in the previous subsection.

Since the digital oscillator can perform any operation that a standard VCO can perform, but usually with greater precision and stability, its application to the synchronization problem of future digitalized communication systems is apparent.

SECTION IV  
BREADBOARD DESIGN DISCUSSION

A. GENERAL

A block diagram of a nonrecursive digital oscillator is shown in Figure 4-1. The thumb-wheel read-in's allow one to select the desired output frequency (for frequency synthesizer applications) or the desired quiescent frequency (for VCO applications). The thumb-wheel outputs are binary numbers representing each decimal number selected. These individual outputs enter

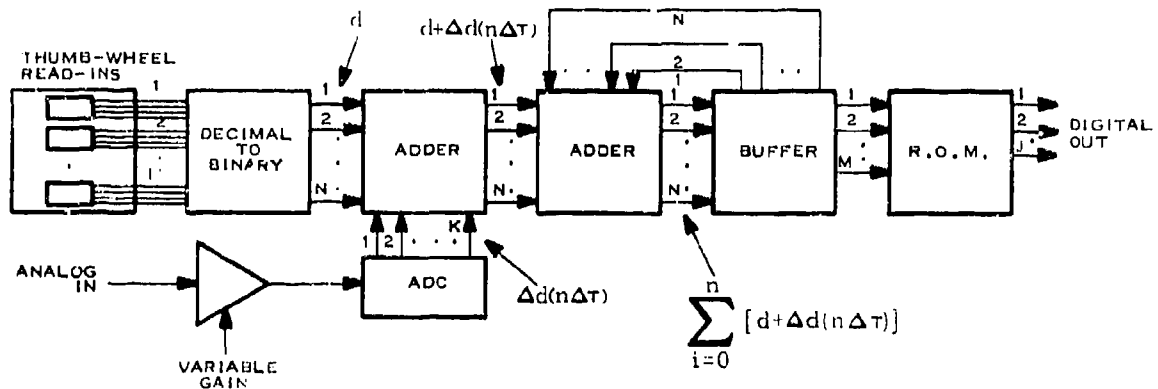


Figure 4-1. Nonrecursive Digital Oscillator

a decimal-to-binary converter (DBC), the output of the DBC, denoted as  $d$ , being an  $N$ -bit binary representation of the desired decimal frequency. This  $N$ -bit number then enters as one input to the first  $N$ -bit adder. The other input, call  $\Delta d$ , to this adder is a  $k$ -bit number coming from an analog-to-digital converter (ADC) the input of the ADC being analog modulating signals for FM modulation or error signals for tracking loop configurations.

The  $k$ -bits from the ADC are added to the  $N$ -bits from the DBC, the  $k$ -bits occupying the  $k$  least significant bits of the  $N$ -bit adder. The resulting  $N$ -bit output,  $d + \Delta d(n\Delta T)$ , is an indication of the rate of speed for stepping around the phase circle as discussed in Section II. B. 1. In the nonrecursive digital oscillator configuration shown in Figure 4-1 the thumb-wheels allow one to determine the interval for selecting points from the phase circle. The ADC output causes perturbations in this interval depending on the input modulating signal.

The second adder performs an integration to maintain a complete history of the inputs  $d + \Delta d(n\Delta T)$ , and has at its output

$$\sum_{i=1}^n [d + \Delta d(n\Delta T)]$$

which is held in a storage buffer. The adder performs a modulo 1 addition so that at any time its output completely specifies some unique point on the phase circle, i. e.,  $(\text{Sum Mod } 1) \cdot (2\pi)$ .

The most significant M bits of this sum are used as an address for look-up in the read-only-memory (ROM), where  $2^M$  sinusoid values are stored. These values are selected at intervals of  $2\pi/2^M$  radians around the phase circle. These M bits serve as the address since the adder performs modulo 1 addition and therefore indicates directly the exact location on the phase circle.

The ROM output is a J-bit binary word representing the sinusoidal value at the position specified by the M-bit address. The order of J may be varied depending on the required significance in the output word, and its selection is independent of other parameters in the system.

An interesting point to be made here is that one can attain any frequency resolution desired by manipulation of the system parameters. The minimum resolution element (MRE), analogous to the elementary bandwidth when taking the discrete Fourier transform, is given by:

$$\text{MRE} = 2^{-N} \cdot f_s,$$

where N is the number of bits in the address. As an example, assume an N of 20 bits and a clock rate of  $f_s = 2^N = 1,048,576$  Hz. The resolution element MRE is then

$$\begin{aligned} \text{MRE} &= 2^{-20} \cdot 2^{20} \\ &= 1 \text{ Hz} \end{aligned}$$

Therefore, 1 Hz resolution may be obtained by making the above selections. A resolution of 0.25 Hz may be obtained by letting  $f_s = 2^{N-2}$ ; i. e.,

$$\begin{aligned} \text{MRE} &= 2^{-20} \cdot 2^{-18} \\ &= .25 \text{ Hz} \end{aligned}$$

These resolutions are however dependent on the stability of the oscillator used in generating  $f_s$  and therefore are minimum bounds.

This oscillator design used in the breadboard has the following specifications. The adders are 22-bits, the sample rate  $2^{22}$  Hz. This combination allows 1 Hz resolution between 1 Hz and 1 MHz. The read-only-memory contains the equivalent of 256 8-bit words.

The ADC has 12-bits operating at a sample rate of 50 kHz. The design criterion is summarized as follows:

$$\begin{aligned}
 N &= 22 \text{ bits} \\
 f_s &= 2^{22} \text{ Hz} \\
 \text{MRE} &= 1 \text{ Hz} \\
 M &= 8 \text{ bits} \\
 J &= 8 \text{ bits} \\
 K &= 12 \text{ bits} \\
 f_{\text{max}} &= f_s/4 = 1 \text{ MHz}
 \end{aligned}$$

## B. BREADBOARD CONFIGURATIONS

This section presents the two basic breadboard operating configurations—frequency synthesizers and VCO replacements. Included in frequency synthesizers are synthesizers themselves and frequency translators; in VCO replacements are tracking loops and frequency modulators.

### 1. FREQUENCY SYNTHESIZERS

#### a. Frequency Synthesizer.

A configuration demonstrating the use of a digital oscillator as a frequency synthesizer is shown in Figure 4-2. A fixed "d" representing the frequency to be synthesized is presented to the digital oscillator. The outputs of the digital oscillator are binary words representing the digitized sinusoid. These words are then digital-to-analog converted (DAC) and low pass filtered (LPF). The output of the LPF is an analog sinusoid of the desired frequency.

#### b. Frequency Translator

A frequency translator configuration is shown in Figure 4-3. A fixed "d" representing some frequency  $f_0$  is input to the digital oscillator. The digital oscillator output, once passed through the DAC and LPF, becomes the required sinusoid of frequency  $f_0$ . This sinusoid and an input signal of fre-

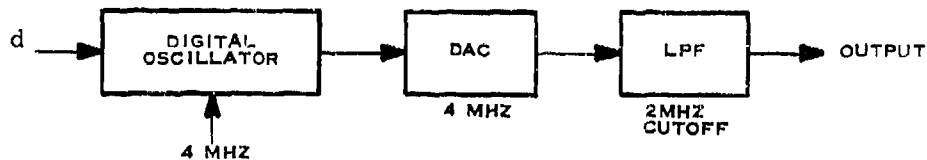


Figure 4-2. Frequency Synthesizer

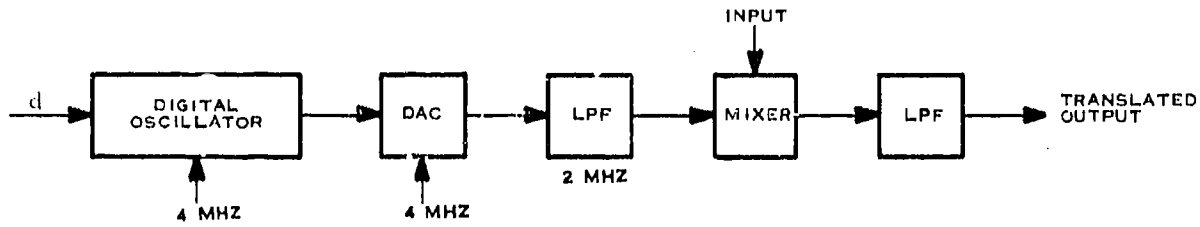


Figure 4-3. Frequency Translator

quency  $f_i$  are then mixed and low pass filtered. The output of the LPF is a signal representing the difference frequency  $f_d = f_o - f_i$ , and is the translated output. The down translation is selected because of its simplicity, but the up translation could also be performed if adequate bandpass filters were constructed.

## 2. VCO REPLACEMENTS

### a. Tracking Filter

The next configuration, the tracking filter, is shown in Figure 4-4. The loop itself is the conventional tracking filter loop with the voltage controlled oscillator (VCO) replaced by the digital oscillator and appropriate converters. The input signal is assumed to have a carrier  $f_c$  and a maximum doppler rate of 100 Hz. This maximum doppler insures that the loop can be constructed in such a way that it will not track audio modulating signals transmitted by the carrier. The quiescent frequency of the digital oscillator is adjusted to be at some frequency  $f_q$ . When initialized, the input carrier and the analog equivalent output of the digital oscillator are mixed and passed through the LPF generating a signal having frequency  $f_q - f_c = f_o$ . This signal is input into a frequency discriminator centered at 100 kHz (for illustrative purposes) with the output being a signal indicating the frequency difference between  $f_o$  and the center frequency of 100 kHz. This difference is low pass filter with a filter having a cutoff of 250 kHz before being fed into the ADC and finally the digital oscillator. The difference frequency will eventually lock to 100 kHz, the center frequency of the frequency discriminator. Low frequency doppler shifts will be tracked out, but high frequency modulating signals will not.

### b. Frequency Modulator

The FM modulator configuration, shown in Figure 4-5, also makes use of a digital oscillator as a replacement for a VCO. The modulating signal is input into the ADC, its output thus supplying an indication of the modulation

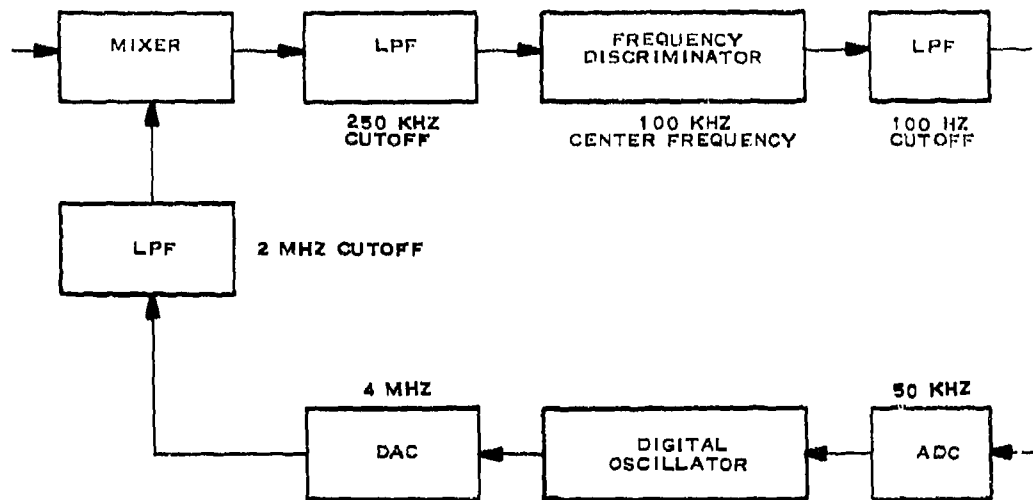


Figure 4-4. Tracking Filter

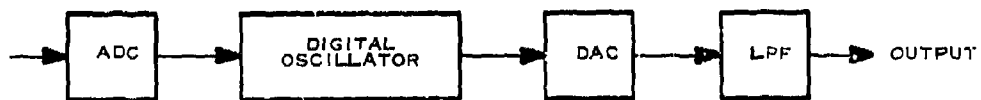


Figure 4-5. Frequency Modulator

around the carrier frequency (the modulation index of the modulator can be varied by adjusting a scale value on the input of the ADC). This digitized FM modulated output of the digital oscillator is then passed through a DAC and LPF, thus generating the analog equivalent output. An interesting side-line to this method of FM modulation is that one can easily select and vary the modulating carrier frequency.

## C. BREADBOARD DESCRIPTION

### 1. MECHANICAL DESCRIPTION

The breadboard construction consisted of dual-in-line integrated circuits mounted in sockets which were wire-wrapped on plug-in cards. The 4 inch by 4 inch cards accommodated 10 to 20 sockets (integrated circuits). The cards, in turn, were mounted on a rack where intercard wiring could be achieved. Analog circuits were mounted on plug-in cards so that the entire system could be contained in a card rack. The card rack and required power supplies were mounted in a 19-inch rack-mountable cabinet. The front panel of the completed breadboard is shown in Figure 4-6.

### 2. OPERATIONAL DESCRIPTION

The digital oscillator (DO) breadboard can be sectioned into 10 functional blocks, each mounted on one printed circuit board (PCB). Nine of these boards are mounted in a card file; the tenth, the power regulator board is mounted at the rear of the chassis along with the remainder of the power supply components.

#### a. Digital Portion

Figure 4-7 shows the seven digital blocks of the digital oscillator. A description of each of these blocks and their functions follow.

- 1) Recursive Adder Board (Board E). The recursive adder board forms the heart of the DO function. This board generates a 9-bit binary digitized sinusoidal whose frequency is specified by a 20-bit binary input board. This is accomplished as follows (Figure 4-7).

The 20-bit word A is applied to the 20 LSB of one input of a 22-bit full adder. The other 22-bit input is tied to the outputs of a 22-bit parallel register. The 22 sum lines from the adder are tied to the inputs of register E. The E-register is clocked at the rate of  $2^{22}$  Hz, and at each clock pulse, the sum of the input word A and the present contents of the register are stored in the register.

The 10 MSB of the register are used to control the sinusoidal generation process. The 8 LSB's of these 10 are fed through controlled inverters to the 512-bit ROM address inputs. The second MSB controls the inversion, with inversion occurring when this line is a logic 0. The MSB (sign) and the eight outputs of the ROM are then routed to the DAC Board, Board F.

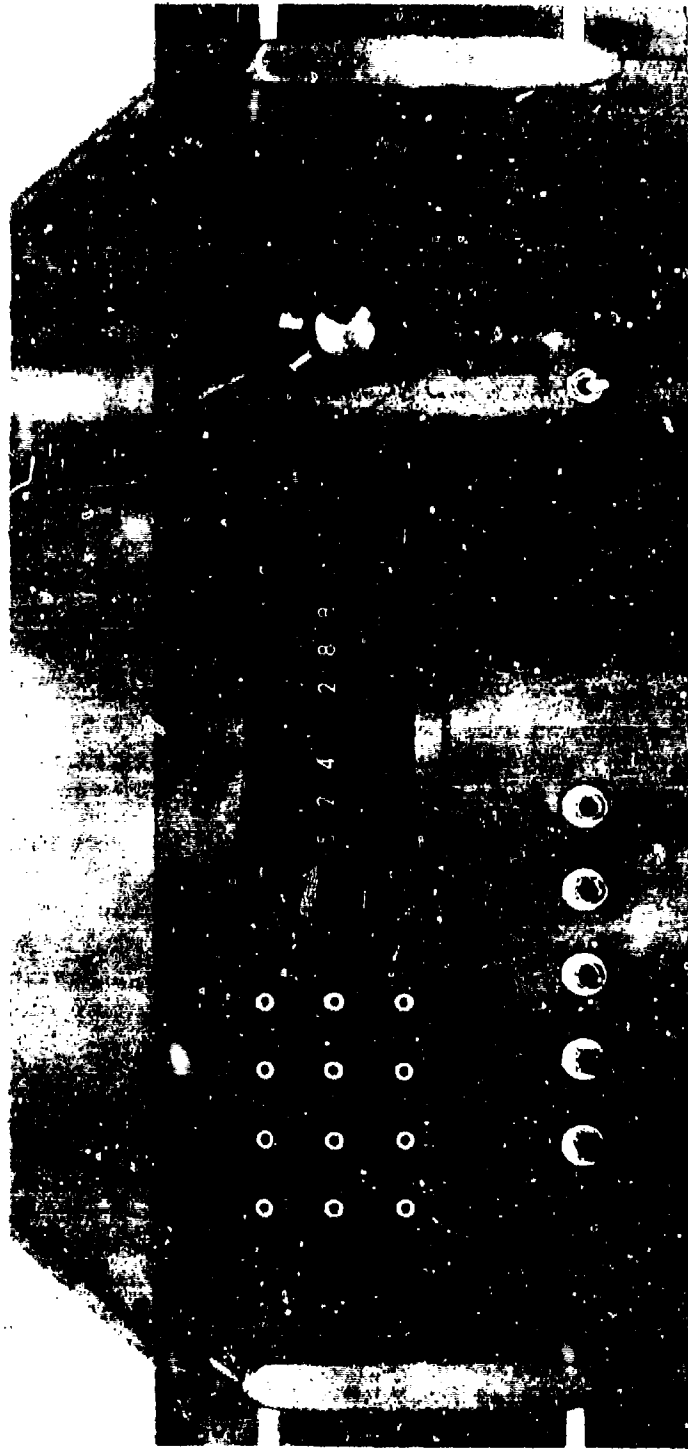


Figure 4-6. Breadboard Mechanical Package

Reproduced from  
best available copy. 

- 2) DAC Board F. The DAC board accepts the nine ROM bits and the sign bit from the Adder Board E, and connects the words to an analog sinusoidal output. The SIGN-bit line controls the MSB input of the DAC and a two's complement operation. The two's complement of the incoming 8-bit word is generated by complementing all the bits and adding a binary 1. These eight bits are buffered by a parallel register clocked at the system rate of  $2^{22}$  Hz.

The analog output of the DAC is buffered by a wideband operational amplifier and made available to a front panel test point. This signal is also passed through a two pole, 2 MHz LPF to partially remove  $2^{22}$  Hz switching rate noise.

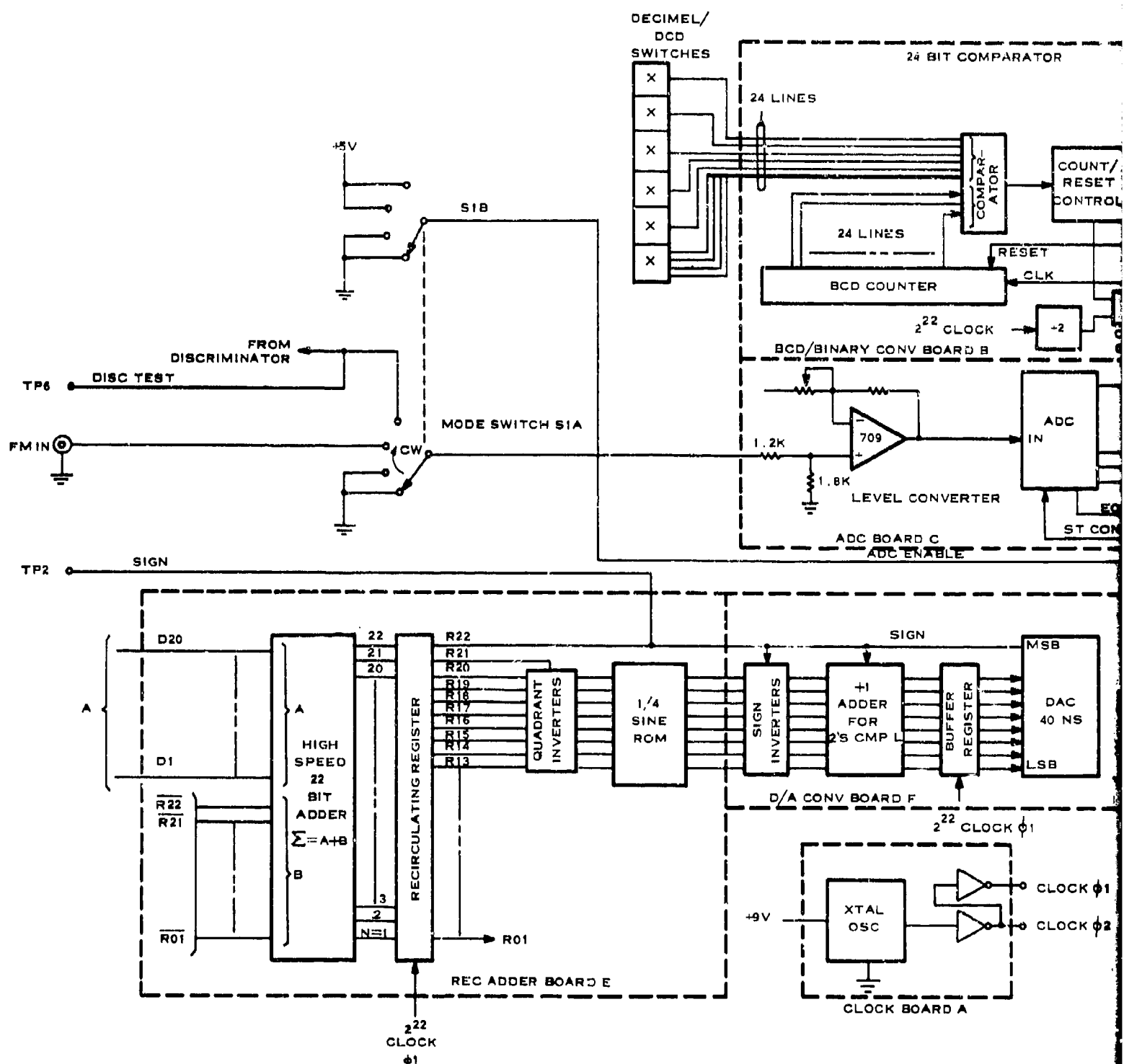
- 3) Buffer Board I. The buffer board provides further low pass filtering for the filtered output from the DAC board. This doubly filtered output is then routed to the OSC OUT connector and the Mixer Board G.
- 4) Modulation Board D. The 20-bit binary input word "A" to the recursive adder board is provided from the Modulation Board D, which provides the sum of the 20-bit front panel word and optionally the 12-bit ADC word (see Figure 4-7).

The 20-bit front panel derived word is generated by providing the proper number of clock pulses to a 20 bit ripple through counter whenever the front panel settings are changed. This clock is supplied by the BCD to Binary Converter Board B.

The 12-bit ADC derived word is supplied from the ADC Board C and made available to the modulation adder through a 12-bit input buffer register. These words are formed in two's complement binary and enable subtraction as well as addition. When modulation by the ADC is not desired (Synthesizer and Translation modes) the register is set to zero by a clear enable line from the mode control switch.

A start conversion clock of 32 kHz is generated from the master clock and provided to the ADC module, and this module in turn supplies the End of Conversion pulse to clock the 120-bit modulator register.

- 5) ADC Converter Board C. This board contains an input buffer amplifier/level converter and the 12-bit ADC module. The input to the buffer amplifier is controlled by the mode switch and is either the FM IN terminal or the internal FM discriminator.
- 6) BCD/Binary Converter Board B. The 24 BCD input lines from the front panel switches are converted to a binary word by enabling a  $2^{21}$  Hz clock to both a binary counter and a BCD counter



B

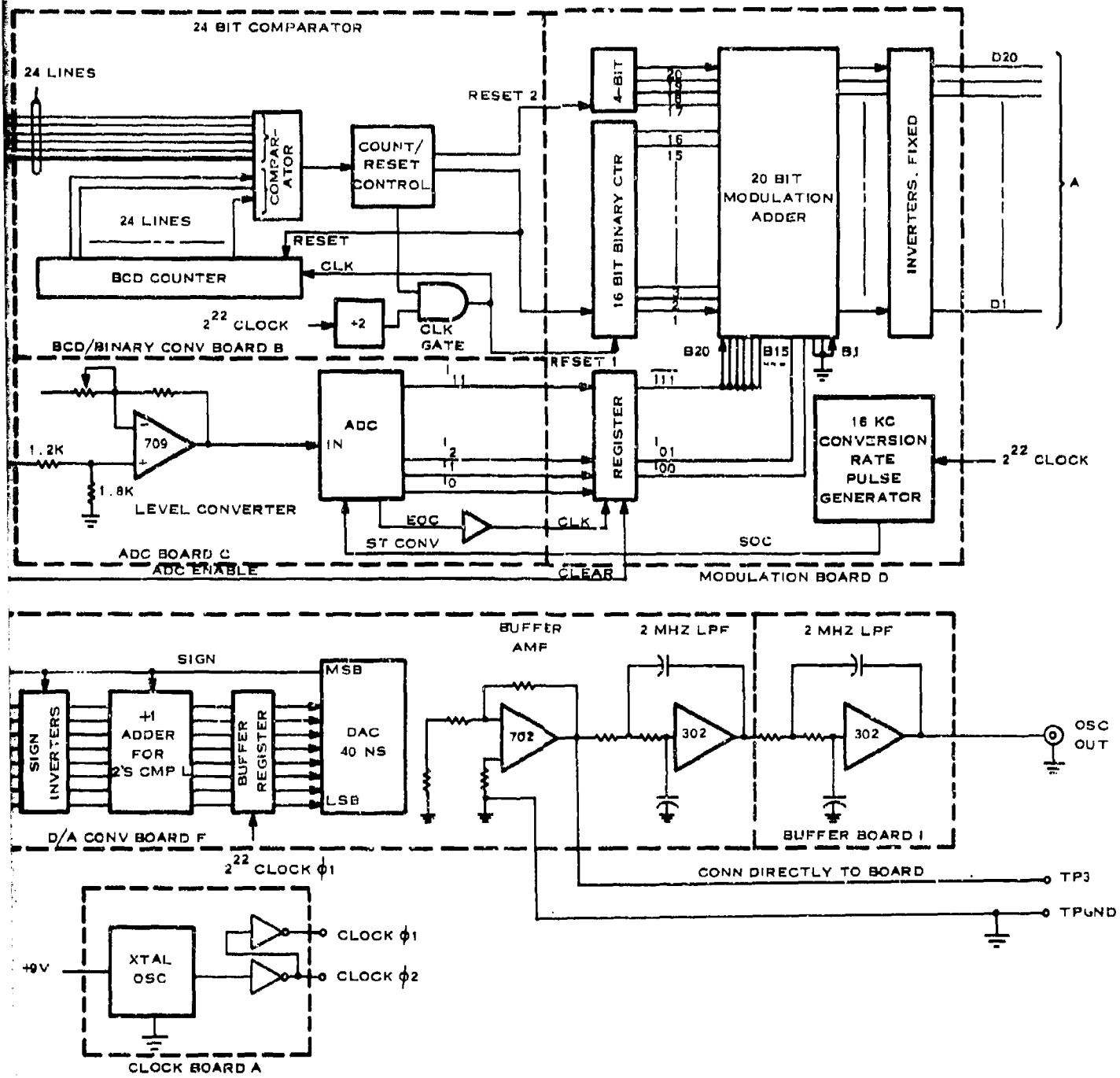


Figure 4-7. Breadboard Digital Layout

until a 24 bit comparator determines that the BCD input and the BCD counter are the same. The count clock is then disabled and the binary counter (located on board D) holds that count in binary form until the 24 bit comparator signals that a front panel change has been made.

- 7) Clock Board A. This board includes a  $2^{22}$  Hz crystal oscillator and digital clock drivers for Clock and Clock.

b. Analog Portion

Figure 4-8 illustrates the two analog boards.

- 1) Mixer Board G. This board includes a balanced mixer and two IF (low pass filters).

One input to the mixer is the digital oscillator, the other the HF IN front panel terminal. The outputs of the 100 kHz LPF are available on the front panel and to the Discriminator Board H.

- 2) Discriminator Board H. This board includes a zero crossing detector and 10  $\mu$ sec one-shot (for frequency discrimination) followed by two parallel filters. One of these is a 100 Hz LPF used in the system tracking loop; the other is an AC coupled 2 kHz LPF providing detected FM to the DISC OUT terminal.

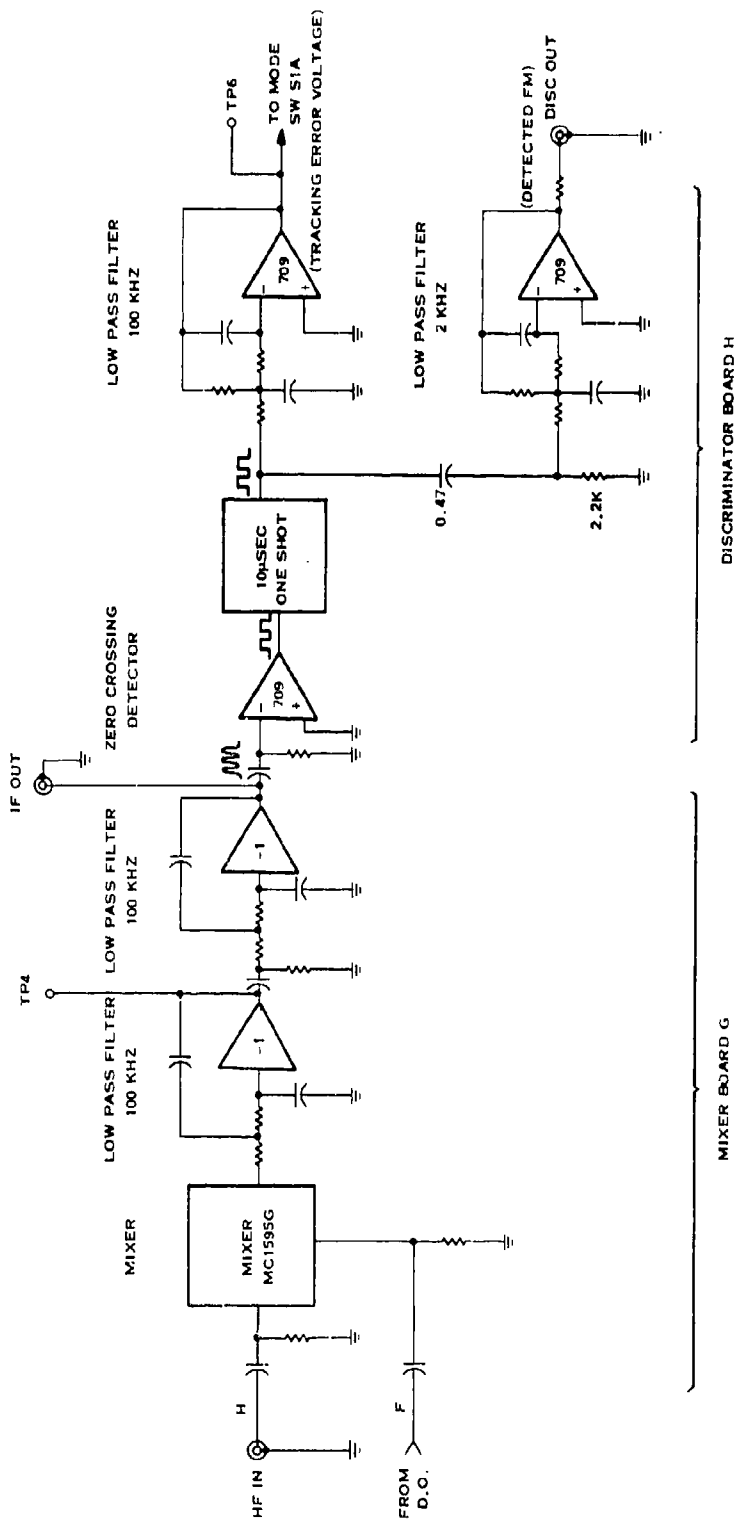


Figure 4-8. Analog Layout

SECTION V  
BREADBOARD DEMONSTRATION AND EVALUATION

The demonstration and evaluation of the digital oscillator operating in the two basic configuration, frequency synthesizers and VCO replacement, are performed by first converting the digital words to analog by digital-to-analog conversion techniques. Once in an analog form, direct comparisons are made between the digital oscillator waveform and that generated by conventional analog equipment. In addition, analog test equipment can be used to measure meaningful properties of the waveform itself.

A. DEMONSTRATION

1. FREQUENCY SYNTHESIZERS

a. Frequency Synthesizer

The breadboard can be demonstrated as a frequency synthesizer using a frequency counter, a distortion analyzer, and a spectrum analyzer. The spectrum analyzer should be of the narrow bandwidth-type to allow the examination of close-in sidebands, and each of these instruments should be capable of 1.0 MHz operation. See Figure 5-1 for the required connections. By placing the breadboard in the SYNTHESIZER mode (see Figure 4-6) and entering the desired frequency on the thumb wheel read-ins, the sinusoid of the appropriate frequency will appear at the OSC OUT connector on the front panel. A check of the frequency is performed by connecting OSC OUT to a frequency counter. To check for harmonic distortion, OSC OUT is connected to the distortion analyzer. The spectrum analyzer when connected to OSC OUT will measure the location of the sidebands and their relative magnitudes. These are meaningful and very appropriate tests for any frequency synthesizer.

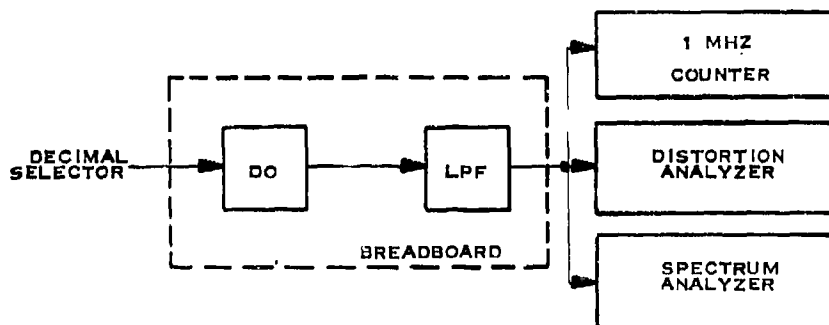


Figure 5-1. Frequency Synthesizer

b. Frequency Translator

The frequency translator function (the TRANSLATOR mode) (Figure 5-2) makes use of the digital oscillator and the mixer contained in the breadboard. The IF output frequency can be observed to be the differences between the HF analog input frequency (HF IN) and the digital oscillator (DO) front panel frequency setting from the decimal read-ins.

$$f_{IF} = |f_{HF} - f_{DO}|$$

The difference (IF) frequency is limited to 150 kHz by the IF low pass filter. The resulting translated signal will appear at the IF OUT connector on the front panel. In this mode a 100 kHz FM discriminator will also detect any frequency modulation of the HF input with the modulation appearing at the DISC OUT connector.

2. VCO REPLACEMENT

a. Frequency Modulation

The frequency modulation (FM) function, performed when the rotary switch is in the MODULATION mode, is illustrated in Figure 5-3. In this

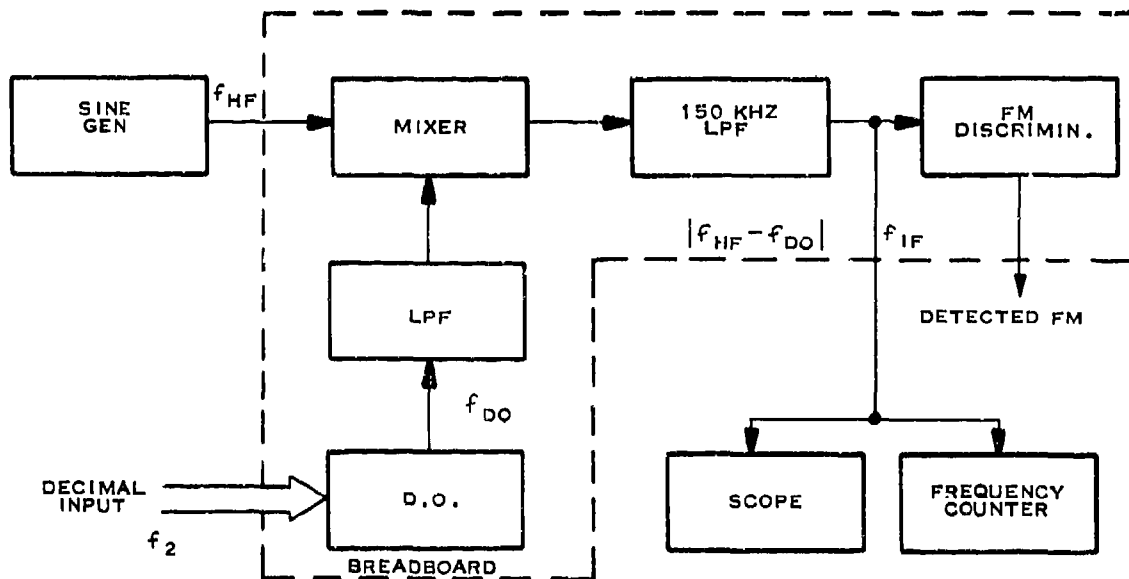


Figure 5-2. Frequency Translation

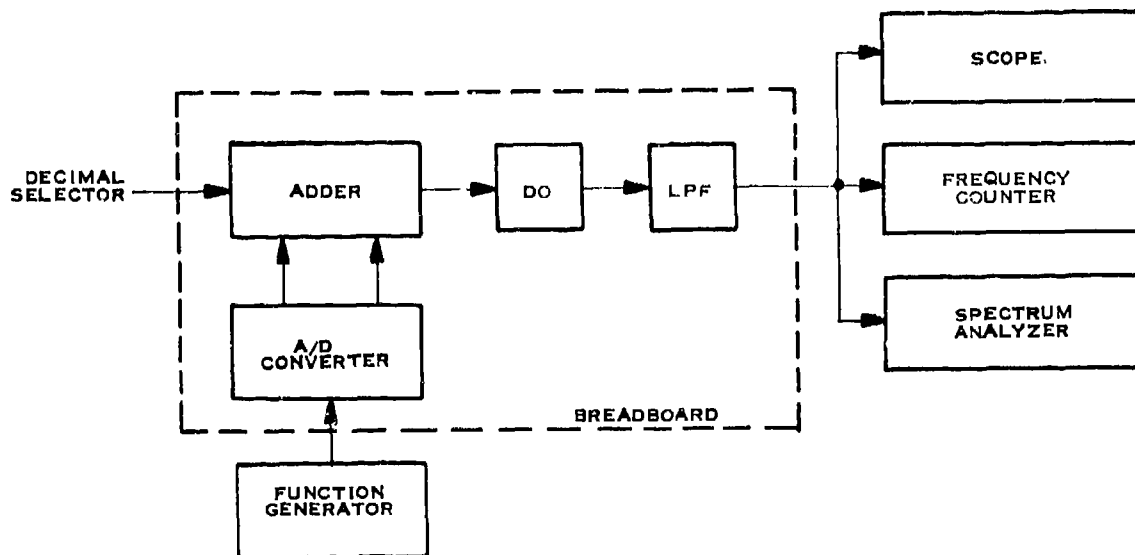


Figure 5-3. FM Synthesizer

mode, the FM center frequency is selected from the thumb-wheel read-ins, and the analog modulating signal is entered at the EXT FM connector on the front panel. The signal at EXT FM is analog-to-digital converted to 12 bits and appropriately added to the binary representation for the center frequency. The frequency modulated output will appear at OSC OUT connector on the front panel. The same tests as in the SYNTHESIZER mode, except for the harmonic distortion test, may now be performed. Frequency shift keying can be demonstrated by applying a square wave input to the EXT FM connector and linear swept frequencies can be generated by application of a sawtooth waveform. FM sidebands should be examined with a spectrum analyzer and the FM waveforms can be observed on an oscilloscope. Modulating frequencies are limited by Nyquist criterion to one-half the ADC conversion rate of 32.768 kHz ( $2^{15}$ ).

b. Tracking Filter

In the tracking filter mode (mode selector switch set to TRACKING FILTER), a loop is formed such that carrier frequency offsets (entered at HFIN) may be corrected to maintain a 100 kHz IF frequency out of the discriminator output. This error voltage is A to D converted, with this now used as a

correction factor added to the DO frequency input word to minimize the offset. This demonstration is illustrated in Figure 5-4.

If an input frequency  $f_{HF}$  is applied to the mixer, the system loop will adjust the DO with bounds such that

$$| f_{HF} - f_{DO} | = 100 \text{ kHz}$$

This 100 kHz IF and the DO frequency can be counted and compared. The loop error voltage from the discriminator is available at a test point and the wideband output of the discriminator at the DISC OUT connector.

### B. EVALUATION

The demonstration procedure discussed in the previous section has been used to evaluate the performance of the nonrecursive digital oscillator breadboard in the two basic operating configurations. The performance results follow:

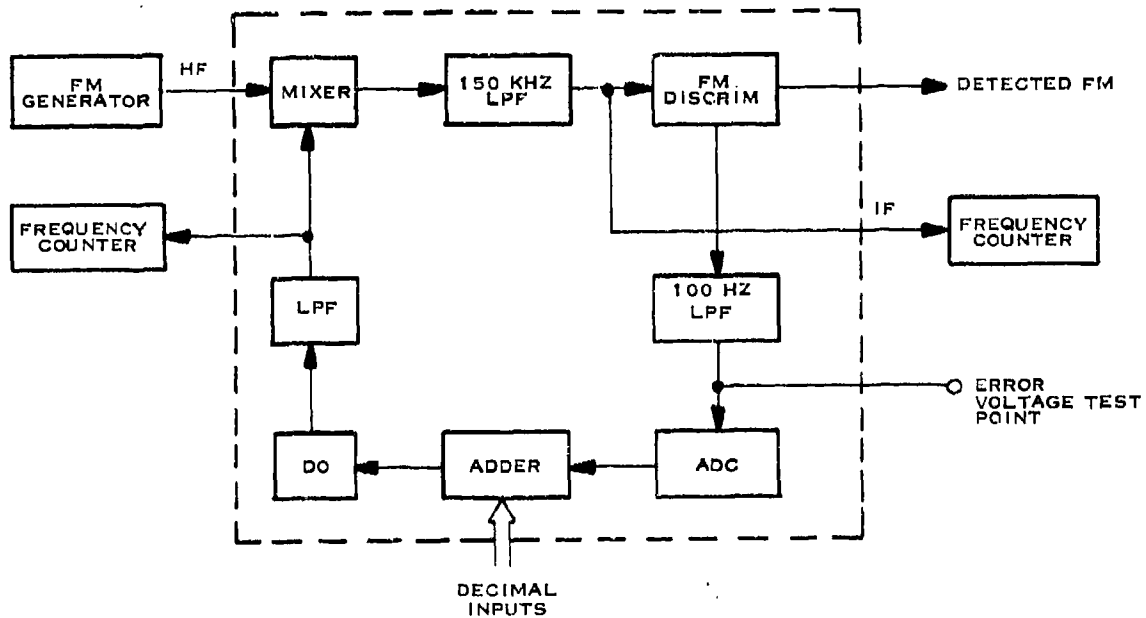


Figure 5-4. Tracking Filter

## 1. FREQUENCY SYNTHESIZERS

The criteria for measuring performance of frequency synthesizers have been stability, frequency distortion, and location and level of sideband energy. These measurements provide a very meaningful and useful description of synthesizer performance.

### a. Stability

The stability of the digital oscillator was measured using the set-up shown in Figure 5-5. These measurements were made using an external oven-controlled-crystal standard as the clock for the breadboard so that any measurable frequency fluctuation could be attributed to the oscillator itself, and not the clock. (There is a BNC connector on the back of the breadboard for external clock inputs, and a switch for selecting either external or internal clock).

The procedure is as follows: an input frequency is selected on the decimal-read-ins on the front panel of the breadboard. The resulting analog output then enters the HP5360A frequency counter. This counter makes a direct frequency to 9-decimal digit conversion; the nine-digits displayed on the read-outs. These nine-digits also enter the HP580A selector and digital-to-analog converter.

The HP580A is a three-digit converter, the three-digits manually selected from the nine-digits available by a front panel knob. This knob was calibrated before hand so that a 1 Hz frequency change on the input would result in a full scale deflection of the brush mark recorder. A frequency of approximately 500 kHz was selected for the stability measurement, with the resulting brush marker output shown in Figure 5-6. Also included in the figure is a comparison stability measurement of a Type 1163A, General Radio frequency synthesizer. Both the DO and the General Radio frequency synthesizers are stable to well below 1 Hz, with the DO having a fluctuation of ap-

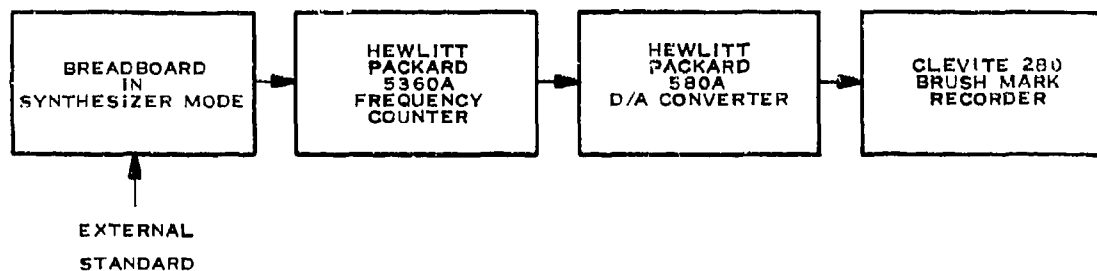


Figure 5-5. DO Stability Measurement

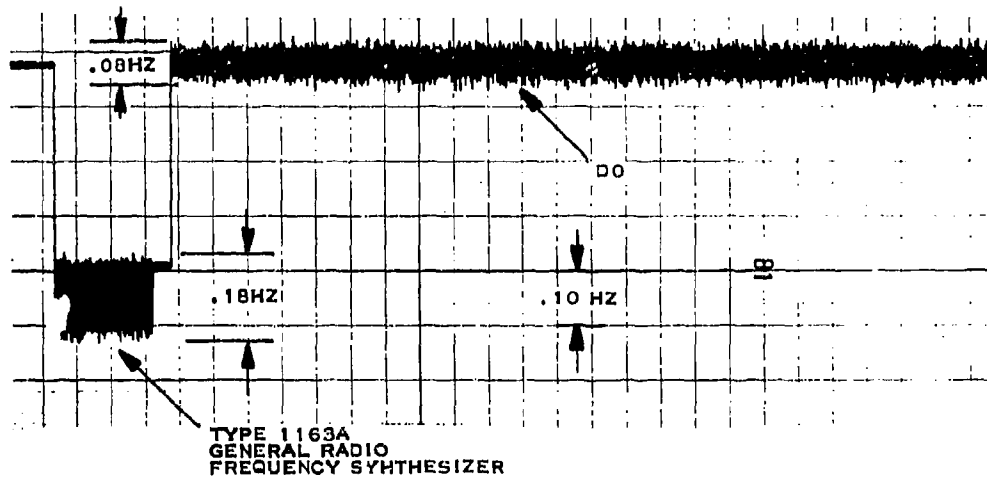


Figure 5-6. Stability Comparison

proximately 0.08 Hz. For the clock rate of 4 MHz, this is stability to fifty parts per million, a figure well below the design objectives of the DO.

b. Harmonic Distortion

A conventional analog distortion analyzer was used to perform these measurements on the breadboard. These analyzers measure the ratio of the sideband energy to total energy. The analyzer was connected to the analog out connector on the front panel, the output frequency from the analog out having been selected by modifying the thumb-wheel read-in's. Figure 5-7 is a plot of frequency versus percent distortion over the frequency range of the digital oscillator. There is less than 0.8 percent distortion up to 10 kHz, and increases to approximately 1.6 percent at 500 kHz. This is good performance for such a relatively inexpensive frequency synthesizer.

c. Harmonic Content

Fourier analysis of simulated digital oscillator outputs were performed and discussed in Section II. B. 2 for various frequency to sample rate ratios. In addition to this, an analog spectrum analyzer has been used as back up for the Fourier analysis. A frequency of 186,413 Hz was selected as a test case.



This corresponds to a frequency versus sample rate ratio of  $1/22.5$ , the ratio used in generating the Fourier analysis shown in Figure 2-8. The spectrum analyzer output is shown in Figure 5-8, with the horizontal scale 100 kHz per division and the vertical scale in DB's. Unfortunately the vertical scale on the analyzer could not be calibrated, but a linear examination of the sideband near 360 kHz indicated approximately 50 dB difference between it and the major lobe. This corresponds closely with the theoretical results predicted. The important thing to notice is the location of the various side-lobes. There is one at approximately 93 kHz, the major lobe at 186 kHz, another sidelobe at 279 kHz, and so forth at 93 kHz increments through the band. This sidelobe placement was predicted by the theoretical analysis performed.

## 2. VCO REPLACEMENT

Voltage controlled oscillators are generally evaluated in terms of frequency linearity, amplitude and frequency stability, pull-in range, harmonic distortion ratios, and harmonic content. These are by no means the only criteria used, but are some of the major ones. The evaluation of the digital oscillator in terms of the indicated criteria is included in this section. Also

Reproduced from  
best available copy.

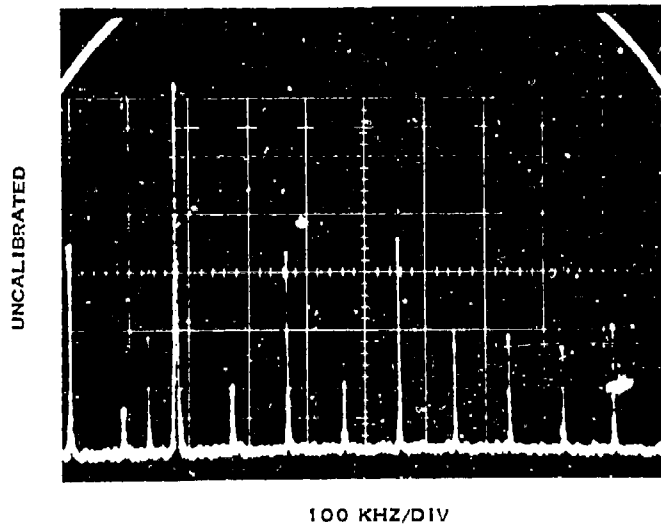


Figure 5-8. DO Spectrum for Input Frequency of 186.413 Hz

included are discussions of the performance of the digital oscillator VCO replacement configuration functioning in linear angle modulation and frequency shift keying applications.

a. Frequency Linearity

Figure 5-9 illustrates the frequency versus dc-input characteristics for the breadboard operating as a VCO replacement. The frequency axis is measured with respect to the quiescent frequency of the VCO, thus the label  $\Delta$ frequency. The curve is obviously very linear in the region  $\pm 16$  kHz of the quiescent frequency.

b. Amplitude and Frequency Stability

There is no reason to even consider amplitude stability of the digital oscillator since the output peak amplitude is fixed and constant for all frequencies. The frequency stability was discussed in Section V, paragraph B. 1. a. The net conclusion is however that amplitude and frequency stability are no problem with the digital oscillator when operating as a VCO replacement.

c. Pull-In Range

The pull-in range of the digital oscillator operating as a VCO is determined by the word size of the analog-to-digital (A/D) converter used in converting the analog control voltage. For a word size of M bits, the pull-in range is  $2^M$  Hz for the 1 Hz resolution of the breadboard. Therefore, any pull-in range can be obtained, at least to within the limitations of conventional A/D converters.

d. Harmonic Distortion and Harmonic Content

Both harmonic distortion and harmonic content were examined in the previous section on evaluation of the frequency synthesizer configurations, and were found to be quite acceptable. The analysis also holds for this configuration.

e. Application Analysis

The digital oscillator has been shown to meet the basic requirements necessary to operate as a VCO replacement. It is of interest therefore, to include some basic applications and the performances for each. The two applications considered are angle modulation and frequency shift keying.

- 1) Angle Modulation. It is generally quite difficult to evaluate the performance of a VCO in an angle modulation application. One method is to examine the frequency spectrum of the modulated output signal from the VCO. For high modulation indices, the frequency spectrum should approach a form similar to the den-

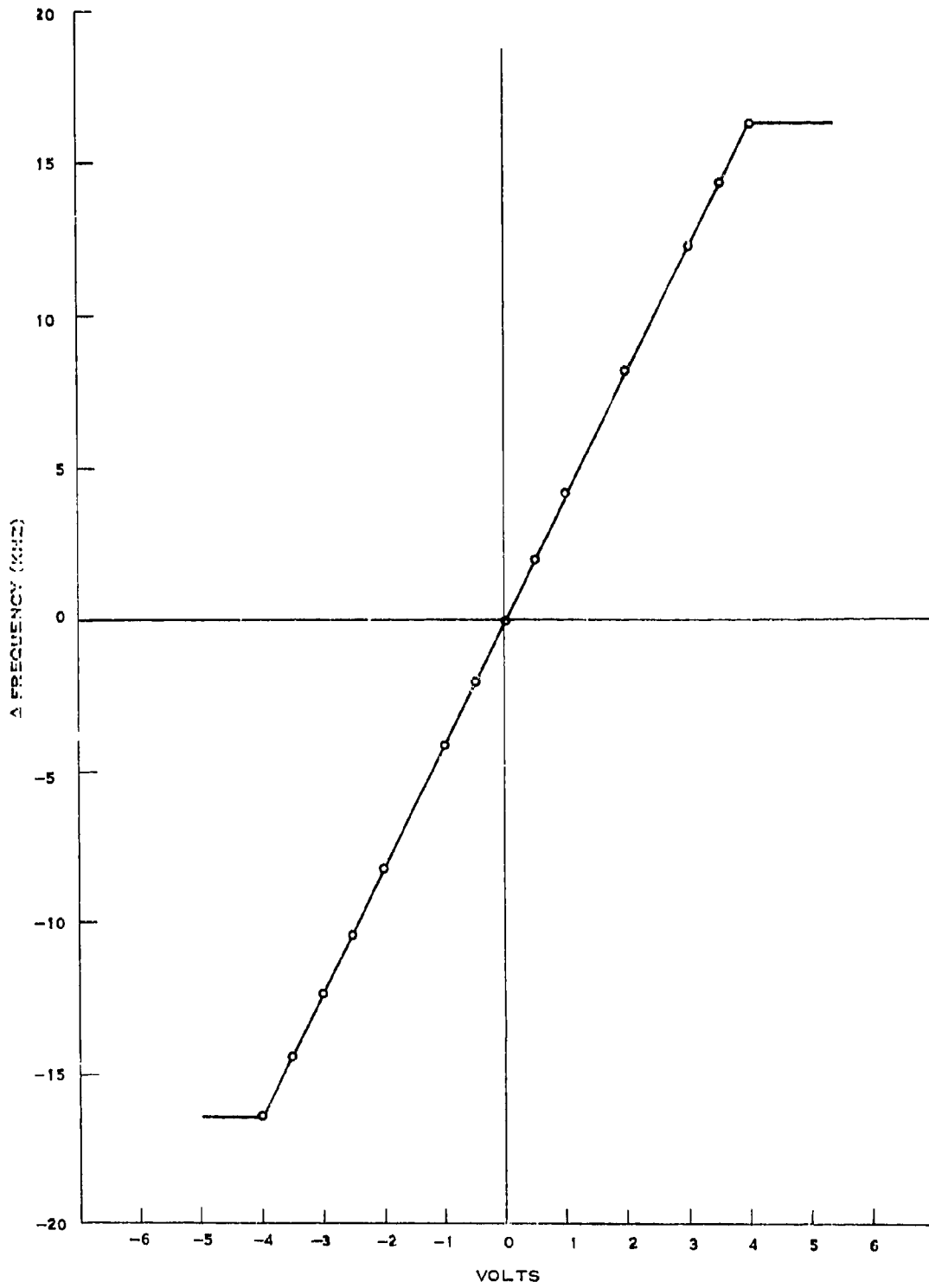


Figure 5-9.  $\Delta f$  vs Voltage FM Mode Digital Oscillator

sity function of the modulating signal. For sinusoidal modulation, the density function is as shown in Figure 5-10 (for uniformly distributed phases)<sup>14</sup>.

The frequency spectrum of the VCO configuration for sinusoidal modulation and a modulation index of 100 is shown in Figure 5-11. The procedure used is the same as that discussed in Section V. B. 1. c. The spectrum does in fact look very much like the density function for a sinusoid shown in Figure 5-10, as theoretically predicted.

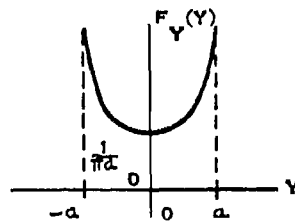


Figure 5-10. Density Function of Sinusoid of Peak  $a$ .

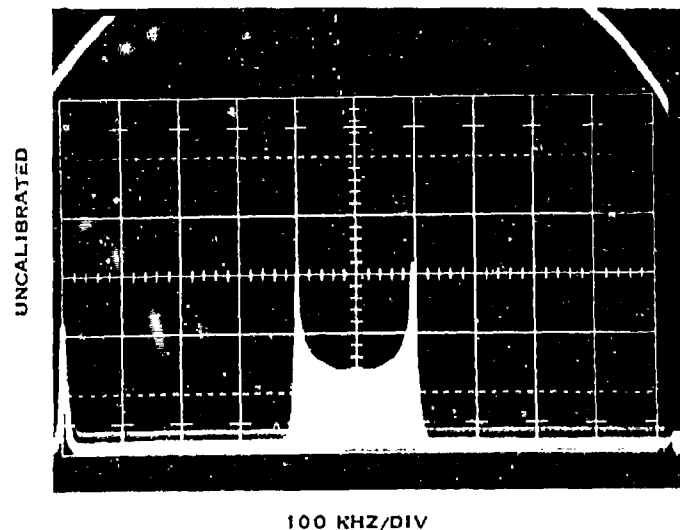
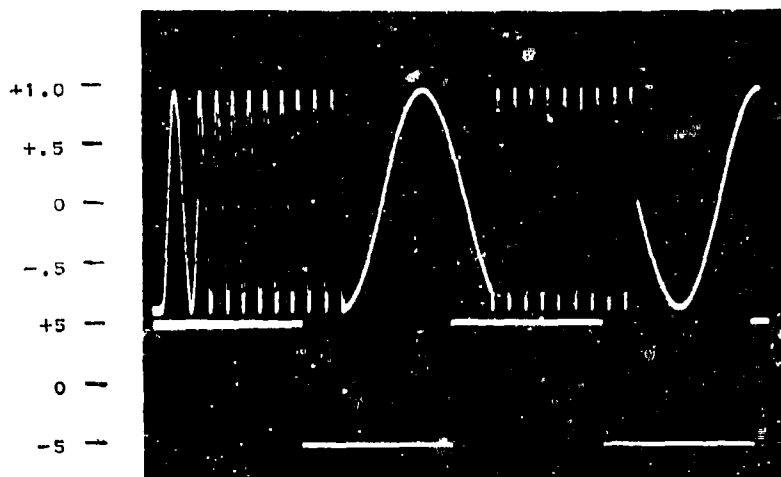


Figure 5-11. Frequency Spectrum for VCO Configuration

- 2) Frequency Shift Keying (FSK). The FSK application is demonstrated by changing the modulating signal from sinusoidal to a square wave, and using the frequency modulation set-up. VCO's operating in FSK applications are generally evaluated in terms of the time required to change from one frequency to the other and in terms of continuity in phase. Figure 5-12 presents the output modulated signal from the digital oscillator (traces a) for a square wave modulating signal (trace b). (The square wave and the output waveform are not synchronized-an operator error). The figure, however, illustrates the instantaneous changes in frequency and the absolute continuity in phase, both very desirable properties of a VCO for FSK applications.



100 KHZ/DIV  
Reproduced from  
best available copy.

Figure 5-12. FSK Application of DO

## SECTION VI CONCLUSIONS

### A. SUMMARY

Two basic techniques for synthesizing digital oscillators have been discussed. The first, the recursive technique, resulted from an examination of the difference equations describing the relationship between the present output and some linear combination of past outputs and inputs. It has been shown that the coefficients of the difference equation result in poles which are on the unit circle (in the  $z$  domain). These poles are, therefore, inherently unstable, with the result being an error build-up in the output sequence. These errors were shown to increase linearly with time - a very undesirable situation. Three techniques were presented for reducing this error build-up, but none could provide perfect or even near perfect error correction.

The second, the nonrecursive technique, uses a read-only-memory (ROM) look-up table where a number of samples from one cycle of a sinusoid have been prestored. These samples are selectively extracted from the ROM to generate the desired output sequence. It is physically impossible to store all samples for one cycle of a sinusoid in a finite size ROM; therefore, errors must occur in the amplitude of the output sequence. These errors are, however, bounded and were shown to be less than 2.45 percent for an ROM containing the equivalent of 256 sample values.

Two basic configurations for application of digital oscillators, frequency synthesizers and voltage controlled oscillator (VCO) replacements, were suggested. The inherent error build-up (either with or without error correction), the complexity, and the required low frequency operation (because of the time required to perform the indicated arithmetic operations) have combined to eliminate the recursive technique for digital oscillator synthesis from use in the two basic configurations. On the other hand, the nonrecursive technique is directly amenable to these configurations as a result of its low cost, relatively high speed (10 MHz upper limit)\*, and bounded error.

A breadboard was constructed utilizing the nonrecursive technique for digital oscillator synthesis. For demonstrating the frequency synthesizer configuration, modes for both frequency synthesizer and frequency translator applications were provided. For VCO replacements, modes for frequency modulation (FM) and tracking filter applications were similarly included.

Experimental evaluation of the breadboard was performed, with favorable results obtained. In frequency synthesizer configurations, the following

---

\*The breadboard has been designed with a 1 MHz maximum frequency, but present logic speeds would allow synthesis up to 10 MHz.

results were obtained: 1. The stability was shown to be entirely dependent on the crystal clock used as the fundamental; 2. The harmonic distortion was less than 2 percent for the entire 1 Hz to 1 MHz range; and 3. The harmonics present were separated in frequency enough to allow conventional filtering techniques to be used where lower harmonic levels are desired.

As a VCO replacement, the frequency linearity around the quiescent was shown to be extremely good, and the pull-in range, determined entirely by system design requirements, may be increased or decreased simply by modifying the digital logic.

All things considered, the nonrecursive technique for digital synthesis of oscillators has been shown to operate as well, if not better, than conventional analog circuits in the basic configurations, frequency synthesizer and VCO replacement.

## B. RECOMMENDATIONS

1. The nonrecursive technique for digital oscillator synthesis has found wide application in communication related areas; many of these have been discussed in this final report. It would therefore, be of benefit to consider the application of large-scale integration (LSI) implementation procedures to the nonrecursive digital oscillator algorithm. The desired result would be a single chip containing the ROM and necessary arithmetic units, where the algorithm would be kept as general purpose as possible.
2. The breadboard has demonstrated that both high resolution (1 Hz resolution for a 4 MHz crystal clock) and high stability are possible using the nonrecursive technique. Many applications, and in particular the instrument landing system (ILS) application, require both high resolution and high stability. In the ILS application, a linear swept frequency is generated and transmitted to incoming aircraft. The aircraft receives a small segment of the sweep-the frequency of the segment indicating position with respect to some reference. Conventional VCO's cannot maintain the sweep accuracy necessary to achieve the required position accuracy, and therefore, are of minimal value. It is therefore suggested that some effort be devoted to this type application, where high resolution and/or high stability are required, to determine: (1) if a nonrecursive digital oscillator is applicable, and (2) if any improvement in system performance would result from the use of the digital oscillator.
3. The recursive nonlinear demodulator (RNLD) discussed in Section III. C of the final report appears to be capable of providing near-optimum threshold extension technique for digitalized FM

receivers. It merits further investigation. Included below are some suggestions for further investigation in this area:

- a. A computer simulation should be developed to compare the SNR performance of the RNLD and other FM demodulation techniques. Both single sinewave modulating signals and synthetic broadband modulating signals should be used in the testing. The effect of different message models (filters) on the SNR performance should be considered.
- b. Simplification of the gain matrix equation should be sought and the effects of these simplification on the SNR performance investigated. It would also be interesting to analyze the threshold phenomena of the RNLD and compare this with the more classical 'click' analysis of FM demodulators contained in literature. Application of the RNLD techniques to other problems of angle demodulation should also be pursued.
- c. Finally, a breadboard model of the RNLD should be fabricated that would be capable of demodulating narrowband FM voice. The above two suggested investigations would help direct the design of the breadboard to the most cost effective configuration.

## REFERENCES

1. Langenthal, I.M., Digital Technique Study, RADC Final Technical Report No. RADC-TR-69-27.
2. Rader, C.M., and Gold, B., "Effects of Quantization Noise in Digital Filters," Proc. SJCC, 1966.
3. Page Comm. Eng., Adaptive Data Modern, RADC Final Technical Report No. RADC-TR-69-296.
4. Kaiser, J. F., "Some Practical Considerations in the Realization of Linear Digital Filters," 3rd Allerton Conference, 1965.
5. Rader, C.M., and Gold, B., "Effects of Parameter Quantization on the Poles of a Digital Filter," Proc. IEEE, May 1967.
6. Viterbi, A. J., Principles of Coherent Communication, McGraw Hill, 1966.
7. Gardner, F.M., Phase-Lock Techniques, Wiley, 1966.
8. Larimore, W. E., "Design and Performance of a Second Order Digital Phase-Locked Loop," Proceedings of Symposium on Computer Processing in Communications, 1969.
9. Pitt, S.P. and Grace, O. D., "Signal Processing by Digital Quadrature Techniques," DRL Report No. DRL-TR-68-39.
10. Jury, E. I., Theory and Application of the Z-transform Method, John Wiley, 1964.
11. Sage, Andrew P., "Optimum System Control", Prentice-Hall, 1968.
12. VanTrees, Harry L., "Detection, Estimation, and Modulation Theory-Part II Nonlinear Modulation Theory," Wiley, 1971.
13. Bennett, W.R., Stein, S. and Schwartz, M., "Communication Systems and Techniques," McGraw-Hill, 1966.
14. Schwartz, Mischa, "Information Transmission, Modulation, and Noise," McGraw-Hill, 1970.

APPENDIX A  
IN-PHASE AND QUADRATURE SAMPLING

APPENDIX A  
IN-PHASE AND QUADRATURE SAMPLING

A. INTRODUCTION

Quadrature sampling techniques have been discussed by Fritchman<sup>1</sup> and by Pitt and Grace,<sup>2</sup> with the latter being a very detailed discussion. A discussion of the technique itself and of the resulting errors introduced are included in this appendix. Also included are discussions of phase incoherent AM, PM, and FM demodulation using quadrature components.

B. QUADRATURE SAMPLING

Let  $y(t)$  be a narrow band-pass signal modulated by a carrier  $f_c$ ; i. e.,

$$y(t) = A(t) \cos [2\pi f_c t + \phi(t) + \theta] \quad (1)$$

where  $\phi(t)$  represents some dynamic phase variation and  $\theta$  an arbitrary but constant phase angle. Reexpressing  $y(t)$  as a function of the quadrature components results in

$$y(t) = u(t) \cos 2\pi f_c t + v(t) \sin 2\pi f_c t \quad (2)$$

where:

$$\begin{aligned} u(t) &= A(t) \cos [\phi(t) + \theta] \\ v(t) &= -A(t) \sin [\phi(t) + \theta] \end{aligned} \quad (3)$$

Since  $y(t)$  is narrow band-pass, the frequencies are confined to the interval

$$f_c - \frac{W}{2} \leq |f_0| \leq f_c + \frac{W}{2} \quad (4)$$

where  $f_c > \frac{W}{2}$ . Therefore, the frequencies of  $u(t)$  and  $v(t)$  are confined to

$$-\frac{W}{2} \leq f_0 \leq \frac{W}{2} \quad (5)$$

The relationship of the quadrature components of  $u(t)$  and  $v(t)$  to the demodulated signal  $x(t)$  is a function of the type of modulation. These relationships, known as inverse modulation techniques, for various modulation types are shown in Table I.

Table I. Relations Between Quadrature Components and Demodulated Signal  $x(t)$

<u>Modulation Type</u>	<u>Modulating Signal</u>
AM-SSB	$x(t) = u(t)$
AM-DSB	$x(t) = u(t)$
Suppressed carrier	$x(t) = u(t)$
Injected carrier	$x(t) = K - u(t)$
PM	$x(t) = \frac{1}{\beta} \tan^{-1} [v(t)/u(t)]$
FM	$x(t) = \frac{1}{\beta} \frac{d}{dt} \tan^{-1} [v(t)/u(t)]$

If, however, a phase incoherent scheme for demodulation is used, the relationships become as shown in Table II.

Table II. Relations Between Quadrature Components and Demodulated Signal  $x(t)$  for Incoherent Phase ( $\phi_0$ )

<u>Modulation Type</u>	<u>Demodulated Signal</u>
AM-SSB	$x(t) = \sqrt{u^2(t) + v^2(t)}$
AM-DSB	$x(t) = \sqrt{u^2(t) + v^2(t)}$
Suppressed carrier	$x(t) = \sqrt{u^2(t) + v^2(t)}$
Injected carrier	$x(t) = K - \sqrt{u^2(t) + v^2(t)}$
PM	$x(t) = \frac{1}{\beta} \tan^{-1} [v(t)/u(t)] - \frac{1}{\beta} \phi_0$
FM	$x(t) = \frac{1}{\beta} \frac{d}{dt} \tan^{-1} [v(t)/u(t)]$

Obviously, if the quadrature components of a received signal are known, the demodulation process is trivial. It is, therefore, of benefit to examine a method for obtaining these components.

The recovery procedure is as follows. Assume  $y(t)$  is sampled at the instants  $(n/fc)$  and  $(n/fc) + (1/4fc)$ : e. g.

$$\begin{aligned}
 y\left(\frac{n}{f_c}\right) &= u\left(\frac{n}{f_c}\right) \cos 2\pi n + v\left(\frac{n}{f_c}\right) \sin 2\pi n \\
 &= u\left(\frac{n}{f_c}\right)
 \end{aligned}
 \tag{6}$$

$$\begin{aligned}
 y\left(\frac{n}{f_c} + \frac{1}{4f_c}\right) &= u\left(\frac{n}{f_c} + \frac{1}{4f_c}\right) \cos\left(2\pi n + \frac{\pi}{2}\right) \\
 &\quad + v\left(\frac{n}{f_c} + \frac{1}{4f_c}\right) \sin\left(2\pi n + \frac{\pi}{2}\right) \\
 &= v\left(\frac{n}{f_c} + \frac{1}{4f_c}\right)
 \end{aligned}
 \tag{7}$$

These sample values are the in-phase and quadrature components evaluated at  $(n/f_c)$  and  $(n/f_c) + (1/4f_c)$  respectively.

Since  $u(t)$  and  $v(t)$  have frequencies less than  $(W/2)$ , Nyquist criterion is satisfied if they are sampled at  $2(W/2)$  or  $WHz$ . It is, therefore, unnecessary to sample  $y(t)$  at  $f_c$  Hz, but instead at  $WHz$  to recover  $u(t)$  and  $v(t)$  completely.

To take advantage of the quadrature sampling technique,  $y(t)$  must, however, be sampled at time instants  $(i/f_c)$  and  $(i/f_c) + (1/4f_c)$  where  $i$  is any integer. If an integer  $k$  is selected such that

$$k \leq \frac{f_c}{W} \tag{8}$$

then  $nk$  will be an integer. The samples  $y(nk/f_c)$  and  $y[(nk/f_c) + (1/4f_c)]$ , therefore, satisfy the Nyquist requirements for sampling  $u(t)$  and  $v(t)$  and also those requirements necessary for quadrature sampling. These samples are given by

$$\begin{aligned}
 y\left(\frac{nk}{f_c}\right) &= u\left(\frac{nk}{f_c}\right) \\
 y\left(\frac{nk}{f_c} + \frac{1}{4f_c}\right) &= v\left(\frac{nk}{f_c} + \frac{1}{4f_c}\right)
 \end{aligned}
 \tag{9}$$

and are the quadrature components. They are, however, taken at sample times differing by  $(1/4f_c)$  seconds. To take advantage of the relations in Tables I and II the samples must be taken at the same time. Errors are therefore introduced; methods of handling these errors are discussed next.

### C. ERROR ANALYSIS

Pitt and Grave have discussed the errors associated with quadrature sampling very thoroughly and subsequently define three types of errors; 1) those due to the time difference between the quadrature components, 2) those due to imprecise sampling such as that expected from any A/D converter, and 3) errors resulting from sampling at some rate other than  $(f_c/k)$ .

The errors of 1) are a result of making the following assumption:

$$v\left(\frac{nk}{f_c} + \frac{1}{4f_c}\right) \cong v\left(\frac{nk}{f_c}\right) \quad (10)$$

The error (in percent) in making this assumption is given by:

$$\epsilon = \left| v\left(\frac{nk}{f_c} + \frac{1}{4f_c}\right) - v\left(\frac{nk}{f_c}\right) \right| \cdot 100 \text{ percent} \quad (11)$$

If  $v(t)$  is a sine wave of maximum frequency  $W/2$ , the maximum error occurs at  $(nk/f_c)$  equal to  $0, \pm\pi, \pm2\pi, \text{ etc.}$  Therefore,

$$\begin{aligned} \epsilon_{\max} &= \left| \sin \left[ 2\pi \frac{W}{2} \left( \frac{1}{4f_c} \right) \right] \right| \cdot 100 \\ &= \left| \sin \frac{\pi W}{4f_c} \right| \cdot 100 \text{ percent} \end{aligned}$$

Letting  $\ell = f_c/W$ , the carrier frequency vs. bandwidth ratio, the error becomes

$$\epsilon_{\max} = \left| \sin \frac{\pi}{4\ell} \right| \cdot 100 \text{ percent}$$

The error  $\epsilon_{\max}$  as a function of  $\ell$  is shown in the following:

$\ell = 1$	$\epsilon_{\max} = 70.7\%$
$\ell = 10$	$\epsilon_{\max} = 7.8\%$
$\ell = 100$	$\epsilon_{\max} = 0.78\%$
$\ell = 1000$	$\epsilon_{\max} = 0.078\%$

This analysis is worst case since the maximum possible frequency for  $v(t)$  was selected, and clearly indicates that the time difference error becomes trivial for relatively large carrier versus bandwidth ratios.

The errors of type 2) have been thoroughly discussed by Radar and Gold<sup>3</sup> and Kaiser<sup>4</sup>, to name a few, and will not be included here.

Errors of type 3) result from inexact knowledge of the carrier frequency, and therefore, incorrect sampling. This is illustrated by assuming a sampling rate of  $(f_c/k)$  for a carrier of frequency  $(f_c + \Delta i)$ ; i. e., the estimate of  $u$ ,  $\hat{u}$ , becomes:

$$\begin{aligned}
\hat{u} &= y\left(\frac{nk}{f_c}\right) = u\left(\frac{nk}{f_c}\right) \cos\left[2\pi(f_c + \Delta f)\frac{nk}{f_c}\right] + \\
&\quad v\left(\frac{nk}{f_c}\right) \sin\left[2\pi(f_c + \Delta f)\frac{nk}{f_c}\right] \\
&= u\left(\frac{nk}{f_c}\right) \left[\cos 2\pi nk \cos \frac{2\pi nk \Delta f}{f_c} - \sin 2\pi nk \sin \frac{2\pi nk \Delta f}{f_c}\right] \\
&\quad + v\left(\frac{nk}{f_c}\right) \left[\sin 2\pi nk \cos \frac{2\pi nk \Delta f}{f_c} + \cos 2\pi nk \sin \frac{2\pi nk \Delta f}{f_c}\right] \\
&= u\left(\frac{nk}{f_c}\right) \cos \frac{2\pi nk \Delta f}{f_c} + v\left(\frac{nk}{f_c}\right) \sin \frac{2\pi nk \Delta f}{f_c}
\end{aligned} \tag{12}$$

The estimate of  $v$ ,  $\hat{v}$ , is similarly obtained and is given by:

$$\begin{aligned}
\hat{v} &= y\left(\frac{nk}{f_c} + \frac{1}{4f_c}\right) = -u\left(\frac{nk}{f_c} + \frac{1}{4f_c}\right) \sin\left[2\pi\left(nk + \frac{1}{4}\right)\frac{\Delta f}{f_c}\right] \\
&\quad + v\left(\frac{nk}{f_c} + \frac{1}{4f_c}\right) \cos\left[2\pi\left(nk + \frac{1}{4}\right)\frac{\Delta f}{f_c}\right]
\end{aligned} \tag{13}$$

The resulting terms  $\hat{u}$  and  $\hat{v}$  might at first appear to be simple  $u(nk/f_c)$  and  $v(nk/f_c + 1/4f_c)$  respectively, since  $\Delta f/f_c$  is a small quantity. This, however, is not the case because the multiplier  $nk$  is linearly increasing with time. Each estimate actually tends to move in and out of phase with its respective quadrature component. These estimates  $\hat{u}$  and  $\hat{v}$  can, therefore, not be expected to be the exact quadrature components as a result of the phase error.

#### D. AM, PM, AND FM DEMODULATION USING $u$ AND $v$

The question naturally arises as to what effect the error type 3 will have on the demodulation schemes as defined by Tables I and II. This will now be considered.

Non-coherent AM demodulation will be unaffected if the following holds:

$$\hat{u}^2\left(\frac{nk}{f_c}\right) + \hat{v}^2\left(\frac{nk}{f_c}\right) = u^2\left(\frac{nk}{f_c}\right) + v^2\left(\frac{nk}{f_c}\right) \tag{14}$$

which is simply the requirement that the envelopes be identical. The envelopes for the estimates are obtained as follows from Equations (12) and (13):

$$\begin{aligned}
\hat{u}^2\left(\frac{nk}{f_c}\right) &= u^2\left(\frac{nk}{f_c}\right) \cos^2 \frac{2\pi nk \Delta f}{f_c} + v^2\left(\frac{nk}{f_c}\right) \sin^2 \frac{2\pi nk \Delta f}{f_c} \\
&\quad + u\left(\frac{nk}{f_c}\right) v\left(\frac{nk}{f_c}\right) \sin \frac{4\pi nk \Delta f}{f_c}
\end{aligned} \tag{15}$$

$$\begin{aligned} \hat{v}^2\left(\frac{nk}{f_c} + \frac{1}{4f_c}\right) &= u^2\left(\frac{nk}{f_c} + \frac{1}{4f_c}\right) \sin^2\left(\frac{2\pi nk\Delta f}{f_c} + \frac{\pi\Delta f}{2f_c}\right) \\ &\quad + v^2\left(\frac{nk}{f_c} + \frac{1}{4f_c}\right) \cos^2\left(\frac{2\pi nk\Delta f}{f_c} + \frac{\pi\Delta f}{2f_c}\right) \\ &\quad - u\left(\frac{nk}{f_c} + \frac{1}{4f_c}\right) v\left(\frac{nk}{f_c} + \frac{1}{4f_c}\right) \sin\left(\frac{4\pi nk\Delta f}{f_c} + \frac{\pi\Delta f}{f_c}\right) \end{aligned}$$

Assuming  $\frac{1}{4f_c} \ll \frac{k}{f_c}$ ,  $\hat{v}^2$  reduces to:

$$\begin{aligned} \hat{v}^2\left(\frac{nk}{f_c}\right) &= u^2\left(\frac{nk}{f_c}\right) \sin^2\frac{2\pi nk\Delta f}{f_c} + v^2\left(\frac{nk}{f_c}\right) \cos^2\frac{2\pi nk\Delta f}{f_c} \\ &\quad - u\left(\frac{nk}{f_c}\right) v\left(\frac{nk}{f_c}\right) \sin\frac{4\pi nk\Delta f}{f_c} \end{aligned}$$

Combining  $\hat{u}^2$  and  $\hat{v}^2$  and remembering that  $\cos^2\theta + \sin^2\theta = 1$  for arbitrary  $\theta$  results in:

$$\hat{v}^2\left(\frac{nk}{f_c}\right) + \hat{u}^2\left(\frac{nk}{f_c}\right) = u^2\left(\frac{nk}{f_c}\right) + v^2\left(\frac{nk}{f_c}\right)$$

The estimates  $u$  and  $v$  can thus be used for non-coherent AM demodulation since the envelopes have been shown to be identical.

To use  $\hat{u}$  and  $\hat{v}$  for PM and FM, the following conditions must hold:

$$\begin{aligned} \text{PM: } \tan^{-1}\left(\frac{\hat{v}}{\hat{u}}\right) &= \tan^{-1}\left(\frac{v}{u}\right) \\ \text{FM: } \frac{d}{dt} \tan^{-1}\left(\frac{\hat{v}}{\hat{u}}\right) &= \frac{d}{dt} \tan^{-1}\left(\frac{v}{u}\right) \end{aligned} \quad (16)$$

Forming the ratio of  $\hat{v}$  and  $\hat{u}$  results in:

$$\frac{\hat{v}}{\hat{u}} = \frac{-u\left(\frac{nk}{f_c}\right) \sin\frac{2\pi nk\Delta f}{f_c} + v\left(\frac{nk}{f_c}\right) \cos\frac{2\pi nk\Delta f}{f_c}}{u\left(\frac{nk}{f_c}\right) \cos\frac{2\pi nk\Delta f}{f_c} + v\left(\frac{nk}{f_c}\right) \sin\frac{2\pi nk\Delta f}{f_c}} \quad (17)$$

Letting  $u(nk/f_c) = \cos\alpha$ ,  $v(nk/f_c) = \sin\alpha$ , and  $\xi = 2\pi nk\Delta f/f_c$ ,  $(\hat{v}/\hat{u})$  becomes:

$$\begin{aligned} \frac{\hat{v}}{\hat{u}} &= \frac{-\cos\alpha \sin\xi + \sin\alpha \cos\xi}{\cos\alpha \cos\xi + \sin\alpha \sin\xi} \\ &= \frac{\sin(\alpha - \xi)}{\cos(\alpha - \xi)} = \tan(\alpha - \xi) \end{aligned}$$

Taking the arctangent of  $(\hat{v}/\hat{u})$ ,

$$\tan^{-1} \left( \frac{\hat{v}}{\hat{u}} \right) = \alpha - \xi$$

and substituting for  $\alpha = \tan^{-1} \left( \frac{v}{u} \right)$  and for  $\xi$ ,

$$\tan^{-1} \left( \frac{\hat{v}}{\hat{u}} \right) = \tan^{-1} \left( \frac{v}{u} \right) - \frac{2\pi nk \Delta f}{f_c} \quad (18)$$

it is obvious that the condition specified in equation (16) for PM demodulation does not hold, and instead has an additive linearly increasing function of time as an extra term. This additive term eliminates the possibility of using quadrature samples where there is a possible frequency error for PM demodulation unless a third order loop is used to perform the demodulation. To check for FM demodulation, the time derivative of Equation (18) is taken and becomes:

$$\frac{d}{dt} \tan^{-1} \left( \frac{\hat{v}}{\hat{u}} \right) = \frac{d}{dt} \left[ \tan^{-1} \left( \frac{v}{u} \right) - \frac{2\pi nk \Delta f}{f_c} \right] \quad (19)$$

The condition in Equation (19) also does not hold for FM, but the difference is an additive constant phase rather than a ramp. The FM demodulation can now be accomplished using a second order loop.

#### E. PHASE INCOHERENT RECEIVER

The underlying assumption in the analysis up to now has been that the transmitter and receiver are in phase; i. e., phase coherent, but incoherent in frequency. Transmitters and receivers are generally frequency locked but incoherent in phase. The estimates  $\hat{u}$  and  $\hat{v}$  for an arbitrary but constant phase shift  $\theta$ , corresponding to a phase incoherent system, are:

$$\begin{aligned} \hat{u} \left( \frac{nk}{f_c} \right) &= u \left( \frac{nk}{f_c} \right) \cos \theta + v \left( \frac{nk}{f_c} \right) \sin \theta \\ \hat{v} \left( \frac{nk}{f_c} \right) &= -u \left( \frac{nk}{f_c} \right) \sin \theta + v \left( \frac{nk}{f_c} \right) \cos \theta \end{aligned} \quad (20)$$

Using the same method as in Equation (15) and after making the assumption that  $1/4f_c \ll k/f_c$  results in:

$$\hat{u}^2 \left( \frac{nk}{f_c} \right) + \hat{v}^2 \left( \frac{nk}{f_c} \right) = u^2 \left( \frac{nk}{f_c} \right) + v^2 \left( \frac{nk}{f_c} \right)$$

and thus indicates equivalence of the envelopes. To determine equivalence of the conditions specified in Table II for PM and FM, the steps resulting in Equations (17), (18), and (19) are followed with these results obtained:

$$\tan^{-1}\left(\frac{\hat{v}}{\hat{u}}\right) = \tan^{-1}\left(\frac{v}{u}\right) - \theta \quad (21)$$

$$\frac{d}{dt} \tan^{-1}\left(\frac{\hat{v}}{\hat{u}}\right) = \frac{d}{dt} \tan^{-1}\left(\frac{v}{u}\right)$$

These favorable results indicate that quadrature sampling techniques are also well suited to phase incoherent receivers.

#### REFERENCES

1. B. Fritchman, C. Gumacos, A. Wright, and T. Hornsby, Digital Equivalent Transceivers Study, Final Report No. RADC-TR-68-539.
2. S. P. Pitt and O. D. Grace, Signal Processing by Digital Quadrature Techniques, Final Report No. DRL-TR-68-39.
3. C. M. Rader and B. Gold, "Effects of Quantization Noise in Digital Filters", Proc. SJCC, 1966.
4. J. F. Kaiser, "Some Practical Considerations in the Realization of Linear Digital Filters", 3rd Allerton Conference, 1965.

APPENDIX B  
A NONLINEAR DIGITAL PROCESSOR FOR FM DEMODULATION

## ABSTRACT

A recursive estimator is derived that will optimally estimate the message of a noisy sampled FM process. The incoming analog FM process is in-phase and quadrature sampled to reduce the bandpass RF waveforms to a sampled baseband process. It is shown that the angle process can be modeled as a discrete linear filter amenable to state variable description. The maximum a posteriori (MAP) criterion is used to develop a recursive cost function. Minimization techniques used in optimal control theory are employed to derive the two-point boundary-value (TPBV) problem from this cost function. Discrete invariant imbedding techniques are then used to solve the TPBV problem and obtain the recursive solution. A single-pole message filter example is reviewed, where computer simulations indicate threshold extension of approximately 6 dB above the conventional discriminator. An above-threshold-linear model is also discussed.

## APPENDIX B

### A NONLINEAR DIGITAL PROCESSOR FOR FM DEMODULATION

#### A. INTRODUCTION

Threshold extension for FM demodulators has been an active area of investigation for the past 20 years. Numerous demodulator configurations have been developed that achieve better threshold performance than the fundamental (conventional) discriminator. Such descriptors as FM with feedback<sup>1</sup> (FMFB), phase-locked loop demodulators (FMPLL), extended range phase-locked loop demodulator (ERPLL), etc., have been used in the analog world to describe low-threshold FM demodulators. At high signal-to-noise (SNR) above threshold the demodulators have almost identical performance in that they provide a linear (in DB) relationship between output SNR and input carrier-to-noise (CNR) ratio. As the CNR decreases, the threshold phenomenon is encountered which results in a drastic decrease in output SNR for a small decrease in CNR; the purpose of the threshold extension FM demodulator is then to lower this critical CNR where threshold occurs and thus extend the operating range of the radio link. As is usually the case, the better the threshold performance of a demodulator the more complex the circuit configuration becomes.

A stored or wired program digitalized FM demodulator can do a simple or a very complex demodulation algorithm while using the same basic circuit configuration; the operations per second may change, but not the network configuration. The objective of this paper is to present the synthesis and evaluation of a digitalized FM demodulator obtained by employing the principles of Bayesian estimation theory coupled with optimal control minimization techniques. The demodulator is necessarily a threshold extension demodulator since it is synthesized to provide near optimum estimation of the message in the presence of noise. Some optimum estimators only provide bounds and are not feasible to implement. In this synthesis scheme, however, a recursive estimation or filtering solution is derived which calculates the best estimate as each data word arrives. Accordingly, the configuration becomes a recursive digital feedback filter which also has time varying gain.

First to be discussed is in-phase and quadrature sampling and how it is related to sampling FM carrier processes. It is shown that this sampling technique permits baseband samples to be obtained directly from the received carrier or IF signal. Next, the modulator is characterized by a continuous-time state variable model. This model is then transformed to a discrete state variable modulator model which is used to derive the general recursive solution algorithm. Both Bayesian estimation theory and optimum control theory are employed to develop the solution. After this, a realization of the algorithm is discussed where the message spectrum is characterized by a single-pole filter. This configuration was simulated and tested for a sinewave

modulating signal and signal-to-noise performance curves obtain from this simulation are presented. The demodulator exhibits threshold extension capability of approximately 6 db better than the conventional discriminator demodulator. Better threshold performance is predicted for more complex message filters. The form of the demodulator resembles a phase-locked-loop demodulator with a time-varying gain processor. It is shown that these time-varying gain elements approach steady state values for above-threshold operation of the demodulator, hence, linearization of the demodulator is possible. Finally, characteristics of the linear model are discussed.

## B. IN-PHASE AND QUADRATURE SAMPLING OF AN FM PROCESS

The fundamental equation for the output  $s(t)$  of a frequency modulated waveform is:

$$s(t) = \sqrt{2}a \cos [2\pi f_0 t + \theta(t)] \quad (1)$$

where  $\sqrt{2}a$  is the amplitude,  $f_0$  is the carrier frequency, and  $\theta(t)$  is the angle modulated process which for FM is given by:

$$\theta(t) = c \int_{t_0}^t x(u) du \quad (2)$$

In this expression for  $\theta(t)$ , the modulating waveform is  $x(t)$  and  $c$  is the so-called frequency deviation. Simple trigonometric identities permit  $s(t)$  of Equation (1) to be rewritten in a convenient form for explaining in-phase and quadrature sampling:<sup>2</sup>

$$s(t) = \sqrt{2}a [\cos(2\pi f_0 t) \cos\theta(t) - \sin(2\pi f_0 t) \sin\theta(t)] \quad (3)$$

Suppose that  $s(t)$  is a bandpass process with bandwidth  $W$  and let  $s(t)$  be sampled at  $t = kI/f_0$ , where  $f_0$  is the carrier frequency,  $k$  is the sample time index, and  $I$  is an integer such that  $I \leq f_0/W$ , then it can be shown\* that

$$s(kI/f_0) = \sqrt{2}a \cos\theta(kI/f_0) \quad (4)$$

which is called the in-phase sample. Similarly, if  $s(t)$  is sampled at  $1/4f_0$  seconds later, i. e.,  $t = (kI/f_0 + 1/4f_0)$ ; then,

$$s(kI/f_0 + 1/4f_0) = -\sqrt{2}a \sin\theta(kI/f_0 + 1/4f_0) \quad (5)$$

---

\*See Appendix A for a more detailed discussion of in-phase and quadrature sampling.

This is called the quadrature sample. Usually,  $f_0 \ll 1$ , then,

$$\theta(kI/f_0 + 1/4f_0) \approx \theta(kI/f_0) \quad (6)$$

and the bandpass process is reduced to a baseband process by an appropriate sampling technique. Since two samples are necessary to describe the baseband sample, a vector description becomes a natural representation, i. e.,

$$\underline{h}(kT) = \begin{bmatrix} h_1 \\ h_2 \end{bmatrix} = \sqrt{2}a \begin{pmatrix} \cos\theta(kT) \\ -\sin\theta(kT) \end{pmatrix} \quad (7)$$

where  $T$ , the sample interval, is  $T = 1/f_0$ .

When the FM process of equation (1) is passed through a noisy channel the observed in-phase and quadrature sample vector  $Z(k)$  will consist of the signal sample vector as well as in-phase and quadrature noise vector.

$$Z(k) = \begin{pmatrix} z_1 \\ z_2 \end{pmatrix} = \underline{h}(k) + \underline{N}(k) = \begin{pmatrix} h_1 + n_c \\ h_2 + n_s \end{pmatrix} \quad (8)$$

A block diagram description of this concept is illustrated in Figure 1 where the message  $x(t)$  is generated by passing a random process  $u(t)$  through a

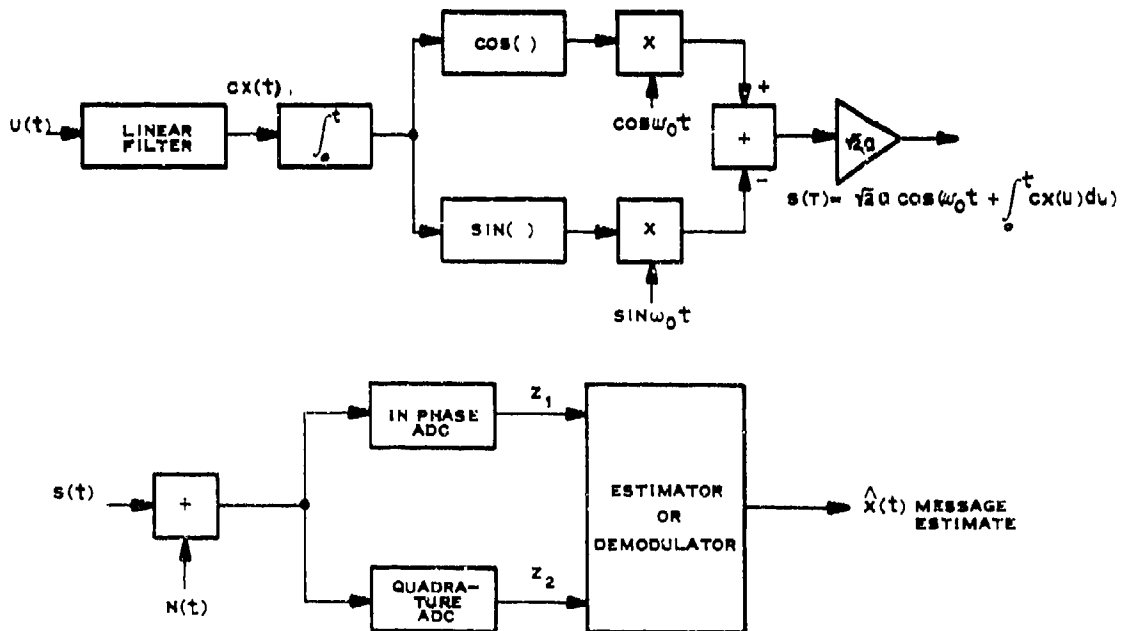


Figure 1. Block Diagram for Modulator and Demodulator for an FM Process

linear filter. The ultimate purpose of this configuration is to use the in-phase and quadrature samples ( $z_1, z_2$ ) to generate an estimate  $\hat{x}(t)$  of the message  $x(t)$ .

The bandpass FM process illustrated in Figure 1 can be reduced to an equivalent baseband process of Figure 2 when in-phase and quadrature sampling is used. In this baseband equivalent configuration, a dc term,  $2\pi\Delta f$ , is added to the output of the linear message filter. This term represents the unavoidable frequency uncertainty that exist between the transmitter and receiver frequencies for the typical FM link. This frequency uncertainty will be reflected in the observed samples at the receiver, and its removal becomes part of the estimator's task. In this situation, the output of the modulation integrator  $\theta(t)$  is represented by:

$$\theta(t) = \int_0^t cx(u)du + 2\pi\Delta ft + \theta(0). \quad (9)$$

### C. STATE VARIABLE MODEL

In recursive estimation, it is usually desirable to model linear filters by the state variable technique. A simple example will illustrate this concept.

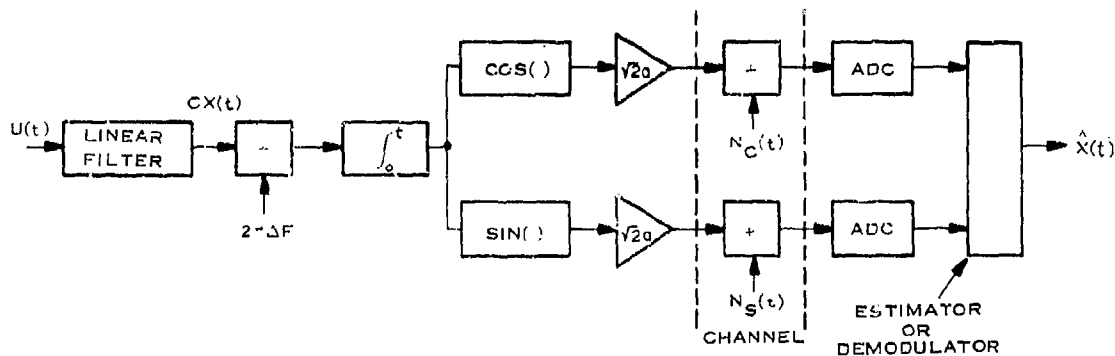


Figure 2. Block Diagram for Equivalent Baseband FM Process

Suppose that the filter is a simple single-pole filter described by the differential equation:

$$\dot{x}(t) = -\alpha x(t) + \alpha v(t) \quad (10)$$

If the output of the integrator of Figure 2 is  $\theta(t)$ , then its input is  $\dot{\theta}(t)$  given by:

$$\dot{\theta}(t) = cx(t) + u_2(t) \quad (11)$$

where  $u_2(t)$  represents the frequency uncertainty. To construct a vector state equation of the process shown in Figure 2 (up to the sine and cosine functions), combine equation (10) and equation (11) as a vector equation:

$$\begin{pmatrix} \dot{x}(t) \\ \dot{\theta}(t) \end{pmatrix} = \begin{bmatrix} -\alpha & 0 \\ c & 0 \end{bmatrix} \begin{pmatrix} x(t) \\ \theta(t) \end{pmatrix} + \begin{pmatrix} u_1(t) \\ u_2(t) \end{pmatrix} \quad (12)$$

where  $u_1(t) = \alpha v(t)$ . In the vector notation, this becomes:

$$\dot{Y}(t) = AY(t) + U(t)$$

where the  $2 \times 2$  matrix  $A$  is sometimes referred to as the system matrix.

The reduction of the modulator configuration to state variable characterization can readily be visualized in Figure 3, Figure 4, and Figure 5. The reduction of an RC single-pole filter to its state variable equivalent is shown in Figure 3 where the filter's output is  $x(t)$ . Figure 4 illustrates the modulator and Figure 5 shows the overall filter modulator configuration.

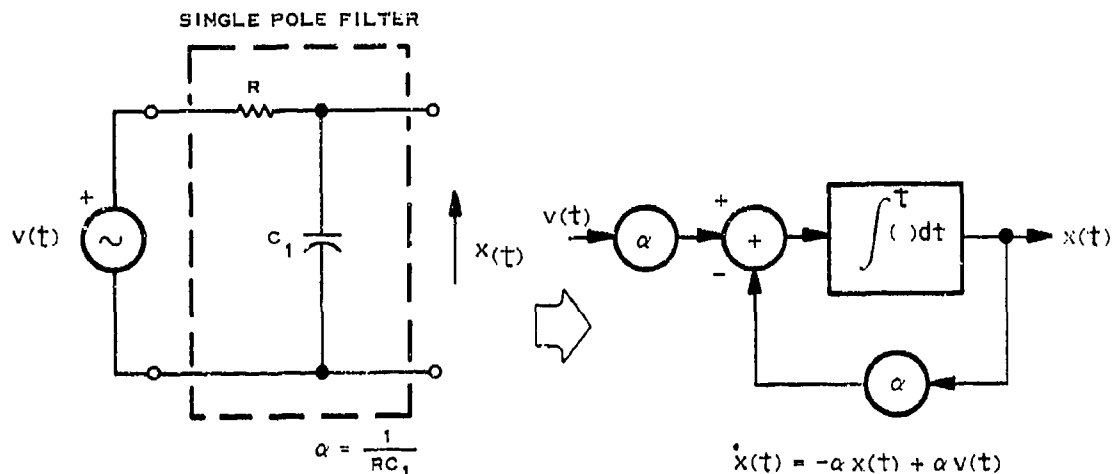


Figure 3. Single Pole Message Model

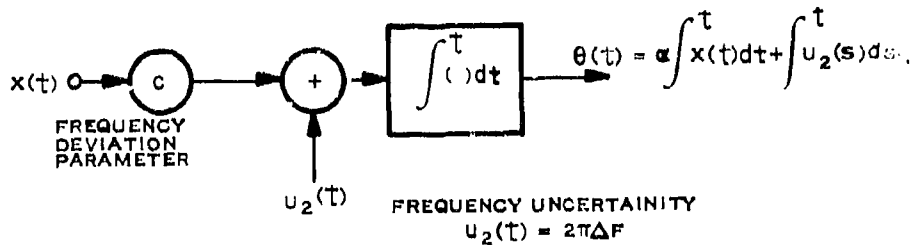


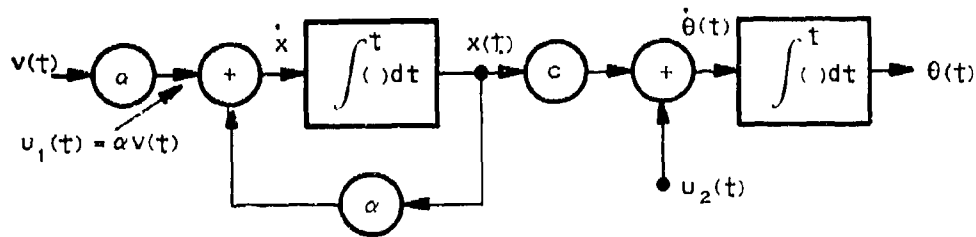
Figure 4. Model for FM

Generalization to a higher order filter is straightforward: For example, Figure 6 illustrates an (N-1) pole filter configuration where the matrix A is the (N-1) x (N-1) system matrix. Techniques are available<sup>3</sup> for transferring a general filter transfer function given in the S-plane to the corresponding A matrix for the state variable representation. In a manner similar to the single-pole filter example just discussed, the differential equation

$$\dot{\theta}(t) = \sum_{i=1}^{N-1} c_i x_i(t) + u_N(t) \quad (14)$$

describing the input to the integrator can be appended to the (N-1) filter state equations to obtain an (Nx1) vector representation as shown:

$$\begin{bmatrix} \dot{x}_1(t) \\ \vdots \\ \dot{x}_{N-1}(t) \\ \dot{\theta}(t) \end{bmatrix} = \begin{bmatrix} a_{11} & a_{12} & \dots & a_{1, N-1} & 0 \\ a_{21} & & & & \\ \vdots & & & & \\ \vdots & & & & \\ a_{N-1, 1} & & & & \\ c_1 & c_2 & \dots & c_{N-1} & 0 \end{bmatrix} \begin{bmatrix} x_1(t) \\ \vdots \\ x_{N-1}(t) \\ \theta(t) \end{bmatrix} + \begin{bmatrix} u_1(t) \\ u_2(t) \\ \vdots \\ u_N(t) \end{bmatrix} \quad (15)$$



$$\begin{pmatrix} \dot{x}(t) \\ \dot{\theta}(t) \end{pmatrix} = \begin{pmatrix} -\alpha & 0 \\ c & 0 \end{pmatrix} \begin{pmatrix} x(t) \\ \theta(t) \end{pmatrix} + \begin{pmatrix} u_1(t) \\ u_2(t) \end{pmatrix}$$

2X1 VECTOR  $\dot{Y}(t) = A Y(t) + U(t)$   
 SCALAR  $\theta(t) = \Gamma^T Y(t); \quad \Gamma^T = \begin{pmatrix} 0, 1 \\ 0, 1 \end{pmatrix}$   
 $\begin{pmatrix} 0, 1 \\ 0, 1 \end{pmatrix} \begin{pmatrix} x(t) \\ \theta(t) \end{pmatrix} = \theta(t)$

Figure 5. Continuous State Variable Representation of FM Process

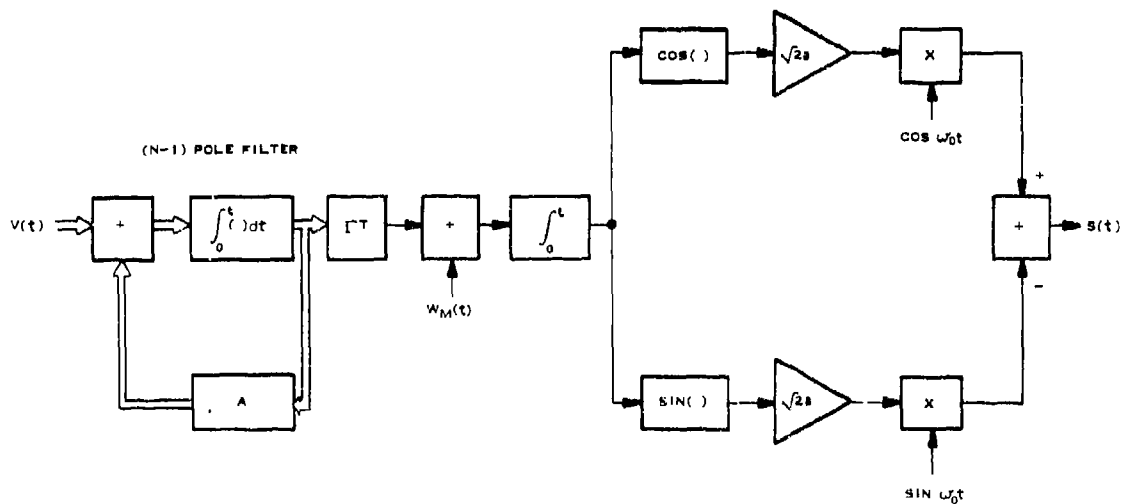


Figure 6. Block Diagram for State Variable Characterization of Message Filter

In vector notation, equation (15) becomes:

$$\dot{Y}(t) = GY(t) + U(t) \quad (16)$$

where the new  $G$  matrix is an  $(N \times N)$  matrix whose elements are the  $(N-1) \times (N-1)$  "A" matrix with another row and column added. For this new augmented system, the scalar input to the integrator is:

$$\dot{\theta}(t) = \Gamma^T Y(t) \quad (17)$$

where  $\Gamma$  is a  $(N \times 1)$  vector given by:

$$\Gamma^T = (0, 0, \dots, 0, 1) \quad (18)$$

The FM output equation is now written as:

$$s(t) = \sqrt{2}a \cos [\omega_0 t + \theta(t)] \quad (19)$$

where  $\theta(t)$ , the angle modulation, is:

$$\theta(t) = \Gamma^T Y(t) + \theta(0) \quad (20)$$

#### D. DISCRETE STATE VARIABLE REPRESENTATION

Since we desire to do the estimation by digital techniques, it is advantageous to convert the message model into a discrete state variable representation. One method for doing this is to convert the vector differential equation, equation (16), into a difference equation. For example,

$$\dot{Y}(t) = \lim_{T \rightarrow 0} \left[ \frac{Y(k+1) - Y(k)}{T} \right]; \quad \begin{array}{l} k = t \\ k+1 = t+T \end{array} \quad (21)$$

Thus, an approximation of equation (16), with  $I$  the  $N \times N$  identity matrix, becomes

$$Y(k+1) = [I + TG] Y(k) + TU(k) \quad (22)$$

However, for high accuracy the sample rate must be rather fast. A better technique is to use the transition matrix or recursive equation from the sampled solution of the continuous time representation  $\underline{Y}(t)$ . This idea will now be illustrated.

The solution to equation (16) can be shown<sup>3</sup> to be

$$Y(t) = \Phi(t, t_0)Y(t_0) + \int_{t_0}^t \Phi(t, \tau)U(\tau) d\tau \quad (23)$$

where  $\Phi(t, \tau)$  is the system transition matrix. A Taylor series expansion of the integral of equation (22) about  $t_0$  results in:

$$Y(t) = \Phi(t, t_0)Y(t_0) + (t - t_0)U(t_0) + R_2 \quad (24)$$

where  $R_2$  is the remaining terms. Suppose that the system is linear time-invariant, then the transition matrix is the exponential matrix:

$$\Phi(t, t_0) = e^{G(t - t_0)} \quad (25)$$

which has a series form:

$$\Phi(t, t_0) = I + (t - t_0)G + \frac{(t - t_0)^2}{2!} G^2 + \dots \quad (26)$$

Let the terms after the linear term be represented by  $R_2'$  such that

$$\Phi(t, t_0) = I + (t - t_0)G + R_2' \quad (27)$$

When we let  $t = (k+1)T$  and  $t_0 = kT$ , then  $t - t_0 = T$ , so that the exact sampled equation for  $\underline{Y}(t)$  is obtained by combining equation (24) and equation (27). Letting  $kT \triangleq k$ , the discrete representation of equation (23) becomes:

$$Y(k+1) = (I + TG)Y(k) + TU(k) + R_2' Y(k) + R_2 \quad (28)$$

The first two terms in equation (28) represent the difference equation approximation which has error proportional to both  $R_2'$  and  $R_2$  and the first three terms represent the Taylor series approximation which has its error proportional only to  $R_2$ . Accordingly, the use of the sampled transition matrix  $\Phi(t, t_0)$  provides a better discrete approximation to the continuous case than does the direct difference equation.

For a linear time invariant system the sampled transmittion matrix depends only upon the sample interval  $T$ , i. e.,

$$\Phi(t, t_0) = e^{GT} = \Phi ; T = t - t_0 \quad (29)$$

For the (2x2) A matrix of equation (12), this transition matrix has the form:

$$\Phi = \begin{bmatrix} e^{-\alpha T} & 0 \\ \frac{c}{\alpha}(1 - e^{-\alpha T}) & 1 \end{bmatrix}$$

The recursive discrete equation is, from equation (24), after appropriate substitution:

$$Y(k+1) = \Phi Y(k) + W(k) \quad (30)$$

where  $W(k) = Tu(kT)$  and  $Y(k+1) = Y[(k+1)T]$

This discrete modulation process with in-phase and quadrature noise terms added is illustrated in Figure 7. The observed process  $Z(k)$  is represented by:

$$Z(k) = \underline{h}[\theta(k)] + \underline{N}(k) \quad (31)$$

where:

$$\begin{aligned} \mathbf{h}^T(\cdot) &= \{h_1(\cdot), h_2(\cdot)\} \\ h_1(\cdot) &= \sqrt{2}a \cos \theta(k) \\ h_2(\cdot) &= -\sqrt{2}a \sin \theta(k) \end{aligned}$$

The discrete phase variable  $\theta(k)$  is given by:

$$\theta(k) = \Gamma^T Y(k) \quad (32)$$

We have now defined the discrete FM process in a form convenient for application of recursive estimation methods. This development will be discussed next.

## E. RECURSIVE ESTIMATION

The methodology used in recursive estimation is to first specify an estimation criterion along with the probability density functions associated with the random variables of the process. These probability density functions are then used in the equation for the estimation criterion to derive a cost function. Finally, the recursive estimation equations are obtained by minimizing the cost function in a recursive manner subject to the systems difference equation. We will use the maximum a posteriori (MAP) criterion in our derivation which follows that given by Sage<sup>4</sup> and McBride<sup>5</sup>.

We assume a vector message and observation model:

$$Y(k+1) = \Phi Y(k) + W(k) \quad (33)$$

$$Z(k) = \underline{h}[\theta(k)] + \underline{N}(k), \quad \theta(k) = \Gamma^T Y(k) \quad (34)$$

where  $Y(k)$  is an  $N$  dimensional state vector,  $Z(k)$  is an  $M$  dimensional observation vector,  $W(k)$  is a  $N$  dimensional message vector and  $N(k)$  is an  $M$  dimensional noise vector.  $W(k)$  and  $N(k)$  are assumed to be Gauss Markov white sequences with:

$$\text{cov} \{W(k), W(j)\} = Q \delta(k-j); E \{W(k)\} = 0 \quad (35)$$

$$\text{cov} \{N(k), N(j)\} = R \delta(k-j); E \{N(k)\} = 0 \quad (36)$$

$$\text{cov} \{N(k), W(j)\} = 0 \quad (37)$$

$$\text{var} \{Y(k_0)\} = P(0); E \{Y(k_0)\} = \bar{Y}(k_0) \quad (38)$$

As usual for discrete problems  $\delta(k-j)$  is the Kronecker delta. Consider the problem of estimating  $Y(k_0), Y(k_1), \dots, Y(k_f)$  having been given the observation sequence  $Z(k_0), Z(k_1), \dots, Z(k_f)$ . It can be shown that the MAP criterion is equivalent to finding a sequence  $Y(k_0), \dots, Y(k_f)$  that maximizes.

$$p[Z(k_0), \dots, Z(k_f) / Y(k_0), \dots, Y(k_f)] \quad p[Y(k_0), \dots, Y(k_f)] \quad (39)$$

where  $p()$  represents the associated probability density functions. Under the assumptions previously outlined, it is straightforward to show<sup>4</sup> that equation (39) reduces to minimization of a scalar  $J$  given by

$$J = 1/2 [Y(k_0) - \bar{Y}(k_0)]^T P^{-1}(0) [Y(k_0) - \bar{Y}(k_0)] + 1/2 \sum_{k=k_0}^{k_f} [Z(k) - h(k)]^T R^{-1} [Z(k) - h(k)] + 1/2 \sum_{k=k_0}^{k_f-1} W^T(k) Q^{-1} W(k) \quad (40)$$

subject to the equality constraint  $Y(k+1) = \Phi Y(k) + W(k)$ , and the associated initial conditions. When we let the summation of  $[Z(k) - h(k)]^T R^{-1} [Z(k) - h(k)]$  stop at  $k_f-1$  by writing this term as  $[Z(k+1) - h(k+1)]^T R^{-1} [Z(k+1) - h(k+1)]$ , the individual summation terms can be included under the same summation, i. e.,

$$J = 1/2 [Y(k_0) - \bar{Y}(k_0)]^T P^{-1}(0) [Y(k_0) - \bar{Y}(k_0)] + 1/2 \sum_{k=k_0}^{k_f-1} \left\{ \left[ [Z(k+1) - h(k+1)]^T R^{-1} [Z(k+1) - h(k+1)] \right]^{(41)} + W^T(k) Q^{-1} W(k) \right\}$$

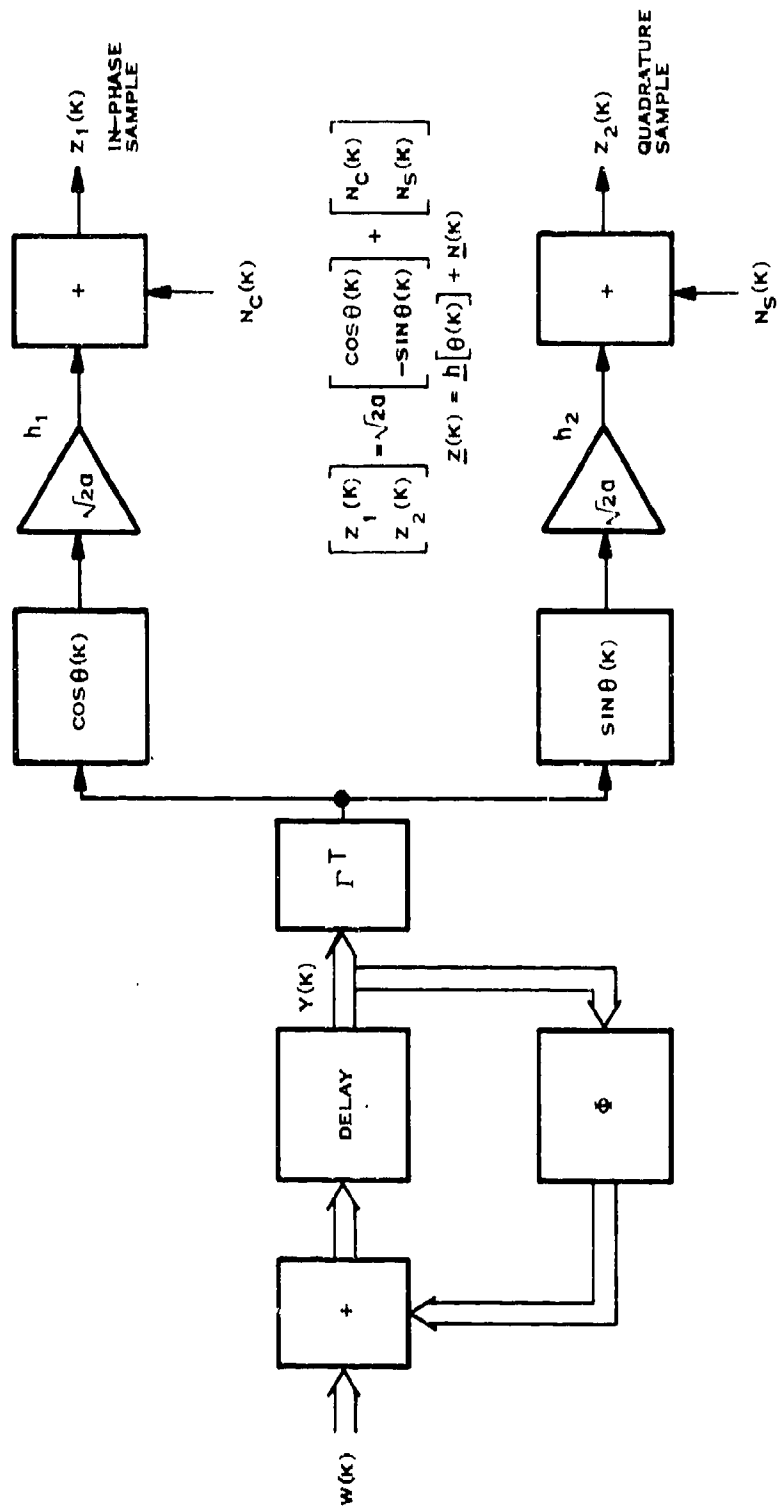


Figure 7. Block Diagram of the Message Process Illustrating Discrete State Variable Characterization of the Angle  $\theta(k)$

The minimization of this scalar  $J$  is a typical optimal control problem.

An equivalent minimization problem has been solved by Sage<sup>4</sup> where he used the minimization techniques of optimal control theory to define the two-point boundary-value problem - a set of vector difference equations which are to be solved simultaneously to obtain the recursive estimation equations. Unfortunately, the resulting set of vector difference equations are not only nonlinear, but also have missing boundary conditions. However, an approximate solution technique called discrete invariant imbedding can be used to overcome this difficulty. Here, we will only state the solution. Interested readers are referred to Sage<sup>4</sup>.

The resulting difference equations that define the two-point boundary-value problem are:

$$Y(k+1) = \Phi Y(k) - Q \Phi^{-T} \underline{\lambda}(k) \quad (42)$$

$$\underline{\lambda}(k+1) = \Gamma \left\{ \frac{\partial h^T(\cdot)}{\partial \theta} \right\} R^{-1} \left\{ Z(k+1) - \underline{h} [\tilde{\theta}(k+1)] \right\} + \Phi^{-T} \underline{\lambda}(k) \quad (43)$$

where:

$$\tilde{\theta} = \Gamma^T [\Phi Y(k) - Q \Phi^{-T} \underline{\lambda}(k)]$$

$$\frac{\partial h^T(\cdot)}{\partial \theta} = \left\{ \frac{\partial h_1}{\partial \theta}, \dots, \frac{\partial h_m}{\partial \theta} \right\} \quad (1 \times M)$$

$$\Gamma^T = (0, 0, \dots, 0, 1)$$

$\Phi = (N \times N)$  system transition matrix

$\underline{\lambda}(k) = (N \times 1)$  adjoint vector

$Z(k) = (M \times 1)$  observation vector

The boundary conditions are:

$$\underline{\lambda}(k_0) = P^{-1}(0)[Y(k_0) - \bar{Y}(k_0)] \quad (44)$$

$$\underline{\lambda}(k_f) = \underline{0} \quad (45)$$

and  $Y(k_f)$  is the missing terminal condition.

To obtain the recursive solution algorithm this set of coupled nonlinear vector difference equation must be solved. An exact solution technique is formidable; however, a solution technique called discrete invariant embedding<sup>4</sup> can be employed to obtain an approximate recursive solution.

The solution algorithm is an Nx1 vector difference equation coupled with an (NxN) matrix difference equation. The matrix equation is sometimes called the gain matrix equations. The general solution algorithm\* is:

$$\hat{Y}_{k+1} = \Phi \hat{Y}_k + P_{k+1} \Gamma \left[ \nabla_{\theta} \underline{h}^T(\theta_k) \right] R^{-1} \left[ Z_{k+1} - \underline{h}(\theta_k) \right] \quad (46)$$

$$P_{k+1} = \left[ \Phi P_k + Q \Phi^{-1} \right] \left\{ \Phi^{-T} + \Gamma \left[ \nabla_{\theta} \underline{h}^T(\theta_k) \right] R^{-1} \left[ \nabla_{\theta} \underline{h}(\theta_k) \right] \Gamma^T \right. \\ \left. \cdot \left[ \Phi P_k + Q \Phi^{-T} \right] - \Gamma \left[ Z_{k+1} - \underline{h}(\theta_k) \right]^T R^{-1} \left[ \nabla_{\theta}^2 \underline{h}(\theta_k) \right] \Gamma^T \right. \\ \left. \cdot \left[ \Phi P_k + Q \Phi^{-T} \right] \right\}^{-1} \quad (47)$$

The following expressions are valid when using in-phase and quadrature sampling, i. e., M = 2.

$$Z_{k+1}^T = \{ z_1(k+1), z_2(k+1) \} = \{ z_1, z_2 \}$$

$$\underline{h}^T(\hat{\theta}_k) = \sqrt{2a} \{ \cos \hat{\theta}_k, -\sin \hat{\theta}_k \}$$

$$\nabla \underline{h}^T(\hat{\theta}_k) = \sqrt{2a} \{ -\sin \hat{\theta}_k, -\cos \hat{\theta}_k \}$$

$$\nabla^2 \underline{h}^T(\hat{\theta}_k) = \sqrt{2a} \{ -\cos \hat{\theta}_k, \sin \hat{\theta}_k \}$$

When these are substituted into equations (46) and (47) and assuming  $R^{-1} = (1/\sigma_n^2)I$ ,

$$\hat{Y}_{k+1} = \Phi \hat{Y}_k - \frac{\sqrt{2a}}{\sigma_n^2} P_{k+1} \Gamma \left[ z_1 \sin \hat{\theta}_k + z_2 \cos \hat{\theta}_k \right] \quad (49)$$

$$P_{k+1} = \left[ \Phi P_k + Q \Phi^{-T} \right] \left[ \Phi^{-T} + \frac{\sqrt{2a}}{\sigma_n^2} \Gamma \Gamma^T (\Phi P_k + Q \Phi^{-T}) \right. \\ \left. \left\{ z_1 \cos \hat{\theta}_k - z_2 \sin \hat{\theta}_k \right\} \right]^{-1} \quad (50)$$

\*To simplify notation the subscript k is sometimes used instead of using (k) in the argument.

The estimate  $\hat{\theta}(k)$  of the angle is  $\hat{\theta}(k) = \Gamma^T Y(k)$ . The parameters of the equations are defined as follows:

- $\phi$  = NxN system transition matrix
- $a$  = rms carrier voltage
- $\sigma_n^2$  = noise power in the input bandwidth
- $\Gamma^T = (0, 0, \dots, 0, 1)$
- $P_{k+1}$  = NxN gain matrix
- $Q$  = NxN covariance matrix of the modulating message source

Next, a simple example using a single-pole message filter model will be reviewed.

#### F. EXAMPLE

For a single-pole message model, the parameters of the recursive algorithm, equations (49) and (50), are:

$$\hat{Y}^T(k) = (x(k), \hat{\theta}(k))$$

$$\phi = \begin{bmatrix} \phi_{11} & \phi_{12} \\ \phi_{21} & \phi_{22} \end{bmatrix} = \begin{bmatrix} e^{-\alpha T} & 0 \\ \frac{c}{\alpha}(1 - e^{-\alpha T}) & 1 \end{bmatrix} \quad (51)$$

$$Q = \begin{bmatrix} \sigma_q^2 & 0 \\ 0 & \sigma_2^2 \end{bmatrix}$$

- $c$  = Frequency deviation
- $\alpha$  = 3 dB frequency of the filter
- $T$  = sample interval

$$\frac{a^2}{\sigma_n^2} = \text{input carrier-to-noise ratio}$$

The  $x(k)$  element of  $Y(k)$  is the estimate of the message that is sought. In the Q matrix,  $\sigma_q^2$  is the variance of the message filter input,  $u_1(t)$ , and  $\sigma_2^2$  is the variance of the frequency uncertainty ( $2\pi\Delta f$ ) where for convenience  $\Delta f$  is assumed to be a Gauss-Markov white sequence. The part of the last assumption pertaining to the white sequence is difficult to justify; however, when crystal controlled frequencies are used  $\sigma_2^2$  is quite small compared to  $\sigma_q^2$  and the degradation is most likely insignificant\*.

A realization of these estimation equations is illustrated in Figure 8. In the absence of noise, the input to the fixed gain  $G_1$  is  $\sin(\theta_k - \hat{\theta}_k) \approx \theta_k - \hat{\theta}_k$ . Under the same input situation, the input to the nonlinear time-varying gain processor is  $\cos(\theta_k - \hat{\theta}_k)$ . It is clear that the form of the demodulator resembles a PLL demodulator where the loop filter and the digitized VCO (digital oscillator) constitute the other elements of the loop. The main departure from the phase-locked loop demodulator is the time-varying gain processor; the algorithm for this processor is defined by equation (50).

The gain term  $G_1$  is given by:

$$G_1 = \sqrt{2a}/\sigma_n^2 \quad (52)$$

where  $\sigma_n^2$  is the noise power, defined in the input IF bandwidth, and "a" is the rms carrier voltage. It is interesting to note that the input to the time-varying gain processor is the quadrature phase component which is often used for automatic gain control (AGC) in phase-locked loop receivers. This might be the reason that matching  $G_1$  to the input carrier and noise power was not too critical as far as the demodulator performance was concerned. This fact was discovered during the simulation of the demodulator.

The simulation of the demodulator of Figure 8 was accomplished using digital computer simulation techniques. Of particular importance in determining the performance of FM demodulators are curves relating to the output signal-to-noise ratio in the message bandwidth (SNR) to the carrier-to-noise ratio in the IF bandwidth\*\* ( $CNR_{IF}$ ). Consequently, the ultimate purpose of the simulation was to obtain these SNR performance curves; Figure 9 illustrates the SNR performance curves obtained by simulation of the single-pole message filter example of Figure 8.

In these curves  $\beta$ , the modulation index, is defined as:

$$\beta = \frac{c}{\alpha} \quad (53)$$

where  $c$  is the radian frequency deviation and  $\alpha$  is the ? db bandwidth of the single-pole filter. Curve A is the SNR performance curve for the demodulator for  $\beta = 5$  and fixed gain  $G_1$  matched to  $CNR = 20$  dB. Both curves were obtained for a sinewave test signal of normalized frequency  $(1/50) T$  where  $T$

\*In all simulation tests,  $\sigma_2 = 0$ .

\*\*In the simulations, the Carson rule bandwidth was used.

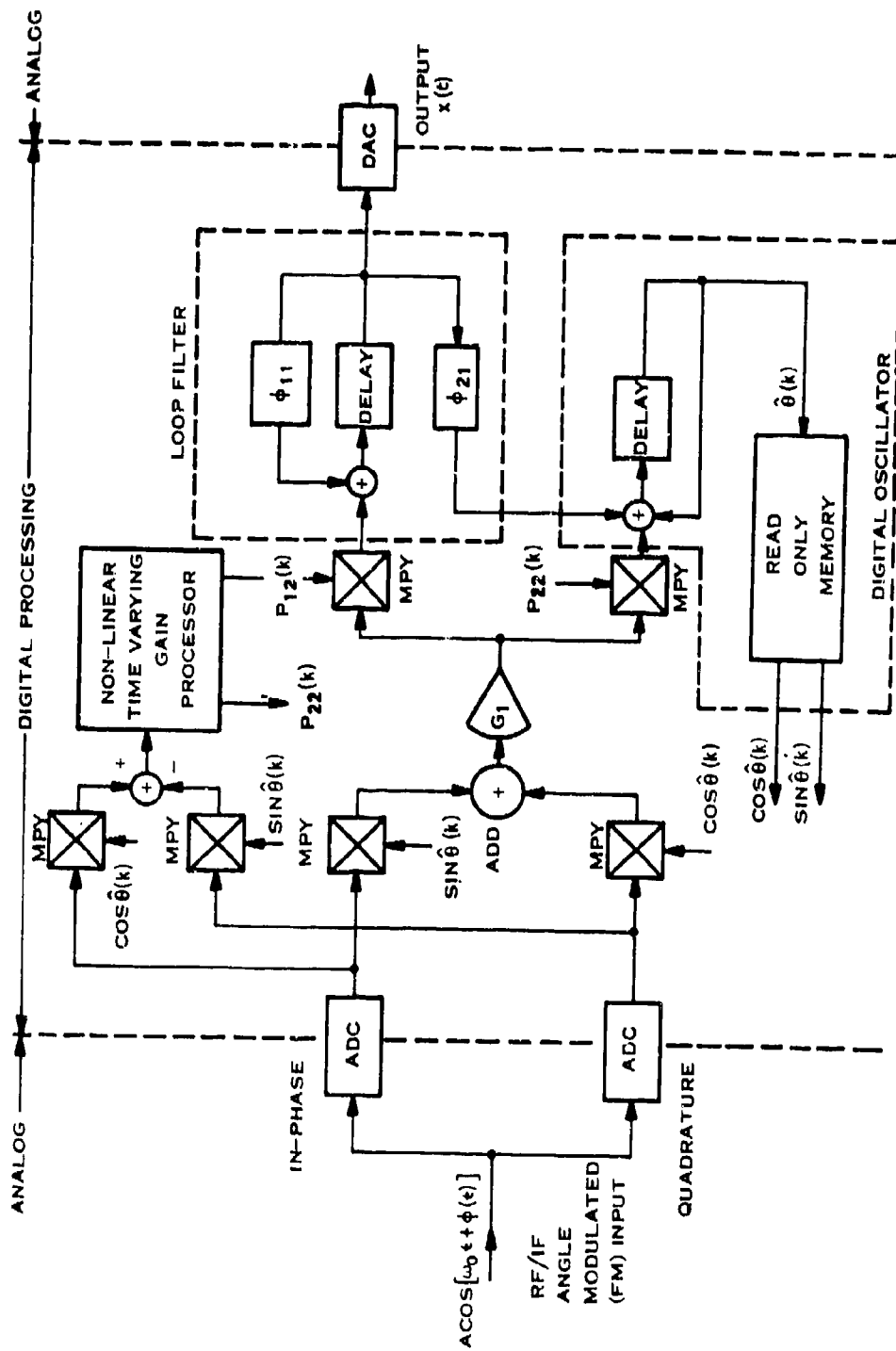


Figure 8. Block Diagram Realization of the Recursive Nonlinear Demodulator for a Single-Pole Message Filter

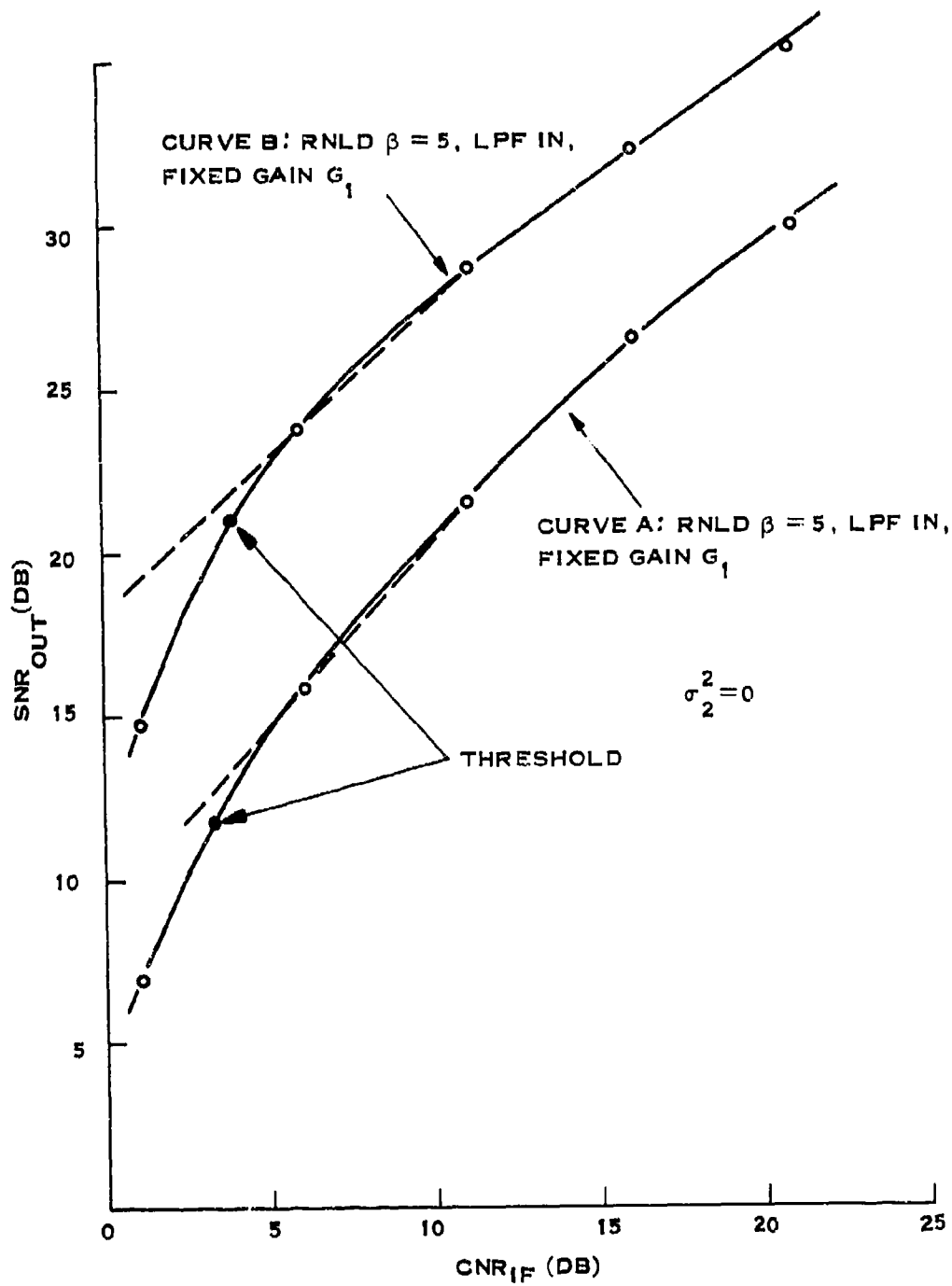


Figure 9. Signal-To-Noise Performance Curves  
Obtained from Simulation

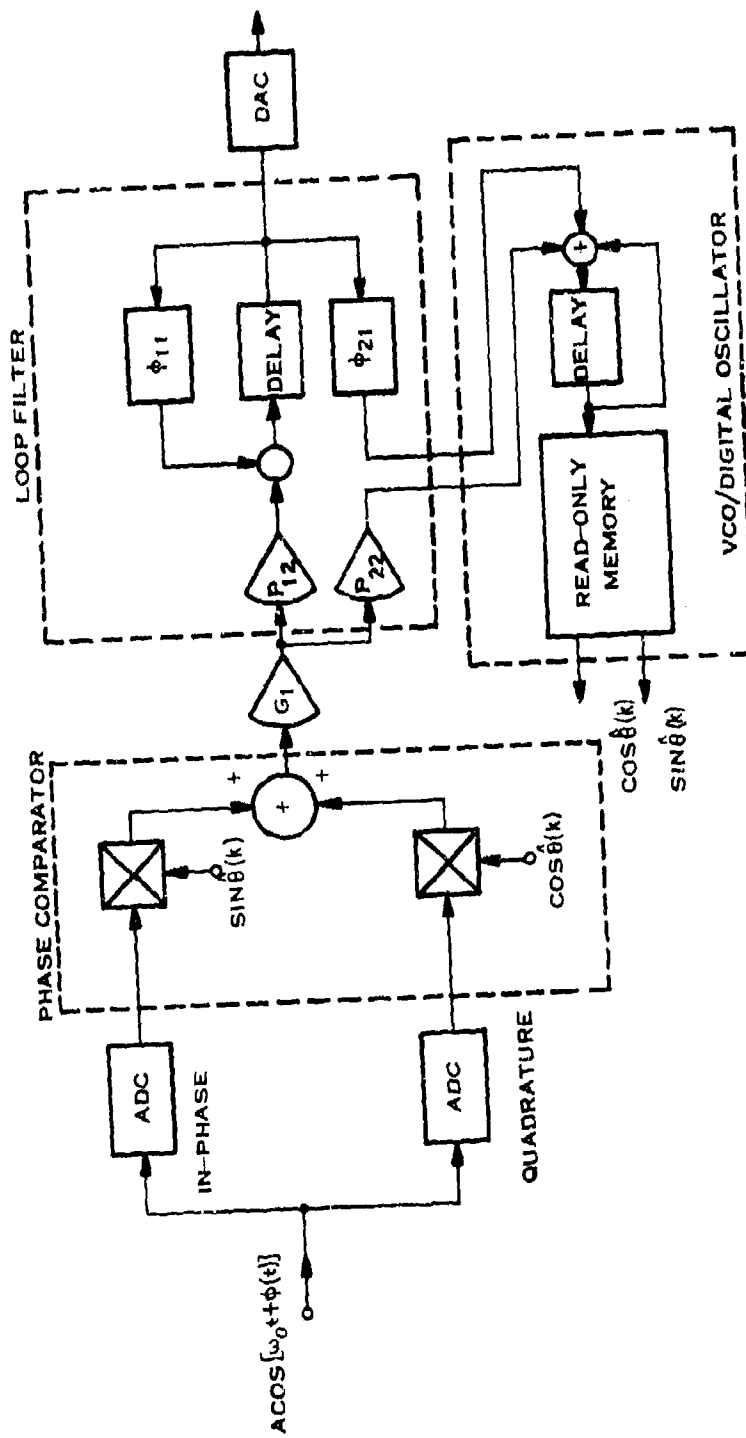


Figure 10. Simplified Block Diagram of the Demodulator when  $P_{12}(k+1)$  and  $P_{22}(k+1)$  are Replaced by Fixed Constants

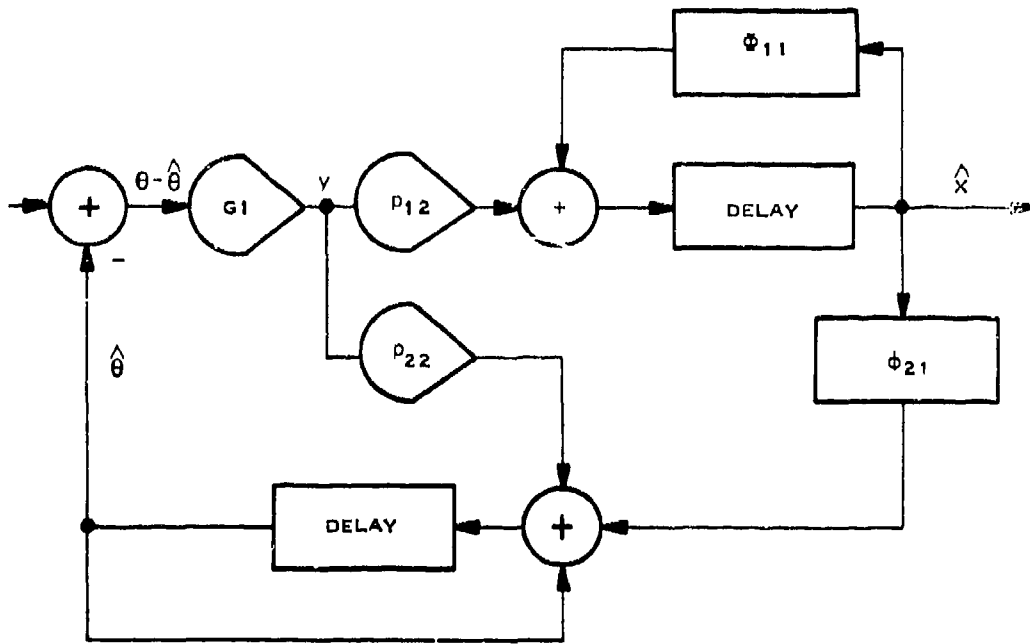


Figure 11. Small Signal Linear Approximation of Demodulator

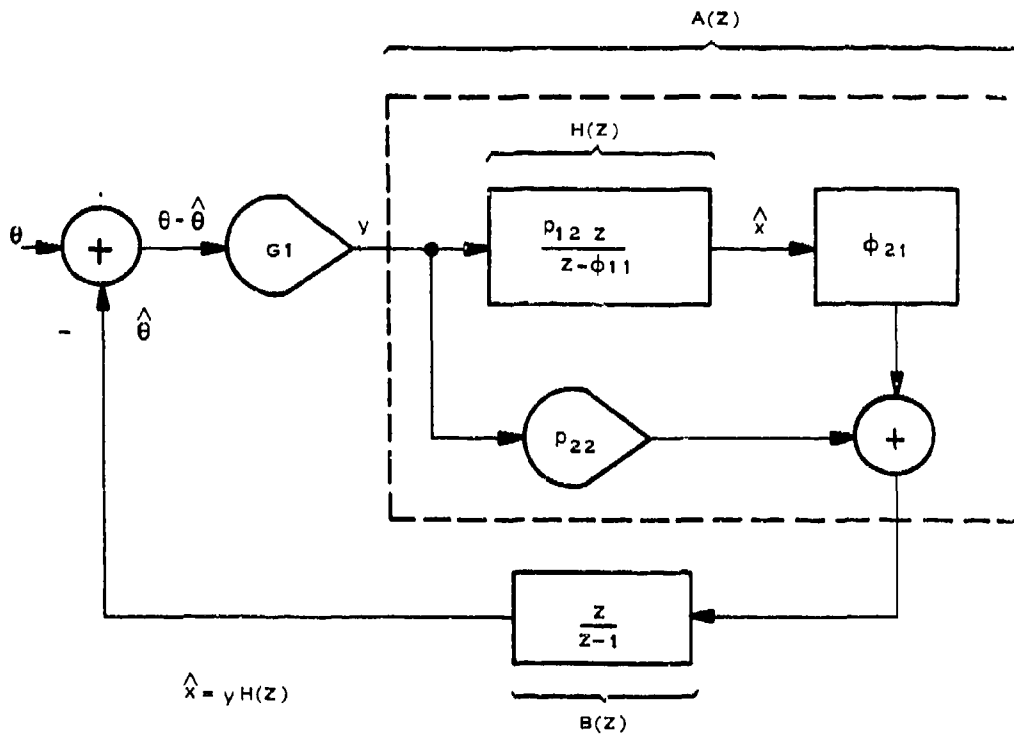


Figure 12. Block Diagram Used for Calculating Transfer Function of Demodulator

The block diagram of Figure 12 is further reduced to the diagram of Figure 13, where:

$$A(z) = H(z) \phi_{12} + p_{22} \quad (55)$$

$$B(z) = \frac{z}{z-1} \quad (56)$$

$$H(z) = \frac{p_{12}z}{z - \phi_{11}} \quad (57)$$

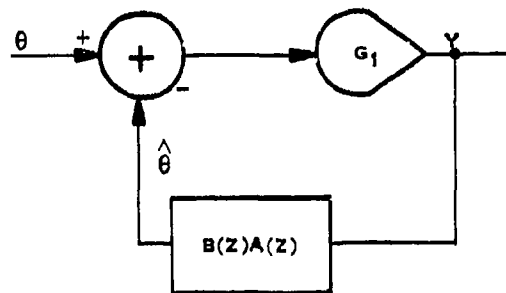


Figure 13. Reduced Block Diagram

The transfer function  $y/\theta$  is, from Figure 13, given by:

$$y/\theta = \frac{G_1}{1 + B(z)A(z)G_1} \quad (58)$$

The desired transfer function  $\hat{x}/\theta$  is derived from equation (58) using the results of equation 54. We have

$$\hat{x}/\theta = \frac{H(z) G_1}{1 + B(z)A(z)G_1} \quad (59)$$

substituting in the values of  $H(z)$ ,  $B(z)$  and  $A(z)$  defined in equations (55) through equation (57), the desired transfer function  $\hat{x}/\theta$  becomes

$$\hat{x}/\theta = \frac{\frac{G_1 p_{12} z}{z - \phi_{11}}}{1 + \frac{p_{22} G_1 z}{z-1} + G_1 p_{12} \phi_{12} \left(\frac{z}{z - \phi_{11}}\right) \left(\frac{z}{z-1}\right)} \quad (60)$$

This is the Z-transform transfer function of the above-threshold approximation of the demodulator. The noise bandwidth can be obtained directly from equation (60) by a technique discussed by Gupta<sup>7</sup>. Here, however, it is more convenient to first obtain the S-transform (Laplace transform) of the transfer function, and then obtain the noise bandwidth from the S-transform transfer function.

The S-transform transfer function is obtained from the Z-transform by first making an intermediate transformation to the zeta-transform. This transformation technique is discussed by Gupta<sup>8</sup> and proper application of his technique permits equation (60) to be written as:

$$\frac{\hat{x}(s)}{\theta(s)} = h(s) = \frac{G_1 p_{12} s}{s^2 + s(\alpha + G_1 p_{22}) + G_1(p_{12} \beta \alpha + p_{22})} \quad (61)$$

The poles of  $h(s)$  are:

$$s = -A \pm jB \quad (62)$$

where:

$$A = \frac{\alpha + G_1 p_{22}}{2}$$

$$B = \sqrt{G_1(p_{12} \beta \alpha + p_{22}) - \left(\frac{\alpha + G_1 p_{22}}{2}\right)^2}$$

For white noise input of spectral density  $N_0/2$ , the equivalent noise power,  $P_N$ , out of the demodulator model is:

$$P_N = \frac{1}{2\pi} \int_{-\infty}^{\infty} \frac{N_0}{2} |h(j\omega)|^2 d\omega \quad (63)$$

where  $h(j\omega)$  is defined by using equation (61). This integral can be evaluated by using complex variables integration techniques. The result is:

$$P_N = \frac{N_0}{2} \left( \frac{K_0^2}{4A} \right) \quad (64)$$

where  $K_0 = G_1 p_{12}$  and  $A$  is defined in equation (62). The loop noise bandwidth,  $2B_N$ , is obtained from the following relationship:

$$P_N = \frac{N_0}{2} (2B_N) \quad (65)$$

Solving for  $2B_N$ , we have:

$$2B_N = \frac{K_o^2}{4A} = \frac{G_1^2 p_{12}^2}{2(\alpha + G_1 p_{22})} \quad (66)$$

We see that the loop noise bandwidth is a function of  $\alpha$ ,  $G_1$ ,  $p_{12}$ , and  $p_{22}$ . To investigate how the noise bandwidth varies we need the steady state values of  $p_{12}$  and  $p_{22}$ .

Some approximate values for the steady state gain terms have been obtained by computer simulation of the demodulator for a sinewave input test signal. Curves showing P-matrix gain versus carrier-to-noise ratio in the IF bandwidth ( $CNR_{IF}$ ) for each of the four gain terms are sketched in Figure 14; a, b, and c. Two types of curves were obtained for each P-matrix gain: curves for variable  $G_1$ , i. e.,  $G_1$  is matched to each new input  $CNR_{IF}$  and curves for fixed  $G_1$  set at  $CNR_{IF} = 20$  dB. Notice that the variable  $G_1$  and fixed  $G_1$  (at  $CNR_{IF} = 20$  dB) for  $\beta = 5$  approximately intersect at  $CNR_{IF} = 20$  dB. These steady state values were obtained after a 500 point run and are representative of data taken on numerous different runs.

Figure 15 is a sketch of the real part A and imaginary part B of the linearized demodulator poles as they vary with input  $CNR_{IF}$ . In these curves,

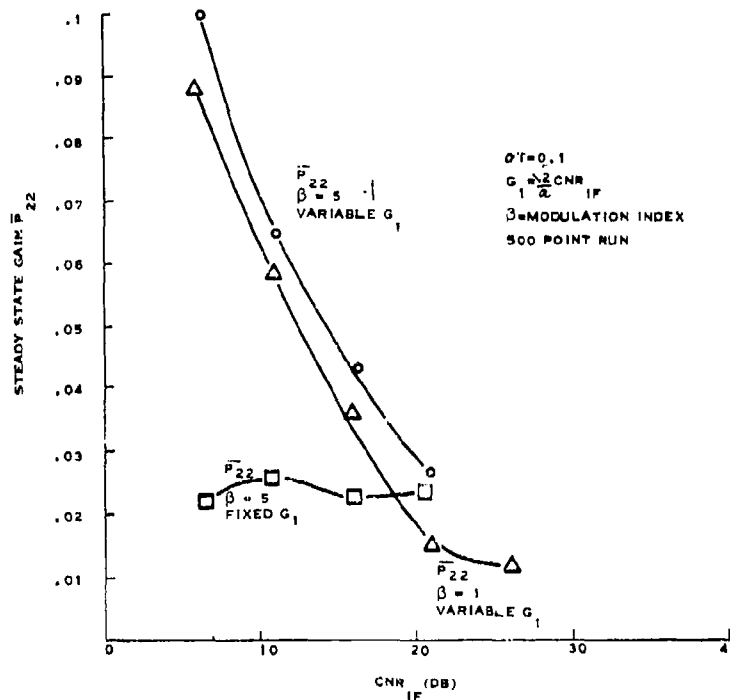


Figure 14a. Variation of Steady State Gains for Fixed and Variable  $G_1$  and  $\beta=1$  and  $\beta=5$

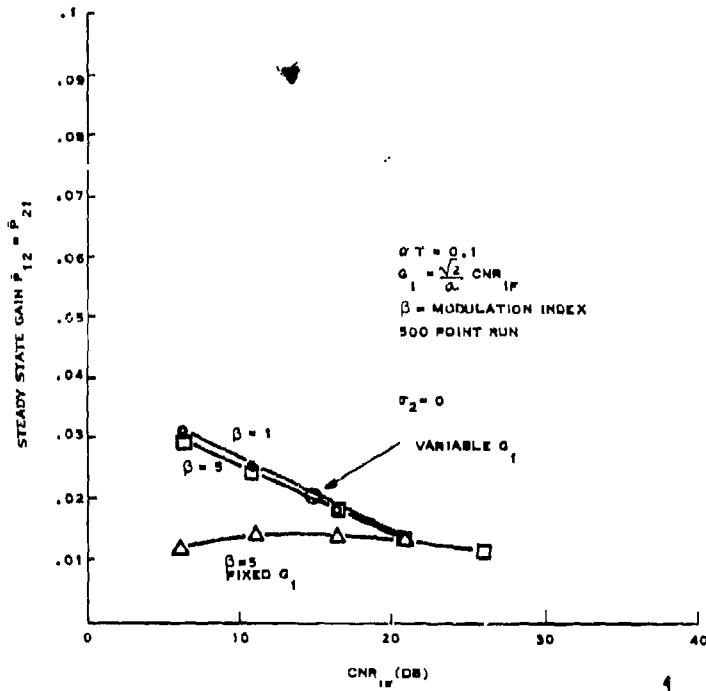


Figure 14b. Variation of Steady State Gains for Fixed and Variable  $G_1$  and  $\beta=1$  and  $\beta=5$

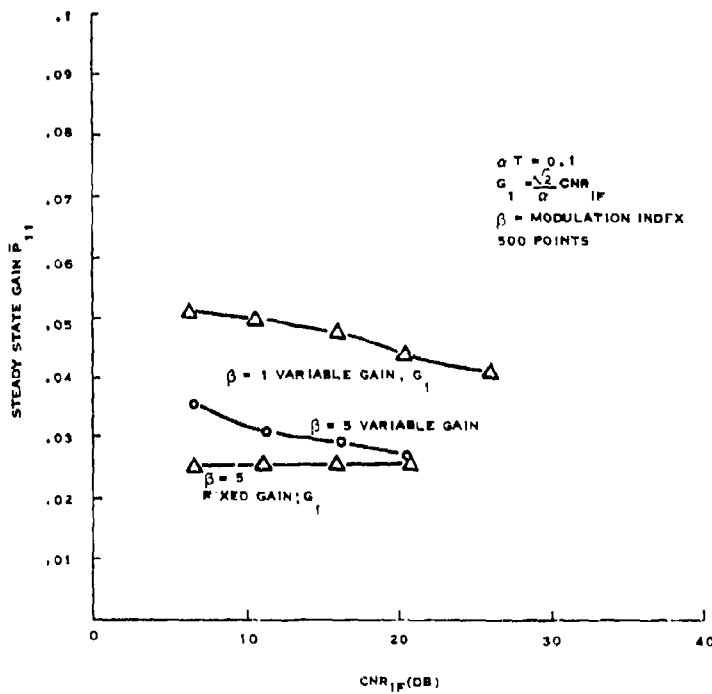


Figure 14c. Variation of Steady State Gains for Fixed and Variable  $G_1$  and  $\beta=1$  and  $\beta=5$

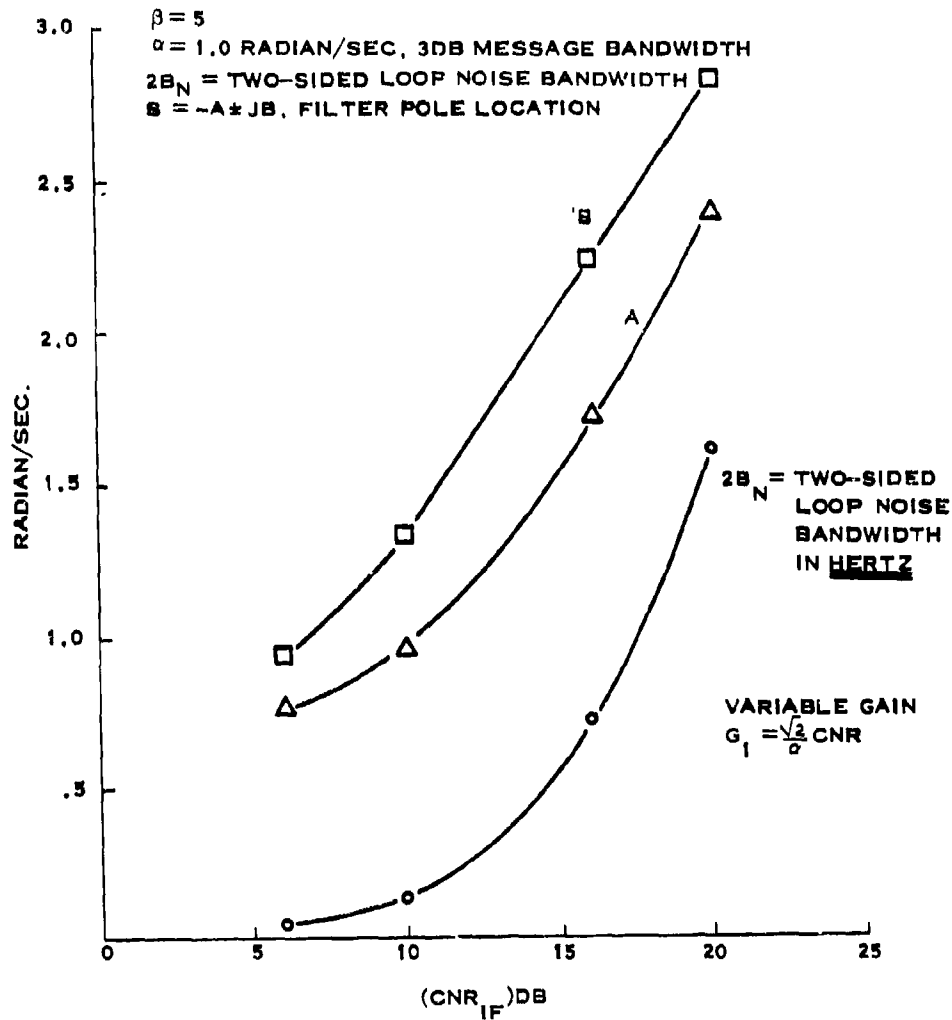


Figure 15. Two-Sided Loop Noise Bandwidth,  $2B_N$ , and Demodulator Pole ( $s = -A \pm jB$ ) Location as Function of Input  $\text{CNR}_{IF}$

the gain  $G_1$  is variable and matched to each new input  $\text{CNR}_{IF}$ . Also sketched in Figure 15 is the loop noise bandwidth that is obtained from equation (66). The noise bandwidth increasing with increased  $\text{CNR}_{IF}$  indicates that as the  $\text{CNR}_{IF}$  increase, the apparent bandwidth of the linearized demodulator opens to better accommodate the signal.

The spectrum of the demodulator transfer function is sketched in Figure 16. For low frequencies,  $\omega < |A - B|$ , the logarithmic plot indicates a parabolic frequency characteristic. This is similar to spectrum characteristics associated with conventional discriminators. The upper cut-off

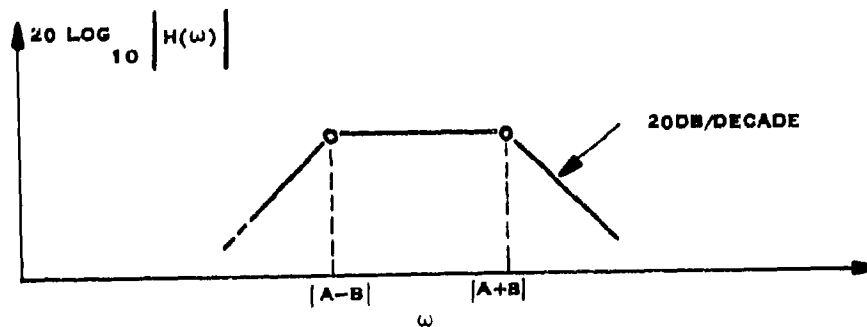


Figure 16. Above Threshold Spectrum of the Demodulator

frequency,  $\omega = |A + B|$ , is also similar to that provided by the low-pass filter in the discriminator demodulator. Figure 17 is a sketch illustrating how the 3 dB bandwidth of the demodulator varies with input  $\text{CNR}_{\text{IF}}$ .

#### H. CONCLUSION

The recursive nonlinear demodulator has been shown by simulation techniques to perform satisfactory; it appears to provide threshold extension capability beyond that of the discriminator of about 6 dB for single-pole message characterization. The above-threshold steady state performance is similar to that obtainable using phase-locked-loop demodulators. An integral part of the demodulator is the time-varying gain processor. During acquisition these gain terms tend to widen the apparent\* bandwidth of the demodulator. Once the signal is acquired, the bandwidth is automatically narrowed.

Obviously, more work is required to reduce the algorithm to a practical digitalized demodulator. However, the work presented here is the necessary first step in applying modern estimation theory and control theory to the problem of optimum digitalization of communication equipment. To the author's knowledge, this is the first realization of an optimum digitalized FM demodulator.

---

\*Apparent bandwidth is used here since bandwidth is rather meaningless in nonlinear processors.

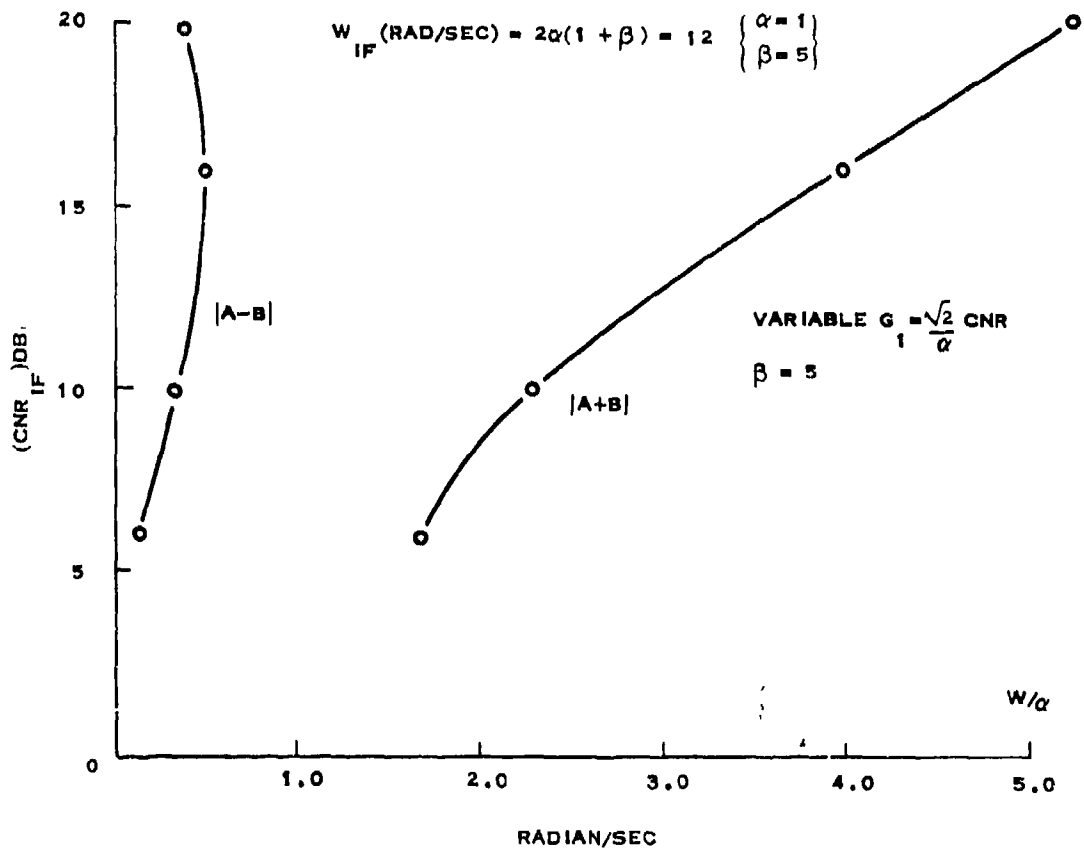


Figure 17. Above-Threshold 3 dB Bandwidth of the Demodulator

## REFERENCES

1. Schwartz, M., Bennett, W., and Stein, S., "Communication Systems and Techniques", McGraw-Hill, 1966.
2. Pitt, S. P. and Grace, O. D., "Signal Processing by Digital Quadrature Techniques" Final Report No. DRL-RT-6839 Naval Ship Systems Command Contract No. N00024-68-C-1117.
3. Athans, M., and Falb, P., "Optimal Control; An Introduction to the Theory and Its Applications," McGraw, 1966.
4. Sage, Andrew P., "Optimum Systems Control," Prentice-Hall, Inc., 1968.
5. McBride, Alan L., "An Estimation Theory Approach to Bit Synchronization", National American Astronautical Society Meeting Record 1969.
6. Van Trees, Harry L., "Part II, Nonlinear Modulation Theory -- Detection, Estimation, and Modulation Theory", Wiley, 1971.
7. Gupta, S., "On Optimum Digital Phase-Locked Loops", IEEE Transactions on Communication Technology, COM-16 pp. 340-344, April 1968.
8. Gupta, S., "Transform and State Variable Methods in Linear Systems", Wiley, 1966.